Dynamic Tidal Power

Spatial analysis and feasibility study

T. J. Verhoeven

12 july 2023

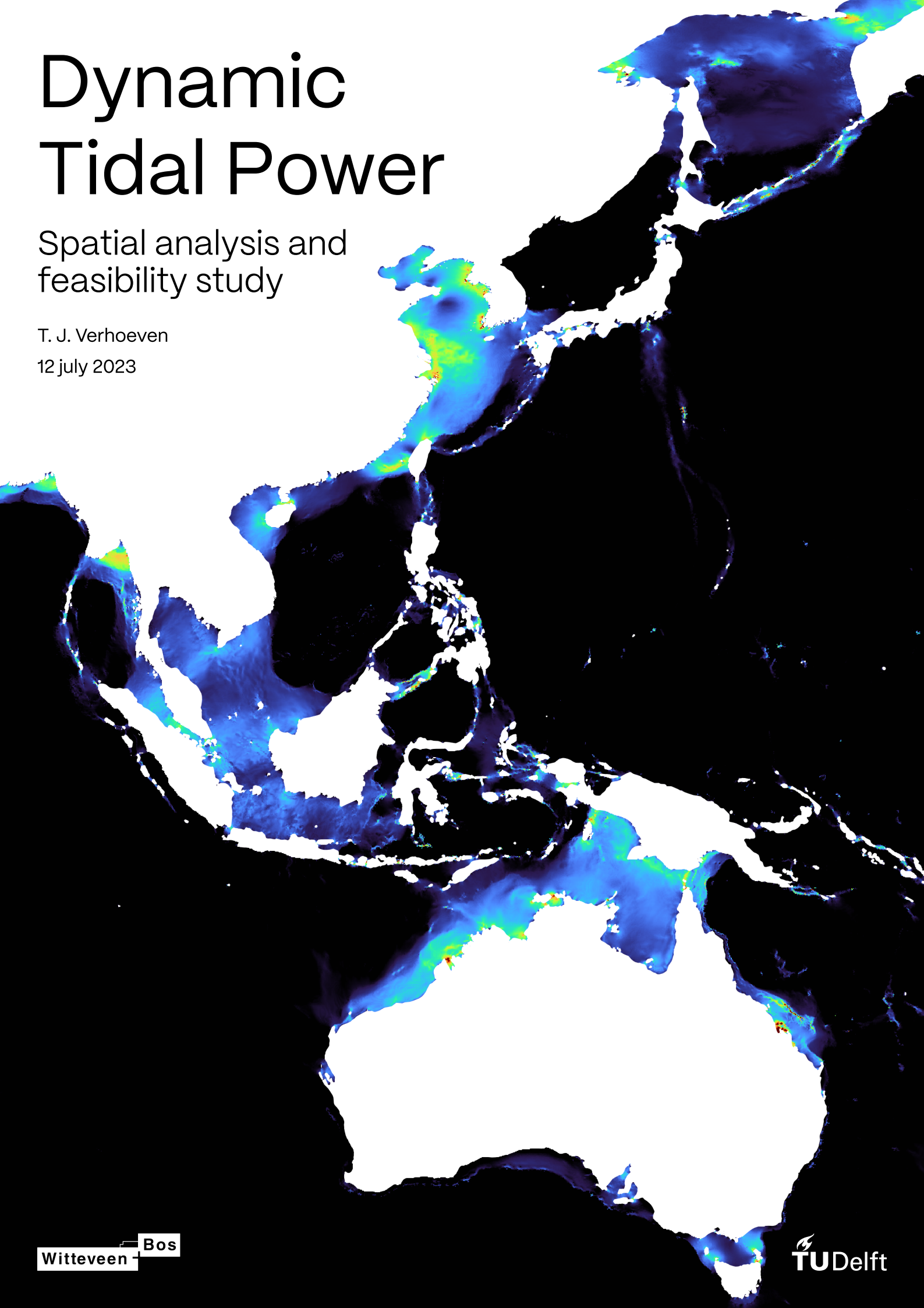

Witteveen + Bos

TU Delft

Dynamic Tidal Power

Spatial analysis and feasibility study

by

T. J. Verhoeven

to obtain the degree of Master of Science
at the Delft University of Technology,
to be defended on July 12, 2023

Project duration:	September 12, 2022 – July 12, 2023	
Assessment committee:	Dr. Ir. A. Antonini,	TU Delft, Chair
	Dr. Ir. C. Kuiper,	TU Delft, Daily supervisor
	Dr. Ir. D. Wüthrich,	TU Delft, Member
	Ms. Ir. A. Rijnink,	Witteveen+Bos, Daily supervisor

TU Delft Witteveen + Bos

Preface

In this master thesis, my study on the global feasibility of Dynamic Tidal Power is presented. It was written to achieve the Master of Science degree in Hydraulic Engineering at the Faculty of Civil Engineering and Geosciences at Delft University of Technology. This research was carried out in cooperation with the company Witteveen+Bos.

First, I would like to express my gratitude to my daily supervisor, Alexandra Rijnink, for her warm welcome at Witteveen+Bos, her guidance and assistance, her expertise, and her helpful feedback. Additionally, I want to thank her for the fun W+B exam.

Secondly, I would like to thank all members of my graduation committee. I want to thank Coen Kuiper for helping me structure the report, providing detailed feedback, and giving me confidence when I was unsure on how to proceed. Alessandro Antonini, thank you for your assistance with the tidal currents dataset, for asking critical questions during our progress meetings, and for encouraging me to include the secondary criteria. Davide Wüthrich, thank you for taking the time to help me assess the flow through the turbine, offering support and asking insightful questions during the meetings.

And last, but certainly not least, I would like to thank my family for supporting me all the way, and my dog Filou for relieving stress when needed. I'm grateful for my friends who made my student time memorable. And I would like to express my gratitude to my girlfriend Fabienne, who always supported and believed in me.

T. J. Verhoeven
Rotterdam, July 2023

Summary

In 2008, a new concept to extract tidal energy was introduced called Dynamic Tidal Power (DTP). In this concept, the natural tidal wave propagating along a coastline is blocked using a long dam, inducing a water level difference between both sides of the dam. This water level difference, called the hydraulic head, can be exploited by placing turbines inside the dam. This is a promising concept, but the feasibility and suitable locations for DTP are largely unknown yet.

This study aimed to identify locations that have the highest potential to implement the DTP concept. By investigating the feasibility criteria and their influence and translating these criteria to spatial analysis, geographic regions with high potential were identified. Additionally, linkage opportunities were assessed and identified to possibly improve the feasibility of DTP.

Based on a sustainable feasibility study framework, the key aspects can be categorized into three main categories; technical, economic and social-ecological feasibility. These aspects were translated into criteria, whose influence was investigated using a hydraulic model. Considering the technical criteria, the tidal flow velocity proved to be more influential on the feasibility than the depth, finding weighting factors of 0.87 and 0.13, respectively. In order to define a threshold of the feasibility of DTP, the technical and economic criteria were combined by assessing the upper threshold of the Levelized Costs Of Energy (LCOE) of 0.1 €/kWh to find a minimum required average flow speed of 0.63 m/s. This threshold was used in the spatial model. The island linkage opportunity proved to be highly valuable. Connecting an island increases the effective blockage length, resulting in a hydraulic head and power output increase with approximately the same dam construction costs. This lowers the mean tidal current speed required for feasibility to 0.39 - 0.57 m/s.

The spatial analysis used a Multi-Criteria Weighted Overlay Analysis (MCWOA) approach, combining datasets and weighting factors for each criterion to find a total Potential Index (PI) score. In total 41 potentially feasible locations for DTP were identified. The geographic regions with the highest potential to implement DTP are the Yellow Sea, the seas in Southeast Asia, and the seas of Oceania. This is due to a combination of high tidal current velocities, relatively modest water depths and a good combination of secondary criteria (energy usage, population size & low shipping disruption). A high share of the island linkage opportunity was found in the locations with the highest potential (44%).

It is recommended to investigate whether additional island linkage opportunities can be identified, by lowering the tidal current velocity threshold in the spatial model. Additionally, 233 locations were discarded, mostly due to their remote location. However, since these locations are technically feasible, it is recommended to investigate the possibility of transmitting the energy over long distances using Ultra High Voltage Direct Current transmission lines and study the total feasibility of DTP at these remote locations.

This study assessed the feasibility of DTP and identified that the Yellow Sea, the seas in Southeast Asia, and the seas of Oceania have the highest potential for a DTP project. Additionally, it provided new insights regarding the influence and thresholds of certain influential criteria, and it presents a hydraulic model and GIS tool that can be adjusted based on the preference of the user. These findings could be useful in future research on the DTP concept.

Contents

1

Introduction

In 2015, the United Nations (UN) adopted 17 Sustainable Development Goals (SDGs) as a shared blueprint to promote peace and prosperity worldwide; see Figure 1.1 for an overview of all goals (United Nations & Development, 2015). Tidal power is a technology that has the potential to help achieve two of these goals (goals 7 and 13) by harnessing the energy of the tides to generate clean and renewable power.

A new concept to extract tidal energy was introduced in 2018, called Dynamic Tidal Power (DTP). In this concept, the natural tidal wave propagating along a coastline is blocked using a long dam, inducing a water level difference between both sides of the dam. It is a promising concept, but so far, the feasibility and suitable locations for DTP are largely unknown.

Figure 1.1: Sustainable development goals (SDGs). Highlighted are Goal 7: *"Ensure access to affordable, reliable, sustainable and modern energy for all"* and goal 13 *"Take urgent action to combat climate change and its impacts"* (United Nations & Development, 2015)

1

1.1. Problem definition

Although Dynamic Tidal Power (DTP) is a promising concept to help achieve the UN SDGs 7 and 13, no global overview of the potential of DTP is available.

Several studies have examined the theoretical proof and functioning of a DTP dam, but the feasibility has not been examined fully. Additionally, The DTP method requires other locational properties than traditional tidal energy extraction methods. Therefore, it could be applicable at locations where the traditional tidal extraction methods are not viable. Currently, only the Yellow Sea and the North Sea are investigated for applying DTP; no research has been conducted to evaluate the worldwide potential. Therefore, there is a lack of knowledge regarding the feasibility of DTP on a global scale.

Identification of regions or locations with high potential could be a starting point for further research, case studies, or to potentially discover a suitable site for the first DTP dam in the world. Therefore, a global assessment of the potential of DTP could be helpful to identify suitable locations, potentially providing a starting point for increasing renewable tidal energy in the world.

1.2. Objective

This research focuses on the development of a Geographic Information System (GIS) tool to demonstrate the feasibility of DTP globally. First, the general feasibility is assessed, after which feasible locations are identified. Hence, the main objective is to gather additional insights regarding the feasibility of DTP and identify the geographical regions or specific locations with the greatest potential for DTP worldwide.

This thesis will explore the feasibility of dynamic tidal power and its potential as a renewable energy source. To achieve this, the following research question will be answered:

"Which worldwide locations have the highest potential to implement Dynamic Tidal Power?"

This will be achieved by first addressing and answering the following sub-questions:

1. What are the key criteria concerning the feasibility of DTP?
2. How do the key criteria influence the energy production of a DTP dam, and what is the optimum configuration, considering energy production and cost?
3. How do the criteria translate to finding locations with high potential, and what geographic regions have the highest potential for DTP?
4. How can the feasibility of DTP be improved, considering linkage opportunities?

1.3. Approach and report outline

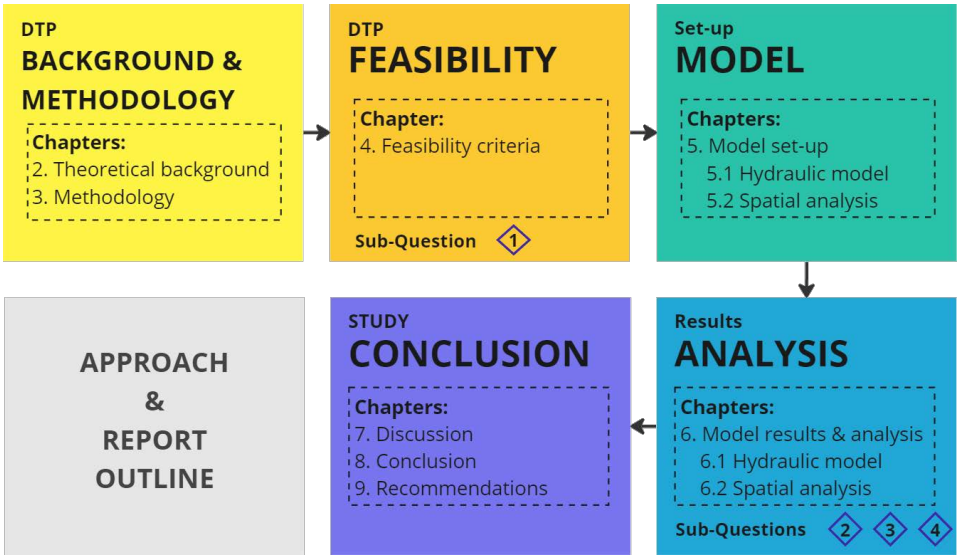

Figure 1.2: Schematic illustration of the approach and report outline

The report outline is summarized in figure 1.2. **Chapter 1** presents the problem definition, objective and approach. **Chapter 2** presents the background information on Dynamic Tidal Power. In this chapter, the basic physical processes behind DPT are explained, a theoretical proof of concept is presented, and a literature review is shown, including the current studies and knowledge about DTP. In **chapter 3**, the methodology of the research is described. **Chapter 4** contains the feasibility study on DTP, where the key criteria of the feasibility are identified, answering sub-question 1. **Chapter 5** shows how both the hydraulic model and the spatial analysis are set up, using the background information and feasibility study as a basis. **Chapter 6** provides both model results and the corresponding analysis. Here, sub-questions 2, 3 and 4 are answered. Lastly, **Chapters 7, 8 and 9** present the discussion, conclusions and future recommendations.

2

DTP: Theoretical background

This chapter aims to provide an introduction to the Dynamic Tidal Power concept and the theoretical background information needed to understand the upcoming chapters of this report. An introduction to tidal energy and DTP is provided in sections 2.1 and 2.2. Then, a literature review is presented in section 2.3, where the current knowledge on DTP is stated and summarized. This provides a basis of knowledge and gives insight into how much is known of the DTP concept. Section 2.4 provides basic information on the global energy mix and demand. Chapter 2.5 provides a brief comparison between DTP and other renewable energy sources. Chapter 2.6 provides the basis of the feasibility study. And lastly, chapter 2.7 provides possible linkage opportunities of DTP. To provide additional information, appendix B provides a theoretical substantiation of the DTP concept.

2.1. Tidal energy

2.1.1. Tides

The tide is generated by the gravitational pull of the moon and the sun on the Earth's oceans, causing a rise and fall in sea levels. The rotation of the earth and the movement of the moon and sun influence the location of the pull of gravitational forces, resulting in long tidal waves. On Earth, three basic tidal patterns can be distinguished; semidiurnal, diurnal and mixed semidiurnal tides. Semidiurnal tides have two high and two low tides every day. Mixed semidiurnal tides also have two highs and lows but differ in height. Diurnal tides have one high and one low each day (Bosboom & Stive, 2021). See appendix A for additional information about tidal processes on a global scale, including an overview of the tidal classifications in figure A.1.

2.1.2. Energy extraction methods

Currently, two main methods exist to extract tidal power; the tidal basin method and the tidal stream method (see figure 2.1). The tidal basin method involves blocking a water body (basin) from the ocean, using the natural high tidal range to generate energy. The tidal stream method extracts kinetic energy directly using turbines or other devices. This method is applied in straits with naturally high tidal current velocities.

Both methods require different area properties; the tidal basin method requires a basin and a large natural tidal range, while the free stream turbines require a large natural tidal current velocity (Mendi et al., 2016). A rough estimate of the global tidal energy potential is approximately 500 Gigawatt, as shown in figure A.5 (Bluespring, 2016).

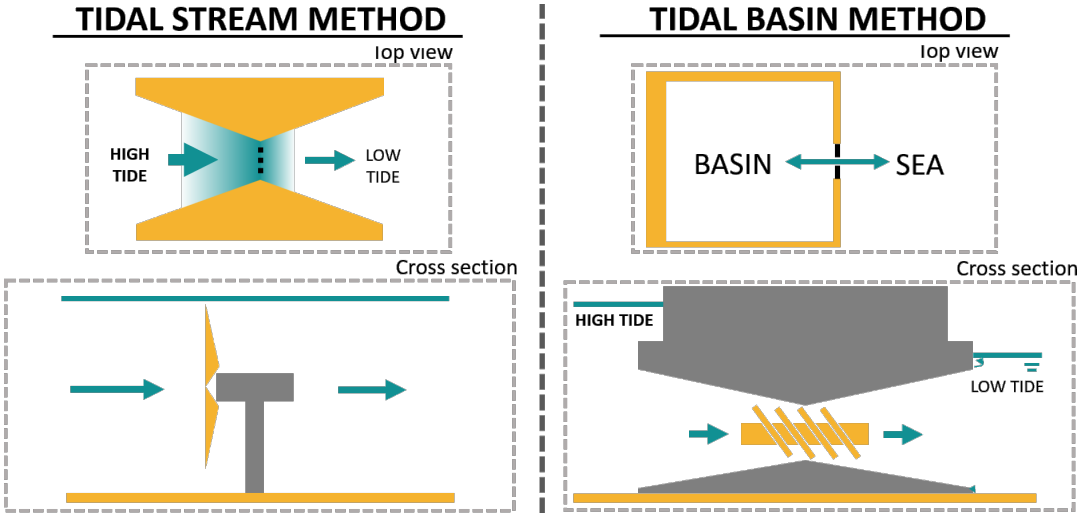

Figure 2.1: Traditional tidal energy extraction methods.

2.2. Dynamic Tidal Power

In 2008, a new concept called Dynamic Tidal Power (DTP) was proposed by Hulsbergen et al., 2008. In this concept, the natural tidal wave propagating along a coastline or between an island and the coast (Kelvin wave) is blocked by a long dam with 30-50km lengths. Due to this blockage, the tidal wave decelerates, and the tidal wave energy converts to height energy, resulting in a water level rise on one side of the dam. Additionally, the water level decreases on the ”low water” side of the dam because of the gravitational pull of the moon and sun on the water body. This results in a water level difference between both sides of the dam, called the hydraulic head difference. This hydraulic head difference can be exploited by placing turbines across the dam to generate energy. See figures 2.2 and 2.3 for 2D and 3D illustrations of the DTP concept. See appendix B for the theoretical substantiation of the concept.

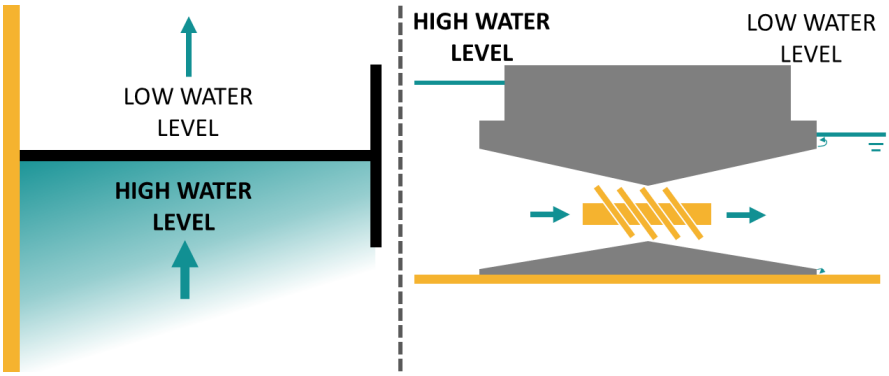

Figure 2.2: Dynamic tidal power concept, top view (left) and cross-section view (right).

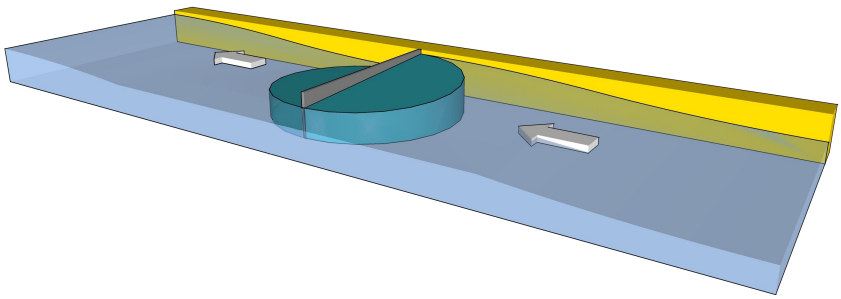

Figure 2.3: Illustration of a tidal wave blocked by a DTP dam, including the trapped water mass area shown in dark-green.

2.3. Literature review

A few academic papers described and investigated the potential of DTP. These papers assess the concept and validate the idea using basic analytical calculations and by using complex numerical models. A brief list of these papers is stated in table 2.1, including their relevance and their contribution to the literature study. These papers will be addressed in more detail in the rest of this chapter.

Author(s)	Description & relevance	Key findings
(Hulsbergen et al., 2008)	First paper on DTP	- Introduction to DTP - Equation B.4 by P. Kolkman
(Talstra & Pak, 2020)	Description physical concept behind DTP Schematized case added value + full numerical model Numerical calculations of DTP configurations	- Schematized case observations - Difference between numerical model - Note on larger-scale wave diffraction-
(Park, 2018)	Modelling DTP configurations (T-bars)	- No dramatic improvement found with attached T, L, or Y-bar - Connected and detached DTP dam study
(Berlee et al., n.d.)	Ecological effects and opportunities	- Ecological effects, see chapter ...
(Mei, 2011)	Derived eq. B.4 using different approach	- Same analytical equation B.4 found
(Dai et al., 2018)	Numerical model observations	- Longitudinal profile: quarter ellipse shape
(Shao et al., 2017)	Triple small dams compared to one large dam	- Thriple small dam may more beneficial

Table 2.1: Main relevant literature on DTP

2.3.1. Dam properties

Hydraulic head

The water level difference between both sides of the DTP dam is called the hydraulic head difference, as illustrated in figure 2.2. The magnitude of the induced hydraulic head is mainly dominated by the tidal current velocity (Mei, 2011). Therefore, the harmonic velocity range is important and not the original tidal range (Hulsbergen et al., 2008).

Longitudinal profile

The head is not constant along the dike length. The maximum hydraulic head occurs at the shore attachment, decreasing towards the tip of the dam by following a quarter ellipse shape (Hulsbergen et al., 2008), (Dai et al., 2018). An example of the longitudinal water level profiles is shown in figure C.1.

Analytic approximation

The hydraulic head can be approximated using equation 2.1, first derived by P. Kolkman (Hulsbergen et al., 2008) by describing an oscillating plate in a fluid at rest. Using a different approach, Mei, 2011 discussed the interaction of a harmonic tidal wave with a long-perpendicular dike, where the same equation (eq. 2.1) was found. Appendix B shows the derivation of this equation and additional information on the physics behind the DTP principle. As can be seen, the maximum hydraulic head depends on the maximum tidal velocity, the dam length, the angular velocity of the tidal signal and the gravitational acceleration.

$$\Delta h_{max} = \frac{2\omega L V_{max}}{g} \tag{2.1}$$

where:

Δh_{max} = Maximum hydraulic head level difference [m]
V_{max} = Maximum (tidal) flow velocity [m/s]
L = Dam length [m]
ω = Angular velocity of the tidal wave [1/s]
g = gravitational acceleration [m/s^2]

Dam length

As seen from equation 2.1, a larger dam length is favourable regarding the increased hydraulic head, also confirmed in the paper of Q. Liu and Zhang, 2014. This is mainly due to two factors. Firstly, a larger dam increases the phase difference between both sides, which increases water level differences and, thus, the hydraulic head. Secondly, a larger dam length captures a larger water mass, increasing the system's inertia and the hydraulic head. On the other hand, a longer dam usually leads to deeper water depths, increasing the construction costs. The optimal dam length is a balance between an increase in hydraulic head and, thus, power output and construction costs.

Phase difference

The earlier mentioned phase difference greatly influences the resulting hydraulic head difference, as shown in figure 2.5 (Hulsbergen et al., 2008). Figure 2.4a shows two out-of-phase tidal signals of a studied location in China. The hydraulic head is around $\pm$ 1.7 m while the individual tidal signals amplitudes are only $\pm$ 1.4 m. Figure 2.4b shows another location in South Korea with the opposite effect. Here, the signals are almost in-phase. The individual amplitudes are fairly large ($\pm$ 6 to 7m), but the resulting hydraulic head difference is relatively modest at $\pm$ 3m. If, in the example in figure 2.5b, the phase difference could be enhanced, then the hydraulic head could be severely increased.

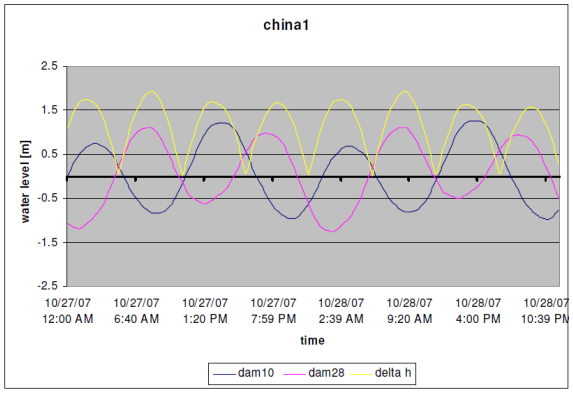

(a) Example of out-of-phase tidal signals, the amplitude of the individual signals is small ($\pm$1.4 m), but the resulting hydraulic head difference is relatively high ($\pm$1.7 m).

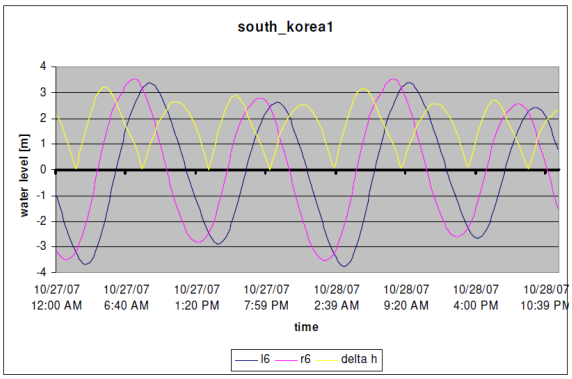

(b) Example of in-phase tidal signals, the amplitude of the individual signals is large ($\pm$ 6 to 7m), but the resulting hydraulic head difference is relatively low ($\pm$ 3m).

Figure 2.4: Tidal signals on opposite sides of the DTP dam and the induced hydraulic head difference (Hulsbergen et al., 2008)

For a regular sinusoidal or cosine tidal wave, the maximum hydraulic head level difference is gained for a phase difference equal to π (180°). For real tidal waves, the more close to π the phase difference is, the higher the hydraulic head (Q. Liu & Zhang, 2014).

Dam shape: T, L or Y-bar

The original research of Hulsbergen et al., 2008 showed that adding a T-bar at the tip of the dam causes an increase in the hydraulic head over the dam. Adding a 20km long T-bar to the head of a 30km long dam, resulted in a hydraulic head increase of 53%. Moreover, a more constant longitudinal water level can be expected, which is beneficial for an equal turbine power output (Hulsbergen et al., 2008) (Talstra & Pak, 2020). This increase can be explained using the added-mass theory, where an increase in trapped water mass increases the hydraulic head difference over the dam (Talstra & Pak, 2020). See figure 2.5a for an example of an additional Y-shaped bar.

Park, 2018 compared the effects of added T and L bars (up and down) for one location in the Yellow Sea, South-Korea. It was found that the added T-bar performed best in terms of induced hydraulic head difference. Following up on this, Q. Liu and Zhang, 2014 found that Y-shaped bars have more advantages than T-shaped bars regarding the induced maximum hydraulic head. This has three main reasons.

- The geometrical gradual narrowing of the Y-shaped bar induces a wave gathering effect (Q. Liu & Zhang, 2014).

- The geometrical shape of Y-shaped bars could induce resonance of the nearby water body, if the inherent frequency of the water body comes close to the tidal wave frequency (Q. Liu & Zhang, 2014). To maximize this resonance, the phase difference should be as close to π as possible. Liu and Zhang found that this is expected when the angle of the Y-shaped bars is $\alpha = 40°$. A DTP dam illustration with a Y-shaped bar configuration can be seen in figure 2.5a.
- Y-shaped bars increase the trapped water mass in two dimensions (parallel and perpendicular to streamwise direction). Due to this increase in two directions, the increase in hydraulic head difference is accelerated (Talstra & Pak, 2020).

Although most studies describing DTP and the applicability of T or Y-shaped bars agree with the positive effects of an additional Y or Y-shaped bar at the end of the DTP dam, there is one research that did not show a significant improvement (Park, 2018). This research concluded that a simple DTP dam without an attachment of a structure would be the best choice to satisfy the energy production and construction costs. However, since the research showed completely different results than other studies, further study on this subject is needed.

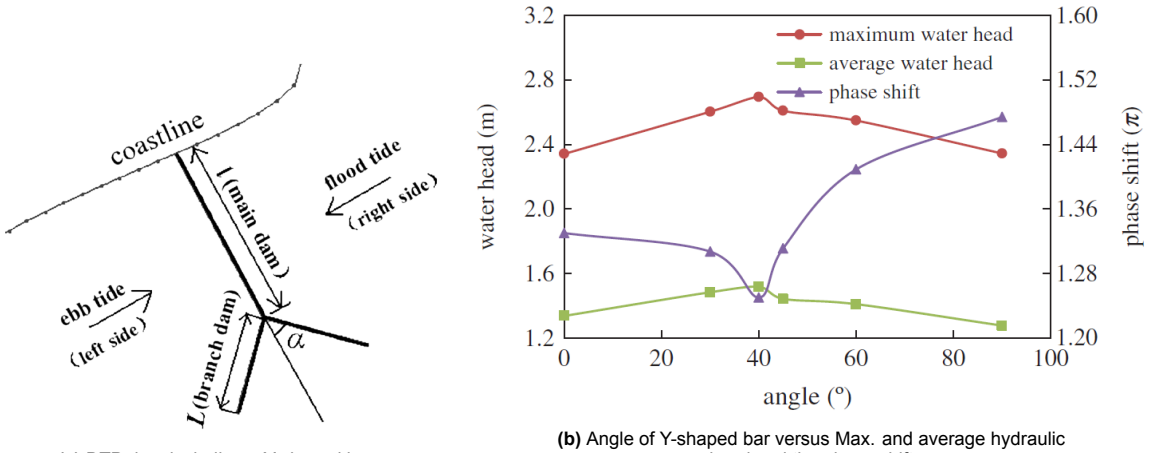

(a) DTP dam including a Y-shaped bar

(b) Angle of Y-shaped bar versus Max. and average hydraulic head and the phase shift

Figure 2.5: DTP dam including Y-shaped attachment and the influence of angle α, from the paper of Q. Liu and Zhang, 2014

Comparison analytical calculations and numerical models

Since this study will use analytical equation 2.1 as the basis for the simplified hydraulic model, the difference between this equation and a numerical model is interesting. Hulsbergen et al., 2008 studied a DTP dam concept at IJmuiden. The hydraulic head of the numerical model was a factor 1.7 higher than the head approximated using the analytical calculation. Similar differences were found by the numerical study of Dai et al., 2018 and by Talstra and Pak, 2020. Since the analytical equation is fairly simple, it only gives an indicative approximation. A numerical model should include the following phenomena that are important for assessing a DTP dam:

- Larger-scale wave diffraction effects (Talstra & Pak, 2020). This scattered diffraction wave is also called a parasitic wave; it scatters away from the dike's attachment (the dam connection to the shore). See the paper of Dai et al., 2018 for more information.
- Wave gathering effects (Q. Liu & Zhang, 2014). Both the geometry of the DTP dam and local bathymetry properties influence the magnitude of the wave gathering effect.
- Resonance of water body (Q. Liu & Zhang, 2014).
- Tidal asymmetry (Talstra & Pak, 2020).
- Including all tidal wave components that form the tidal signal spectrum (Talstra & Pak, 2020).

Twin dams

The possibility of combining two DTP dams was initiated and investigated by Hulsbergen et al., 2008, using an example in the Yellow Sea. The combination of two dams could yield a more constant power

output. The dams should be placed so that the head is maximum for one dam when the head is zero for the other and vice versa. To give an indication, the dams described by Hulsbergen et al., 2008 the mutual distance was 200km. See figure C.2 for a figure showing this study's locations, the hydraulic head and the corresponding power output.

Following on this concept, Shao et al., 2017 examined the use of triple small DTP dams instead of one single large DTP dam. This research used the same locations at the study of Hulsbergen et al., 2008 in the yellow sea. One large DTP dam of 50 km with a branch of 37.5 km was compared with three dams of 25 km with a branch of 18.75 km. It was found that combining two or three small dams may reach or exceed the induced hydraulic head and power output of a single large one working alone.

Connected and detached DTP dam
Park, 2018 compared DTP dams connected and detached from the shore. Detaching the DTP showed a significant reduction in hydraulic head differences (reduction of 33% to 73%, dependent on distance from the shoreline). However, a detached DTP dam has the benefit to has a less environmental, hydrodynamic and morphodynamic impact (Park, 2018). Additionally, it can be positioned inside existing wind parks or at locations where shipping can easily sail around. A summary of the differences between a DTP dam connected or detached from the shoreline is shown in table 2.2 (DTP Netherlands, n.d.).

Aspect	Connected to shore	Detached
Hydraulic head	Higher, maximum at attachment to shore	Significant lower
Morphology	Blocked nearshore sediment fluxes	Nearshore sediment fluxes can pass
Environmental influence	Higher, more hydro - and morphodynamic changes	Lower
Shipping	Large shipping disturbance	Could be positioned to disturb shipping less
Costs	Lower construction costs (shallower depth & easier construction) Lower maintenance costs	Higher construction, power grid & maintenance costs

Table 2.2: Main differences between a connected and detached DTP dam (DTP Netherlands, n.d.)

Dam permeability
The turbines installed in the dam allow water flow through the dam, making it partly permeable. The dam permeability influences the hydraulic head difference. If the dam is fully closed, the hydraulic head difference is highest. If the permeability increases, the hydraulic head difference decreases, since more water is able to flow from the high to the low side of the dam.

Generally, the permeability is determined by the cross-sectional flow area, thus the number of turbines and the turbine diameter. An increase in the number of turbines or the diameter increases the cross-sectional flow area and, thus, the permeability (see chapter 2.3.2). However, other design choices could also affect the dam permeability; two design concepts are stated below. Both concepts reduce the hydraulic head difference significantly, which also reduces the power output and, thus, energy generation by the DTP dam. Therefore it is highly debatable whether these designs are desired.

Dam with partial open bottom

- In large water depths, it is costly to block the full water column. Constructing a partially floating construction at the deeper part could reduce construction costs significantly.
- An open bottom allows for sediments to pass the dam easily, giving less disruption to the natural sediment patterns. Additionally, probably less sediment erosion or accommodation will occur. The scour holes will be significantly less deep, reducing the need for extensive bed protection.
- It allows for larger fish species, such as whales, to pass the dam easily. Alternative ways are fish-friendly turbines, but the diameter should be of significant size for larger species and it should be proven that the fish are not harmed by the turbines. Therefore, leaving the dam partially open could have benefits if the dam is planned in a larger fish migration route.

Dam with small part disconnected from shore

- Near shore, the water depth is shallow. This induces wave action (breaking wave), (rip) currents and other phenomena. Therefore, the sediment transport is higher near the shore. Leaving a part disconnected could allow for easier sediment passage (reducing the effect of the dam on the natural longshore sediment transport). This also reduces the downdraft erosion and updrift accretion normally found at structures at the coastline (Bosboom & Stive, 2021).
- Although the flow velocities are induced, leaving a part of the dam disconnected from the shoreline could possibly allow vessels to pass. Although, the flow velocities will most likely increase significantly, possibly making it unsafe with respect to manoeuvrability. This should be investigated in more detail.

2.3.2. Turbine configuration

To extract power, hydraulic turbines are needed. The power output of a hydraulic turbine is described by equation 2.2. As can be seen, the power output is mainly dependent on the flow rate and hydraulic head difference (pressure).

$$P = \eta \rho g \Delta h Q = \eta \rho g \Delta h V A \tag{2.2}$$

where:

P = Power output [W]
η = Efficiency factor [-]
ρ = Water density [1025 kg/m^3]
g = Gravitational acceleration [9.81 m/s^2]
Q = Flow rate [m^3/s]
Δh = Hydraulic head difference [m]
A = Cross-sectional flow area [m^2]
V = Axial flow velocity [m/s]

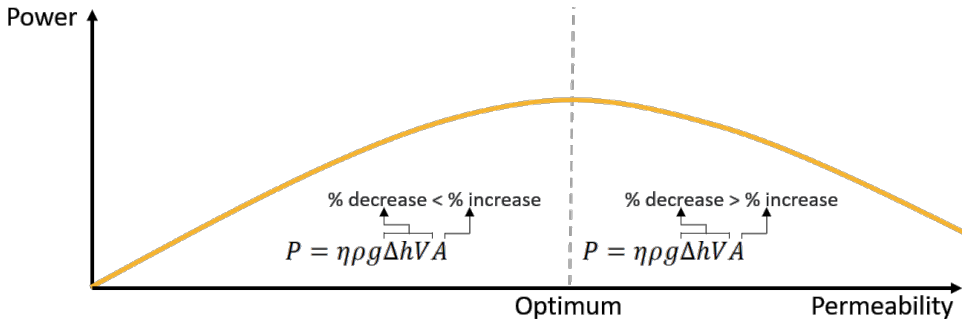

Figure 2.6: The permeability influence on the hydraulic head, flow velocity and flow area. An optimal permeability can be found. Based on (Tidal Bridge bv, 2020)

If a DTP dam with turbines is considered, without any other additional openings, the permeability is fully determined by the number and diameter of the turbines (cross-sectional flow area). For such a situation, figure 2.6 illustrates the balance between permeability and power output. As can be seen, increasing the permeability decreases the hydraulic head difference and the flow velocity, but increases the flow area. At this moment, the percentual increase of the cross-sectional flow area is larger than the percentual decrease in hydraulic head and flow velocity. Increasing the permeability and thus flow area, increases the flow rate through the turbines. An optimum can be found, where the percentual increase of the hydraulic head and flow velocity is equal to the percentual increase in flow area. When a larger permeability is chosen, the power output decreases, since the percentual increase in cross-sectional flow area (A) is smaller than the percentual decrease of the hydraulic head and flow velocity. Therefore, to achieve the maximum power output, there is a balance between the cross-sectional flow area and the hydraulic head level difference.

Turbine openings
The optimal turbine opening and, thus, the permeability of a DTP dam is case-dependent. Hulsbergen et al., 2008 indicated that the optimal turbine opening should lie between 5% and 15% of the lateral dam area. Similar turbine opening rates are found in other researches (Dai et al., 2017), (Anteagroup, 2018), (Tidal Bridge bv, 2020).

Number of turbines
The amount of turbines needed depends on an area's energy potential. With equation 2.2, the maximum power of a design can be estimated. However, the number of turbines needed to extract all potential power is case-dependent.

If the energy production is plotted against the number of turbines, the power does first increase linear and then decreases slowly until the maximum power output is reached. Therefore it could be economically viable not to install the full 100% turbines. Installing fewer turbines could increase the energy generation per turbine and reduce construction and maintenance costs. During an interview with G. Manshanden from fishflow innovations, it was found that one fishflow turbine with a diameter of 10 meters will cost approximately €2.000.000. Knowing this, an optimum between the number of turbines and power generation can be found, where the benefits of additional power production are weighted against the costs of an additional turbine.

Turbine diameter
The choice of turbine diameter depends on several factors, which are listed below:

- Since a DTP dam blocks a large water body, fish migration routes are possibly disturbed. The choice of a large and fish-friendly turbine could allow large fish species, such as whales, to pass the turbine. Therefore, the ecological effect of the dam on the environment can possibly be reduced if the turbine diameter is large enough for the desired fish species to pass.
- A larger diameter turbine has the advantage of being less costly in terms of flow area and costs. According to G. Manshanden from FishFlow Innovations, building one big turbine is generally less costly than producing multiple smaller turbines (keep in mind that area is proportional to the diameter squared). For example, one turbine with a diameter of 10m equals four turbines with a diameter of 5m.
- Multiple smaller turbines could have the advantage of having a smaller starting velocity. Therefore, for smaller flow velocities, having multiple smaller turbines is beneficial compared to one large turbine. However, for large flow velocities, the power output of one larger turbine is higher than for multiple smaller turbines. Therefore, it depends on the expected flow velocities which turbine diameter is preferable. Appendix E.4 investigates this scale effect in more detail, using the results of a flow study (OpenFOAM software) of the FishFlow innovation turbines.
- Considering turbine maintenance, both have benefits and drawbacks. Smaller turbines are less heavy, improving manoeuvrability and ease of assembling and disassembling. However, if large-diameter turbines are chosen, the total number of turbines in the dam is less. Therefore, fewer turbines need maintenance.

2.4. Energy

2.4.1. Energy mix

The global energy mix is shown in figure 2.7. It can be observed that the mix is more diverse than ever before in history. Nonetheless, the dominant energy source is still fossil fuels, accounting for 84% of the total energy consumption. Moreover, the total fossil fuels energy production increased from 116,214 to 136,761 TWh in 10 years and is still increasing each year (Ritchie et al., 2022), see figure G.1 for more detailed information.

2.4.2. Energy demand

Electricity can only be stored to a limited extent and at relatively high costs. Therefore, primary production is typically closely linked to demand ("load"). There are two main energy categories; dispatchable

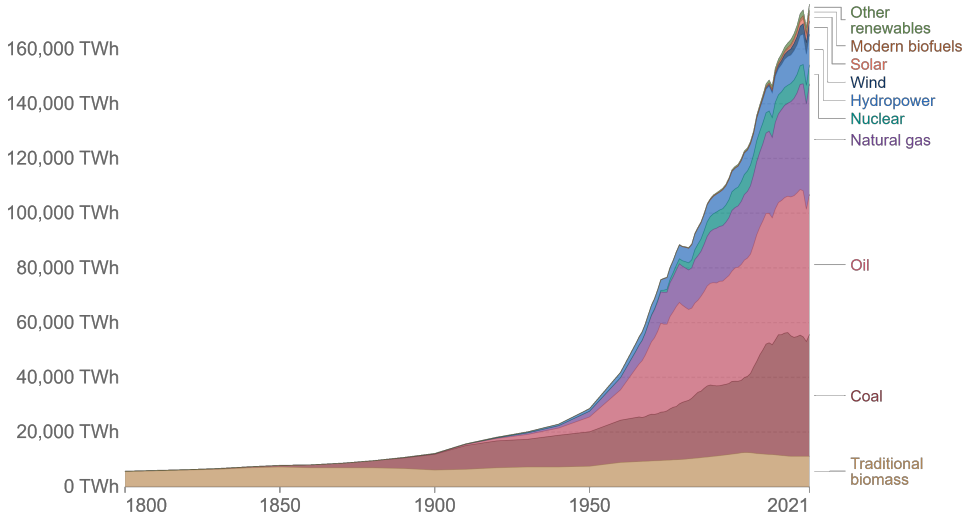

Figure 2.7: Global energy mix change in time (Ritchie et al., 2022)

energy and intermittent energy. The production of dispatchable energy can be controlled, so it can be started or stopped when needed. Intermittent energy, on the other hand, refers to energy sources dependent on external factors, such as solar or wind, that cannot be controlled.

The demand or load type can be categorized into: the variable base, base, intermediate and peak load. The variable base consists of intermittent energy; these cannot be controlled. Moreover, the variable base load has effective priority in the marketplace since these are renewable but cannot be controlled. The base load consists of sources that provide reliable and inexpensive power, but the energy output is not flexible. The intermediate load is more flexible so that it can follow the demand. The peak load is the most flexible and closely follows the peaks in demand; this type is the most expensive. Power plants in the intermediate or peak load categories are called load-following power plants. See table 2.3 for an overview of the main energy sources and their energy and load categories.

As can be seen, hydropower can be utilized as base, intermediate and peak load; if the plant has enough potential energy stored (water behind the dam). Gas can be found in two categories. The combined-cycle gas turbines utilize gas in the intermediate load; the composition gas turbine is used for the peak loads. Tidal can be both a variable base and a base load. This is because tidal power without adjustments has a predictable but variable power output. If the tidal power plant is expanded with battery packs, it could provide constant energy.

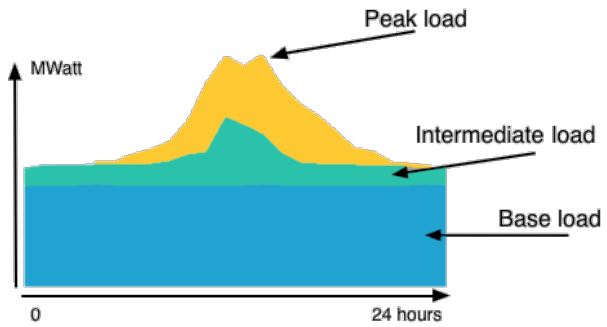

Figure 2.8: Schematic representation of the energy load curve, including the base, intermediate and peak load principle (Weidema, 2014)

	Intermittent energy	Dispatchable energy		
Load type:	**Variable base**	**Base**	**Intermediate**	**Peak**
	Solar Wind Tidal	Coal Nuclear Hydro Tidal	Gas Coal or oil to steam Hydro Biomass	Gas Oil Hydro

Table 2.3: Energy and load types of main energy sources

Energy demand mix change
The use of renewable energy (and thus intermittent energy) is increasing (IEA, 2021), leading to an increased need for flexible energy sources to handle the variable base load, see figure 2.9. It is predicted that intermediate (fossil fuel) load types will play a major role in managing the fluctuations caused by intermittent energy (Pickard & Meinecke, 2011). However, the technique needs further improvement to increase flexibility, including rapid and efficient start-ups and (overnight) shutdowns. Additionally, intermediate fossil fuel power plants must still have a high capacity to provide energy when no renewable energy is available, but a high energy supply is needed. This change in the mix of the energy load curve would induce integration costs and complex challenges; please see the list below. For Europe, Pudjianto et al., 2013 estimated the integration costs of solar power to be between 0.5 and 2.5 eurocents / kWh. For a full elaboration on this subject, please refer to the papers of Martinot, 2016 and Brouwer et al., 2014.

- Re-design of supply-side: flexible power plants
- Higher levels of system reserve capacity, to be used as backup when no renewable energy is available
- Flexibility of electricity demand
- Increase of electricity and heat storage
- Transmission strengthening and grid balancing
- Power system operational measures and improved planning by distribution systems

Predictable tidal power
Considering the impact of tidal power, it is highly predictable, so it can directly replace the current base load fossil fuel types. Additionally, the predictability of tidal power makes energy management more efficient. Including tidal power in the energy mix would provide a stable and highly predictable energy load, reducing the costs and operational challenges mentioned in the list above.

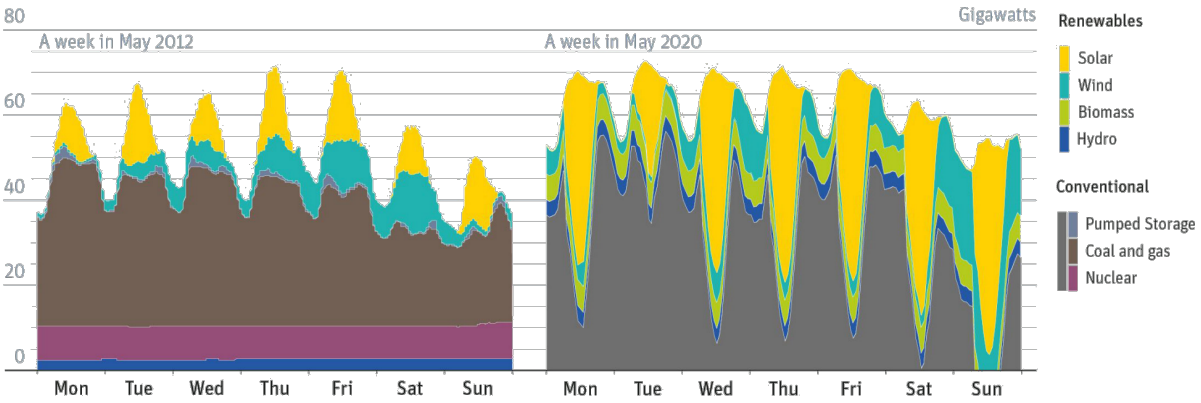

Figure 2.9: Energy load curve comparison between a week in May 2012 and May 2020 in Berlin (Jungjohann & Morris, 2014)

2.5. Renewable energy comparison

2.5.1. DTP compared to traditional tidal energy

As DTP actively interacts with the tidal wave propagating along a coastline, it works differently than traditional tidal power extraction methods such as the basin and stream methods. Therefore, the areas suitable for DTP are different than for other tidal power techniques; see table 2.4 for the areal requirements and common locations for each method. In most cases, the tidal energy methods will not compete with each other since they all have different area requirements. The tidal basin method requires a tidal range generally larger than 3 m (U.S. Energy Information Administration (EIA), 2022). The tidal stream method and DTP both require sufficient tidal flow velocities. The difference lies in the magnitude of flow velocities required. The tidal stream method directly uses the natural tidal currents to generate energy, mean spring peak tidal currents larger than 2 m/s are required. For lower current speeds the energy density is inadequate to be economically viable (Aqua-RET, 2012). DTP actively interacts with the current of a propogating tide to generate a sufficient hydraulic head difference. Therefore, the required tidal current speed is lower (Minimum required $\approx$ 0.6 - 0.7 m/s (Hulsbergen et al., 2008)).

Method	Required area properties	Indication of magnitude	Common locations
Tidal basin	Large tidal range + basin	Tidal range >3 m	Basin or estuary
Tidal stream	High tidal flow velocities	Tidal currents >2 m/s	Strait + shallow water
Dynamic Tidal Power	Propagating tide	Tidal currents >0.6 m/s	Coastline

Table 2.4: Table summarizing required area properties of tidal power extraction methods.

2.5.2. Tidal comparison to solar and wind energy

1. Resource Availability:
   Since the tides are predictable and occur twice or once a day (dependend on a semi-diurnal or diurnal tidal signal), tidal energy is a consistent and reliable energy source. Solar and wind energy are highly dependent on meteorological conditions, which causes fluctuations in energy generation. The energy net needs to process this energy surplus or store it in batteries for later usage, which is a complex and costly process. Additionally, if there is no wind or solar energy available, brown energy sources (coal, gas, oil) or nuclear energy have to be used to fulfil the energy demand.

2. Cost:
   Tidal energy is currently more expensive compared to solar and wind energy. The construction costs of the tidal basin method and DTP are high, large investments are required. As explained in the energy price comparison section (2.5.3), the costs of solar and wind energy both decreased significantly in the last years (see figure G.2). The solar energy price decreased from 0.35 €/kWh in 2010 to 0.04 €/kWh in 2021, the offshore wind energy price from 0.16 €/kWh to 0.06 €/kWh in the same period (IRENA, 2022). Taking into account that the initial investments costs are significantly less for a solar or wind project, makes solar and wind energy currently economically more viable.

3. Environmental Impact:
   Tidal Tidal energy systems can have a relatively low environmental impact. They do not produce direct greenhouse gas emissions, and their installation can create artificial reefs, which can provide habitats for marine life. However, tidal barrages can disrupt marine ecosystems and affect fish migration patterns. Solar Energy: Solar energy is environmentally friendly and has minimal impacts once the panels are installed. However, the production of solar panels involves the extraction of raw materials, some of which can have environmental consequences if not managed properly. Wind Energy: Wind energy is also considered environmentally friendly once operational. However, the manufacturing process of wind turbines requires significant energy and raw materials. Large-scale wind farms may also have visual and noise impacts on local communities and wildlife.

4. Geographic region:
   Tidal energy is limited to coastal regions with tidal activity, therefore it is only applicable at specific locations. Solar and wind energy are more widely applicable, but naturally some locations are more suitable if more solar or wind is available during the year. A spatial analysis could take this into account, by identifying the potential of tidal energy, wind energy and solar energy for all locations, to identify if energy sources are competitive in a geographic region. However, please note that an energy mix is always required, see section 2.4.1).

2.5.3. Energy price comparison (LCOE)

Comparing different energy sources to DTP energy is challenging because the exact costs of DTP are not known precisely. Table 2.5 shows a levelized cost of electricity (LCOE) comparison in € cents (ct) / kWh in the year 2021 (IRENA, 2022). As can be seen, the 5% percentile of all energy sources lies around 2 - 4 €ct/kWh, the 95% percentile lies around 10 - 11 €ct/kWh, except for onshore wind with 5.3 €ct/kWh. The average lies between 3 and 6 €ct/kWh. For DTP to be competitive, the LCOE should approach the average (3-6 €ct/kWh) with 10 €ct/kWh as the upper limit.

	€ cents / kWh		
Energy source	5%	Average	95%
Solar	2.4	4.1	10.1
Onshore wind	1.7	2.8	5.3
Offshore wind	4.4	6.3	10.7
Hydro power	2.4	4.1	11.0
Fossil fuel	4.4	-	11.8

Table 2.5: Energy sources levelised cost of electricity (LCOE) comparison in € cents / kWh in the year 2021. Derived from IRENA, 2022, converted from Dollar to Euro. See figure G.2 for detailed information.

2.6. Feasibility analysis on DTP

A feasibility analysis investigates how a project can be completed and what factors affect the feasibility. Generally, five main categories can be classified to assess the feasibility of a project (TELOS); technical, economic, legal, operational and scheduling feasibility (Mukherjee & Roy, 2017), (Bause et al., 2014), (Hall, 2010), (Burch, 1992). However, assessing the feasibility differs greatly between different sectors or fields (McLeod, 2021). According to Matinmikko et al., 2022, the classic feasibility study (FS) framework should be expanded towards a sustainable feasibility study (SFS) in some cases to consider the investment projects' feasibility beyond the economic perspective. If a project is socially and ecologically feasible, it is more likely to be widely accepted and supported by society and environmental organizations. Since a DTP dam is a project on an immense scale, it is essential to perform an SFS and include social and ecological aspects. This can reduce the likelihood of legal challenges or regulatory obstacles, thus improving the project's legal feasibility. The main feasibility categories identified in literature are stated in table 2.6.

Exclusion of categories

Since DTP depends on a large variety of parameters, the scope of the feasibility analysis has to be restricted to a manageable amount. Therefore, some feasibilities will not be included in the thesis. The included feasibility aspects will be described and assessed in more detail in chapter 4.

Operational, scheduling and delivering feasibilities

The feasibilities that describe the capability of an organization to manage a project, such as the operational, scheduling and delivering feasibilities, are considered internal feasibility categories (McLeod, 2021). Since this report will assess the feasibility and application of DTP in a general context, no internal project management constraints are assessed. Therefore these three feasibilities are excluded from the thesis.

Legal feasibility

Additionally, the legal feasibility is not included in this research. Although the legal feasibility is highly

relevant to the feasibility of DTP, it is country-specific and, therefore, not suitable for assessment on a global scale. However, all protected areas currently acknowledged by the United Nations (UN) are taken into account in the spatial analysis.

Feasibility categories		Description	Inclusion in thesis
General	Technical	The technology readiness, constructability, operability	Yes
	economic	Profit, expenditures, market competitiveness and magnitude of investment	Yes
	Environmental	Assess the sustainability, perform EIA	Yes
	Societal	Assess impact on society and support	Yes
	Legal	Whether it conflicts with legal requirements	No
Capability	Operational	What operational risks are present and how will the project be executed?	No
	Scheduling	Estimating & scheduling if project is finished in time	No
	Delivering	Is the organization or company able to deliver the project?	No
	Maintenance	The management, capabilities and costs of performing maintenance	No

Table 2.6: Feasibility categories, brief description and their inclusion in the study. Included feasibilities will be assessed in more detail in the feasibility analysis (chapter 4).

2.7. Linkage opportunities

An important aspect of the feasibility of DTP is the use of linkage opportunities. The high investment costs can be partly substantiated by the use of linkage opportunities, which could give additional economic or societal benefits. Several possibilities are stated in table 2.7, including a small description.

One interesting linkage opportunity is the use of the natural coastline or islands (see figure 2.10. This offers the potential to connect the island and mainland by building a bridge and a DTP dam at once. High energy production can be achieved while reducing the dam length (and thus dam costs), and, at the same time, the bridge can give additional economic and social improvements for the island.

Another option is to integrate the dam with other renewable energy sources, for instance, by placing wind turbines or solar panels on the dam. Additionally, the dam can facilitate space for offshore wind park maintenance facilities or a hydrogen hub. The energy generated can then be transmitted to the mainland through hydrogen pipelines.

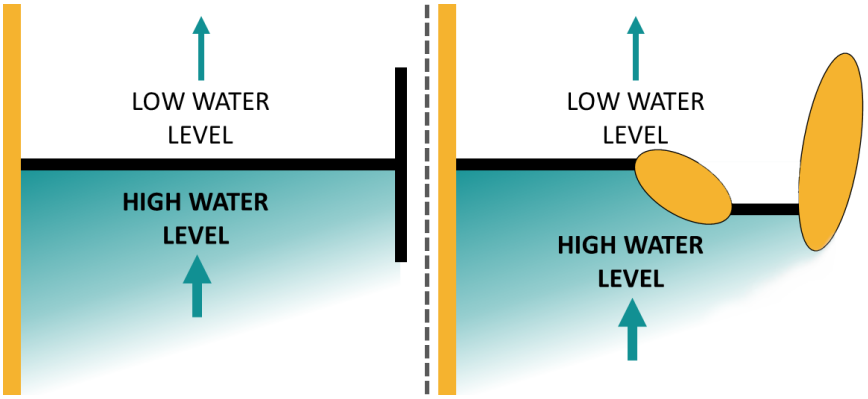

Figure 2.10: DTP options: T-bar (left) and usage of the natural coastline and islands (right)

Category	Opportunity		Description
Infrastructure	Bridge / road		Can function as a bridge towards an island, which increases economic and societal aspects.
	Pipelines		Pipelines can go through the DTP dam, less costly than a new system on the seabed.
	Electricity cables		An island or windmill park can be connected to the mainland by using electricity cables in the DTP dam.
Expansions and Facilities	Energy storage	Pump storage station	The possible Y bar of the DTP dam can also function as a Valmeer. Water will fall into the artificial lake to generate energy by turbines when the windmills produce no energy. Water will be pumped out of the lake when there is an energy surplus by the windmills. This absorbs energy fluctuations on the energy net.
		Batteries	Batteries can be installed in the DTP dam, to absorb fluctuations in energy from DTP and windmills.
		Hydrogen hub	A hydrogen plant including storage facilities can be constructed, to produce hydrogen with DTP and wind energy and transfer this hydrogen through pipelines across the dam towards the mainland. The hydrogen can also be used and transported by ships, if a harbour facility is combined.
	Harbour facilities		The dam will be built in larger depths than at the coastline. If the dam is combined with harbour facilities, there can be an expansion for bigger vessels. This can be combined with opportunities stated earlier, for instance, different energy hubs. The increased flow velocities are an uncertain factor, these should be studied in more detail.
	Wind-park maintenance rooms		If a wind-park is located nearby, maintenance parts and personnel facilities can be placed inside the dam.
	Tourism		It can attract tourists by facilitating restaurants, hotels, dive schools and other tourism attractions. Especially the diving can be interesting, because the dam will probably stimulate the (underwater) biodiversity (provides shelter for many species).
	Airport		Airport (expansions) could be constructed in sea, because this gives less local disturbance in terms of noise and pollution compared to more densely populated areas.
Other	Sand trapping mechanism		The DTP dam could be placed in an angle, using the natural currents to trap sediment at the base of the DTP dam. This could possible also transport sediment from deep water into shallow water, which can be used for coastal reinforcements. Please note, this isn't scientifically proven to work but only a hypothesis.
	Coastal protection		In some cases the DTP dam could block incoming storm waves. This idea needs further research.
	Desalination of water		Area's where little natural fresh water is present could benefit from a DTP dam by combining it with a water desalination plant, to have fresh water for basic needs, agriculture, etc.

Table 2.7: Linkage opportunities

3

Methodology

The methodology to answer the research questions is shown in the flow chart in figure 3.1, which comprises the following steps:

Step **1:** The aspects that influence the feasibility of DTP are assessed and described.

Step **2:** The main feasibility criteria are determined based on the feasibility aspects.

Step **3:** The influence and thresholds of the criteria are investigated using the simplified hydraulic model.

Step **4:** Locations are identified based on the criteria and their importance using the spatial model.

Step **5:** The spatial analysis results are analysed on a global and more detailed regional scale.

The research involves a broad view, where first, the DTP concept is assessed schematically using a simplified hydraulic model and then globally using a spatial analysis. Locations with a high potential to apply DTP will be assessed on a regional scale, where additional secondary criteria and linkage opportunities are considered as well.

Figure 3.1 shows a scheme of the research method. The research method is divided and summarised into three phases. The structure of the report is based on this sequence of steps.

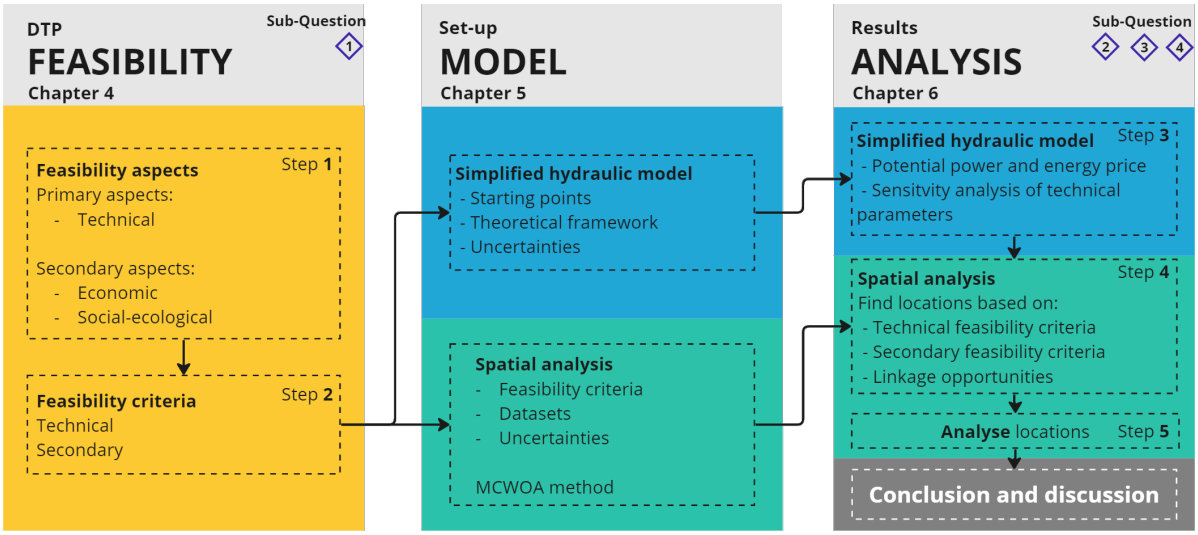

Figure 3.1: Methodology: Research phases and sequence of steps

3.1. Research tools: Model overview

Two models are created; a simplified hydraulic model and a spatial model. The simplified hydraulic model determines the influence and thresholds of the (hydraulic) conditions, answering research question 2. The spatial model uses a Multi Criteria Weighted Overlay Analysis (MCWOA) method to assess the potential of DTP for each area globally. The MCWOA method includes combining several datasets (criteria) and applying weighting factors to these criteria to create an overlay map that shows the potential of DTP in that area (Potential Index).

Figure 3.2 shows the connection between the two models and the process for each model to come to the conclusions of this research. Elaboration on specific components in figure 3.2 can be found in the related chapters.

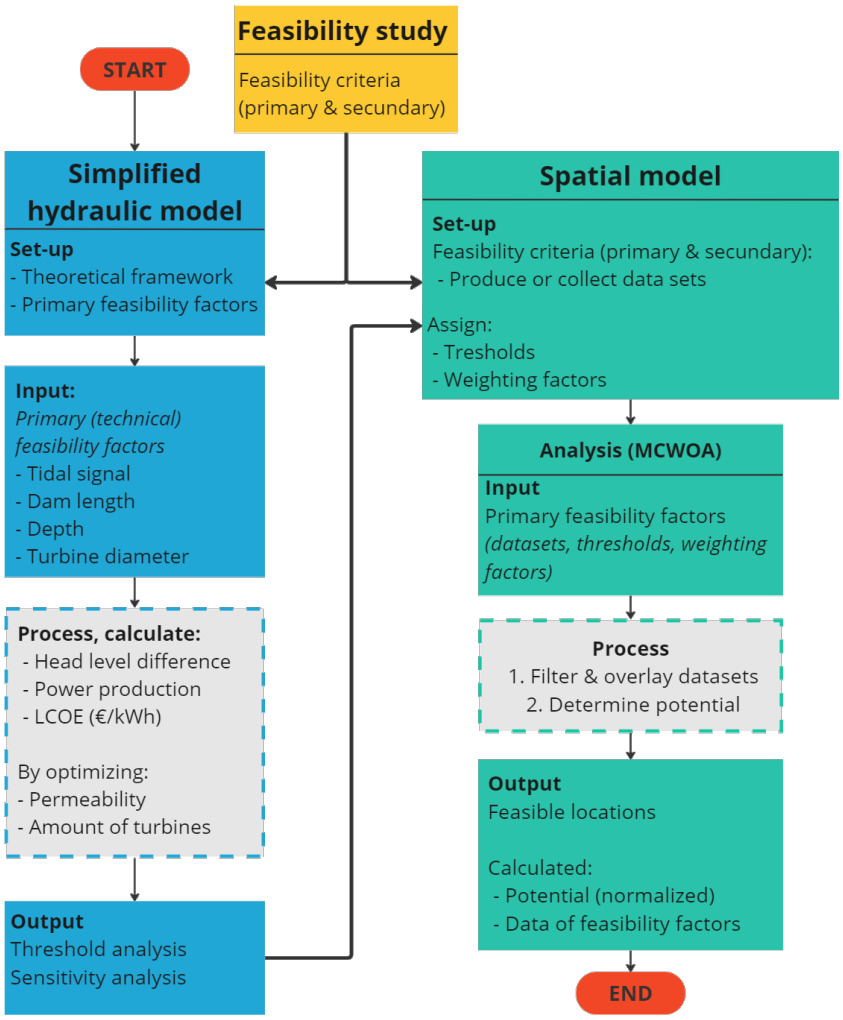

Figure 3.2: Overview of the processes concerning the simplified hydraulic model and the spatial model

Simplified hydraulic model

The simplified hydraulic model will estimate the induced hydraulic head level difference and the corresponding power generation. This model will help assess the effect of technical criteria by performing a threshold and sensitivity analysis. Additionally, it evaluates the power output for specific locations once these are identified.

Set up

The theoretical framework assessed in chapter 2 will be used as a basis to set up the simplified hydraulic model. Additionally, the technical feasibility criteria found in the feasibility chapter 4 will be included.

Process
The maximum induced head level difference and corresponding power production are determined by optimizing the permeability and, thus, the number of turbines. Additionally, it derives the estimated construction costs of the structure so that the LCOE (€/kWh) can be derived.

Output
First, a threshold analysis is conducted, where the feasibility thresholds are approximated for the main input parameters. To do this, the estimated LCOE is compared to the rate of other renewable energy sources, such as solar and wind energy, see chapter 2.5.3. Furthermore, a sensitivity analysis is conducted, where the influence of the main input parameters on the power output is investigated. The thresholds and weighting factors derived from these two analyses will be included in the spatial analysis.

Technical details
The programming language ”python” will be used for the simplified hydraulic model since this is a freely available programming language with many useful functions.

Spatial model
The spatial model identifies feasible locations and regions to apply DTP. Additionally, linkage opportunities will be taken into account.

To perform the spatial analysis, a Multi Criteria Weighted Overlay Analysis (MCWOA) is performed. This method calculates a Potential Index (PI) that ranks each grid cell for its potential to apply DTP (Vu et al., 2019), (Mourão et al., 2014), (Wu et al., 2017). This is done by combining various datasets and weighting factors. It permits for an integrated analysis of objectives (Malczewski, 1996, Malczewski and Jackson, 2000, Braga and Ribeiro, 2006). One benefit of this method is its flexibility. The spatial model can use various input parameters based on the user’s preference and find potentially suitable areas for those weighting and threshold criteria.

Set up
The findings obtained from the feasibility study (chapter 4) will be used to set up the spatial analysis. First, a dataset will be found that spatially represents each feasibility criterion (if possible). For the technical feasibility criteria, these thresholds and weighting factors are derived from the simplified hydraulic model. The secondary feasibility criteria use thresholds and criteria derived from the feasibility chapter.

Process

1. Align and standardize datasets to a common reference system.
2. Filter datasets based on the threshold criteria.
3. Determine the potential for each grid cell by combining the normalized criteria with their respective weighting factor.

Output
The spatial model provides spatial data of locations that comply with the thresholds defined earlier. Additionally, the locations are sorted from highest to lowest potential, and a regional analysis can be performed to identify if the model results are realistic. The marked locations with linkage opportunities can be analysed in more detail since these provide additional opportunities.

Technical details
The geographic information system (GIS) application ”QGIS” will be used to conduct the spatial analysis since it offers various functions and is freely available. This choice enables flexible adjustment and expansion of the model for future research (or practical) purposes. Moreover, since QGIS is built on the Python programming language, it will be simpler to directly integrate the schematized hydraulic model into the spatial model in the future (“QGIS Geographic Information System”, n.d.).

3.2. Research limitations

The research employs a wide perspective; the feasibility aspects are assessed broadly, a global spatial analysis will be performed, and a simplified hydraulic model will be used. Consequently, the research is subject to numerous limitations. The main limitations are stated below. These should be kept in mind prior to, during and after the study.

- The DTP concept has not been tested in the real world. To date, it has only been verified through theoretical and numerical models or analytical solutions. More study on the validation of the concept should be conducted.
- The feasibility study in chapter 4 gives a first indication of the important criteria, but it does not involve all aspects or all details. Further studies should be conducted, especially location-specific case studies and the feasibility of DTP at that specific location. Locations identified in this study could be a starting point for future feasibility studies.
- The hydraulic model gives a rough estimate of the power output using analytical equations. This simplified approach can serve as a preliminary indicator of the expected power output and assess the influence of certain parameters, such as the tidal current signal, depth, dam length, number of turbines and others. While it is suitable to test the potential to apply DTP in an area, it is unsuitable for a detailed case study.
- Since the potential of DTP is assessed on a global scale, a general design is used with corresponding simplified costs. The costs were estimated using a Standardized Costs determination method (SSK) approach, including only construction costs. However, the cost estimates are still subject to a high degree of uncertainty since the final costs are location dependent. Material prices, transportation methods and distances, labour costs, design differences and other factors all influence the final costs of a project. Therefore, the cost estimates should only be used to compare locations generally and provide an estimate of the minimum costs in euro for the reference year 2023.
- The study will use freely available datasets (see tables 5.2 and 5.3). Many factors influence the feasibility, not all can be taken into account by datasets. Consequently, the identified locations should be considered as a preliminary indication of potentially suitable locations, detailed manual assessment will always be required.

4

Feasibility criteria

To assess the feasibility of Dynamic Tidal Power, the main aspects that influence the feasibility of a DTP dam project are identified and briefly described (chapter 4.1) while using the feasibility categories derived in chapter 2.6. Subsequently, the most relevant aspects are simplified into criteria that will be used in the hydraulic model and the spatial analysis (chapter 4.2). Furthermore, this chapter provides more detailed information and assumptions on these criteria to support further chapters in the report, such as the set-up of both models.

4.1. Feasibility aspects

A feasibility study (FS) framework should be adjusted to the subject. As described in chapter 2.6, in the case of DTP, the FS should be extended to a sustainable feasibility study (SFS) to consider the feasibility beyond the economic perspective. Therefore the technical, economic, societal and ecological feasibilities are assessed. See figure 4.1 for a scheme including the main categories and their relation to a DTP project. Below figure 4.1, each feasibility aspect is briefly elaborated.

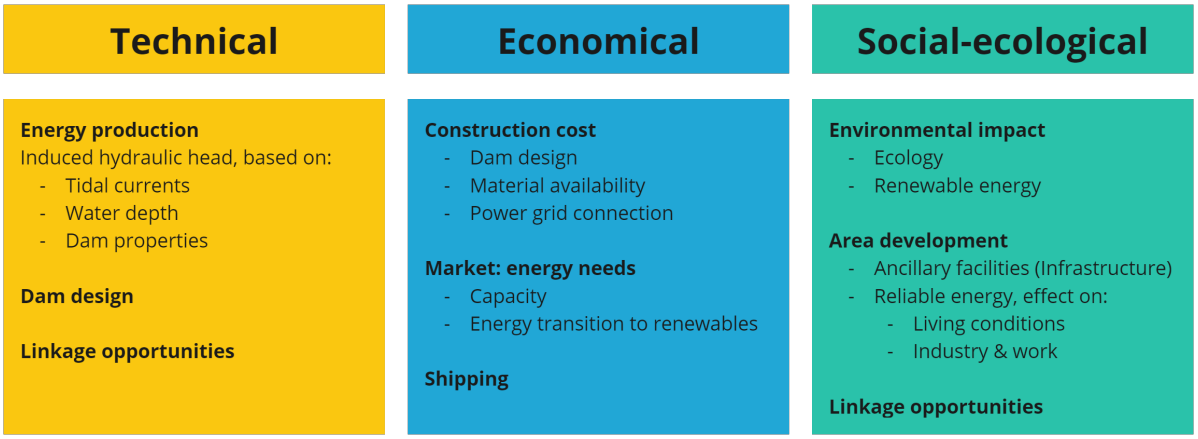

Figure 4.1: Feasibility aspects, based on SFS framework derived in chapter 2.6

4.1.1. Technical aspects

Energy production

The main goal of a DTP dam is to harvest reliable and renewable energy. As described in chapter 2, the energy potential depends on several area properties such as the natural tidal current speed, the water depth and the dam's design. To recap, a location with stronger natural tidal currents can achieve a larger hydraulic head level difference since higher turbine flow speeds can be achieved (more power per turbine) and more turbines installed, increasing the total power output of the DTP

dam. Additionally, a deeper water depth in the area is beneficial for the energy potential because deeper water corresponds to a larger water-mass blockage by the dam. A larger water-mass blockage increases the total momentum and water volume, which results in a larger power output.

Inclusion of tidal currents and water depth in study
The tidal currents and water depth are essential aspects that influence the technical feasibility. Therefore these are investigated in the schematized hydraulic model and included in the spatial analysis.

Dam design
Dam design and power output
The dam design influences power production in multiple ways. The dam length influences the maximum hydraulic head and the initial construction costs. The turbine type, diameter and number of turbines influence the power production and construction, installation and maintenance costs. Additionally, the dam design influences the dam permeability. For example, a floating design results in lower water blockage (resulting in a lower hydraulic head) but also reduces construction costs in deeper areas.

Construction costs
The dam design determines the construction costs. Two main dam categories can be distinguished; Rubble mound breakwaters (made out of loose stones) and monolithic breakwaters (caisson with or without rock foundation) (CIRIA, 2007). The choice of breakwater type mainly depends on the site-specific properties, such as the depth, subsoil material, hydraulic boundary conditions, possible nature disasters (seismic activity, tsunamis) and other aspects. Additionally, factors such as the availability of construction materials and labour prices play an essential role in the design costs. To conclude, the optimal dam design is different for each location.

Inclusion of dam design in study
The dam design is important for the energy production and technical feasibility of DTP, but the design is location dependent. Since this study covers a global feasibility study, making a detailed design for each location is unrealistic. Therefore, a simple and general caisson design is created that is generally representative; see chapter 4.3.1. This design is included in the schematized hydraulic model, and the influence of certain design choices is investigated (i.e. the turbine diameter, number of turbines and depth). Thus, the dam design is not included directly in the spatial analysis but indirectly influences the spatial analysis since it is included in the hydraulic model.

4.1.2. Economic aspects
Construction costs
Various factors influence the dam's construction costs, such as the design, resource availability, and power grid connectivity.

Resource availability
A significant cost factor is the availability of resources, which is also highly location dependent. When designing a DTP dam, it is essential to consider various materials and assess their availability in the area. The material costs correlate with availability and significantly impact the final construction costs. For example, if rocks are broadly available, including large rock volumes in the dam design is beneficial since their purchase value and transportation costs are relatively low. Labour availability in the area is another resource to examine. If the DTP dam is built in a remote location, the labour market may be limited, resulting in a significant increase in labour costs as workers would need to travel from distant places.

Power grid connection
The energy produced by a large dam, such as a DTP dam, can be substantial, ranging from 0.1 to several terawatt-hours (TWh) depending on the dam's size. The energy must be transmitted through a power grid to the required locations to utilize it. Two main factors are important to consider when evaluating the site's suitability for the energy grid connection (International Atomic Energy Agency, 2006):

- DTP power output compared to the grid power capacity
- Distance from the DTP plant location to the grid (the site should have adequate transmission link to the national grid)

Strengthening the grid is necessary to support the integration. The amount of strengthening needed (and thus the impact on the costs) depends on the DTP output capacity relative to the grid power capacity. Additionally, transmission lines and associated infrastructure costs can increase quickly for long distances (Yli-Hannuksela, 2011). For very long distances (>1000km), Ultra-High-Voltage Direct Current (UHVDC) transmission lines could be applied (Humpert, 2012). The construction of UHVDC transmission lines should be examined thoroughly to see if remote locations could be feasible. If the energy production outweighs the total project costs, including the electricity transmission, these remote locations could still be economically feasible.

Inclusion of construction costs in study
As described, construction costs are highly location dependent. To include the construction costs globally, a construction costs index can be used (Arcadis, 2022). This index gives an indication of the construction costs of 100 cities all over the world, compared with the costs in Amsterdam. Since this index is derived using actual construction costs of buildings, the material costs, labour prices, energy prices, inflation, finance costs and other aspects are all included. However, please note that a DTP dam project differs greatly from a standard building project in a city (for example, different building materials and equipment are used). Moreover, a DTP dam is likely to be constructed at a location with limited access (far from a city). The resource availability in a remote area and the power grid costs (strengthening and constructing new grid lines) are not included in the construction costs index. Additionally, locations where construction costs are relatively low generally correspond to locations where energy prices are low as well. This means that the generated energy can be sold with less profit, weighing out the profits against the costs. Therefore, this index can be used as an indication to compare locations, taking the limitations into consideration.

Energy market
The energy market is determined by the principles of supply and demand; see chapter 2.4.2. Three main factors will be addressed; the existing and future energy capacity, the energy price and the transition to renewable energy sources.

Capacity
To gain profit, sufficient energy demand in the area is crucial to selling all produced electricity. To help identify whether an area is suitable in terms of energy needs, a simple decision tree is presented in figure 4.2. This decision tree is based on the state of the energy capacity in an area.

Step **1:** If there are adequate resources on the grid to ensure that the electricity demand is met at all times, the capacity suffices. If the capacity is insufficient, DTP could be a solution to increase the energy capacity in that area.

Step **2:** If the energy capacity currently suffices, the future demand should be approximated. Many factors play an important role, such as population density; energy usage per person; area development (attraction or expansion of industries) and other factors. For example, if the population density is high and the energy usage per person is low, one could argue that with increasing economic development in the area, the energy usage per person will increase, increasing the total energy demand in the area. Additionally, the increase in energy capacity in the area due to a new DTP dam could attract new industries so that DTP could increase economic development in the area. Thus, building a DTP dam could be profitable, even if the energy capacity is sufficient today.

Step **3:** Replacing fossil fuels power plants with renewable energy helps achieve the UN SDG goals 7 and 13. DTP has the benefit of being a predictable energy source. Therefore, it is possible to use this source as a reliable base load of the energy grid, replacing baseload power plants (see chapter 2.4.1). Additionally, if renewable energy sources such as solar and wind are widely available, the capacity could still be insufficient since the energy production of these sources variates highly over time. Therefore, DTP would be a beneficial addition to these areas as well.

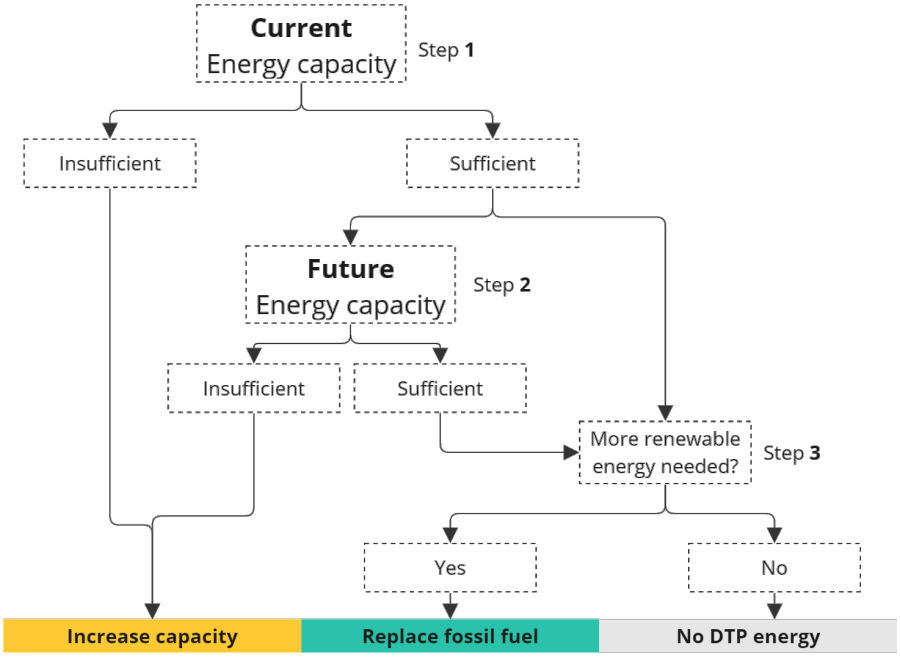

Figure 4.2: Energy need market analysis

Energy market prices - LCOE
For DTP to be competitive with other energy sources, the energy price should be in the same price range. Table 2.5 shows the global LCOE per energy source for the year 2021. DTP should approach an average of 3-6 €ct/kWh, with 10 €ct/kWh as the upper limit to be economically competitive with other energy sources.

Transition to renewable energy: replace fossil fuels
The energy transition from traditional fossil fuels to renewable energy sources is essential to include in the market analysis (step 3 from figure 4.2). As described in chapter 2.4.1, fossil fuels comprise the largest portion of the energy mix. Renewable energy sources such as wind and solar highly variate in terms of power output (dependent on wind or sun availability). Because tidal energy is predictable, it could be a stable base load on the energy grid, replacing existing base load power plants, see chapter 2.4.2. Therefore when analysing the feasibility of DTP in the energy market, the possibility of replacing baseload power plants with a DTP dam should also be analysed.

Inclusion of energy market in study
The current energy capacity of an area is taken into account in the spatial model by using population size and energy usage per person, excluding locations that have insufficient energy consumption (but including future potentially interesting locations). The discussed transition to renewable energy, replacing fossil fuel power plants, is included in the last steps of the spatial analysis by manually evaluating the possibilities to replace base-load power plants at the potential locations found.

Shipping
The blockage of a DTP dam could also block existing shipping lanes, forcing vessels to sail around the DTP dam. Elongating these shipping routes may increase sailing time and fuel usage, thus having a negative economic impact and increasing pollution of emissions in the atmosphere.

Contrarily, shipping could retrieve an economic boost in several ways. First, if a port is situated close by, the energy generated by the DTP dam could stimulate industries and provide additional power to port activities, allowing for port expansion. Second, the DTP dam could be used to facilitate the port expansion. Normally costly port expansions are needed to facilitate larger vessels with significant draught. The depth around the DTP dam is likely significantly deep to facilitate these vessels. Using this linkage opportunity, shipping can be more efficient, the industry stimulated, and renewable energy extracted. Additional research on these opportunities is required.

Inclusion of shipping in study
The blockage of existing shipping lines could have a significant negative effect on the economy of an area. Therefore, the shipping lanes are an important feasibility criterion. A shipping density dataset is used, describing the shipping intensity and, thus, includes the shipping lanes. Using this dataset, the potential for locations located near high-intensity shipping lanes can be decreased.

4.1.3. Social-ecological aspects

Environmental impact
Comprehensive research on the (long-term) environmental impact of a DTP dam is needed. Because of the blockage of a large stretch of water perpendicular to the coastline, it is expected that a DTP dam actively changes hydrological current patterns and the tidal range. This also influences sediment transport patterns, changing the bathymetry and coastal system. However, because DTP does not contain water, it is expected that this reduces environmental problems when compared to the traditional tidal barrage method (Park, 2018). To get a prediction of the hydrodynamic and morphodynamic evolution, an extensive model study could be performed (e.g. (Luijendijk et al., 2017)). Additionally, the impact of the hydrodynamic and morphodynamic evolution on the environment and ecology is unknown. Berlee et al., n.d. explored the ecological effects and socio-economic opportunities for a DTP dam in the North Sea. The main conclusions of this research are stated below:

- A DTP dam disconnected from the coastline has a relatively smaller impact on coastal protection and biodiversity than a DTP dam with a shoreline connection.
- Impact on migratory fish is small (except for bigger species like whales) since the turbines are designed to be fish-friendly.
- A shelter and nursery habitat could be created for a wide range of species, further enhancing biodiversity.
- The dam could be a resting place or breeding ground for migratory birds.
- DTP-dam could enhance biodiversity, creating a spillover effect beneficial for fisheries
- Considering aquaculture; oysters and mussels are economically viable species

Berlee et al., n.d. concludes that the ecological impact of the DTP-dam will be minimal, whilst the potential for improving ecosystem health in the surroundings is high. Although this conclusion is positive concerning the ecological effects of a DTP dam, no other research is available to validate this conclusion.

Inclusion of ecological effects in study
The ecological effects of a DTP dam on its environment are largely unknown and different for each location. Since this study will assess the feasibility on a global scale, the exact impacts of a DTP dam on the environment will not be assessed in detail. However, protected areas will be included in the spatial model as an optional model constraint, using a comprehensive global database of marine and terrestrial protected areas (UNEP-WCMC & IUCN, 2023). Other ecological factors are considered out of the scope of this research.

Area development
The construction of a new power plant affects an area's economic and social development. Affordable and reliable energy increases the productivity of businesses (Abeberese, 2017), (Allcott et al., 2016) (Andersen & Dalgaard, 2013). Furthermore, it leads to an increase in employment (Dinkelman, 2011) and reduces poverty in the long run (Lenz et al., 2017). Thus, if a new power plant induces affordable and reliable energy, this could result in positive economic and social effects. Additionally, these economic and social effects are not only due to the provision of electricity but also due to the following influences (Montrone et al., 2022):

- The infrastructure spillovers related to constructing a new power plant.
- The electricity grid expansion
- Agglomeration economies arise from new industries located around new sites.

The paper of Montrone et al., 2022 found different effects between power plant types. For a coal power plant with 100 MW power capacity, an increase of 0.2% in the 6 years after it becomes operational was found. For a hydro-power plant, an increase in GDP is found before operations start due to the construction. See figure G.3 for more details on the relationship between different power capacities and the GDP per capita.

Comparing a DTP power dam with the types above, it is most comparable to a hydro-power plant. They both provide reliable and clean energy, involve large construction sites and mobilize a large amount of construction-related labour. This construction may attract investments and workers in remote regions (de Faria et al., 2017).

Inclusion of area development in study
Although the effect of constructing a new power plant on the area's development is an important factor, it will not be included further in this research. This is because the effects are complicated and hard or impossible to predict for new projects. The effect will be considered, but the spatial model or analysis will not include the impact on area development.

Linkage opportunities
As described in chapter 2.7, linkage opportunities could add additional benefits or profits. However, since linkage opportunities differ greatly for each location, inclusion in the spatial analysis is challenging. Table 4.1 states all linkage opportunities described in chapter 2.7 and the inclusion of these opportunities in this study.

Category	Opportunity		Further inclusion in study
Infrastructure	Bridge / road		Yes, Hydraulic & spatial model
	Pipelines		No
	Electricity cables		No
Expansions and facilities	Energy storage	Pump storage station	No
		Batteries	No
		Hydrogen hub	No
	Harbour facilities		Yes, spatial analysis
	Wind-park maintenance rooms		No
	Tourism		No
	Airport		No
Other	Sand trapping mechanism		No
	Coastal protection		No
	Desalination of water		No

Table 4.1: Inclusion in this study of linkage opportunities described in chapter 2.7.

4.2. Decision criteria

Table 4.2 shows an overview of the feasibility aspects described in the previous chapter 4.1 and how these are translated to criteria. Their inclusion in the study (hydraulic model, spatial model and/or spatial analysis) can be found.

Not all aspects are included in further analyses. A distinction is made based on their relevance, uncertainties and available datasets. Therefore some criteria, such as resource availability, power grid connection and social impact, are not included further in this study. Other criteria, such as the dam design parameters, are included in the hydraulic model to assess other criteria but are not included in the spatial analysis. Lastly, some criteria are not included in the spatial model but are addressed during the manual assessment of the spatial analysis once regions with high potential are found.

				Included in:		
Category	**Aspects**	**Criteria**	**Details**	**Hydraulic model**	**Spatial model**	**Spatial analysis**
Technical	Energy production	Tidal currents	Min. (threshold)	X	X	X
			Influence (sensitivity)	X	X	X
		Water depth	Min. & max. (threshold)	X	X	X
			Influence (sensitivity)			
	Dam design	Parameters:	Dam length	X		
			Turbines	X		
economic	Construction costs	Dam design		X		
		Resource availability		Not included		
		Power grid connection		Not included		
	Energy market	Market capacity			X	X
		Renewables: energy transition				X
	Shipping	Shipping intensity			X	X
Social-Ecological	Environmental impact	Protected areas			X	
		Renewable energy				X
	Area development	Social impact		Not included		
	Linkage opportunities	Bridge / road		X	X	X
		Harbour facilities				X

Table 4.2: Decision criteria based on the feasibility aspects of chapter 4.1, to be implemented at the spatial analysis.

4.3. Elaboration on criteria

4.3.1. Dam design

The dam design is crucial for giving more information on two decision factors; energy production and construction costs. First, a general and simple design is presented that can be applied to many regions across the globe. Then, the costs of this design are estimated as accurately as possible. The design and the corresponding costs will later be used in the hydraulic model. To include the design in the model, the design is scalable with increasing dam length, increasing number of turbines and depth.

Since no specific location is known, the design is general and simple. The purpose is to give a general idea of a possible design and to include costs in the hydraulic model. Therefore, assumptions and simplifications are made.

Dam type

Three main dam types can be distinguished; rubble mound breakwaters, caisson breakwaters and composite-type breakwaters (Tutuarima & d'Angremond, 1998). Which type is more suitable is strongly dependent on the location, the main influential factors are the depth, wave conditions and material availability. Generally, the rubble mound breakwater type is less costly in shallow water depths. When approaching deeper waters, their material volumes rises exponentially, thus also the costs. In these deeper waters caisson-type breakwaters become more suitable since these are efficient in terms of material volume. For very large depths, the composite breakwaters appear to be more cost-saving, as the increasing height of a caisson alone requires additional widths (Tutuarima & d'Angremond, 1998).

A DTP dam can be located at a depth ranging from 0 to -40 meters, but possibly even deeper. Therefore, it is difficult to determine the dam type based on depth. Since a general design is made, a type must be chosen that is feasible for the majority of depths. Additionally, the dam needs to facilitate space to install the turbines. Considering these two requirements, the caisson type is the most advantageous, as this can be applied in the majority of depths, and the caissons can be constructed to fit exactly the dimensions of the turbines.

Since not the entire span of the dam is required for the placement of turbines, the use of different breakwater types could be beneficial to reduce construction costs. The rubble mound breakwater type can be used in shallow water areas (depth < 10m), and the composite type for deeper water (depth > 40m). In the current design only the caisson type breakwater is considered for simplicity. However, it is advisable to investigate the use of other breakwater types in a detailed case-specific design, if the water depth differs across the dam length. For example at depths smaller than 10 meters, the ruble mound breakwater type can be applied to reduce construction costs. For this general design, the caisson type spans the full dam length.

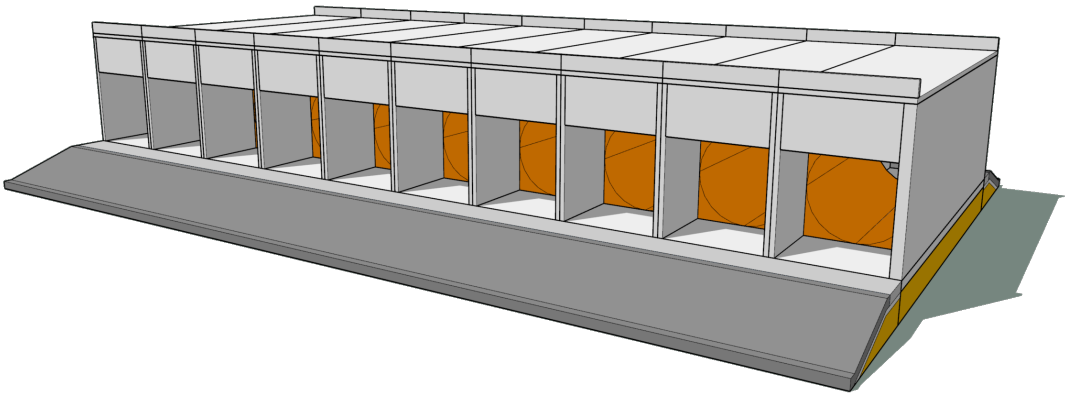

Figure 4.3: 3D illustration of the DTP dam design using caissons

Turbines
First, the turbine type and dimensions are considered, then these dimensions are included in the caisson design. The turbines should comply with the following conditions:

- *Bi-directional:* Since the high and low water level sides of the dam will change over time (every 6 hours in case of a semi-diurnal tidal signal), bi-directional tidal turbines are required.
- *Fish-friendly:* The blockage of a DTP dam could block fish migration routes (Berlee et al., n.d.). Therefore, the turbines should allow fish to pass, reducing the ecological impact of the dam.
- *High efficiency* at both low and high water velocities.
- *Low maintenance* effort and costs.

The Free Flow Turbine of Fishflow innovations (Fishflow innovations, n.d.) complies with both conditions due to its large and slow-rotating rotor, which is designed to be fish friendly while maintaining high efficiency. A rotor diameter of 8 meters is used in the design. The turbine uses spoilers that converge the flow towards the rotor, which results in an inlet diameter of 10 meters.

Longitudinal distribution of turbines
The longitudinal profile of the hydraulic head (chapter 2.3.1) should be considered when designing the placement of turbines. The distribution of turbines along the dam should be well-designed to efficiently harness the hydraulic head difference everywhere. This means that the turbines should have sufficient spacing from each other individually, and the highest density of turbines should be positioned where the hydraulic head is greatest. In most cases, this is the attachment point to the coast.

Turbines placement height
Two main factors influence the placement height of the turbines:

1. Turbines should be fully submerged on the high-tide level side of the dam since then the full flow area of the turbine is used. This results in maximum torque and, thus, maximum power to the turbine.
2. The turbines should be placed low enough to have limited wave action. Wave action induces flow fluctuations, giving unsteady flow conditions, which could induce vibrations and material fatigue issues (X. Liu et al., 2016).

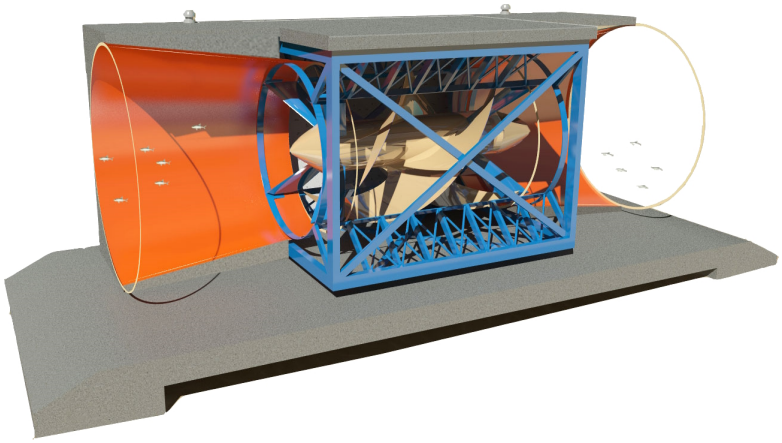

Figure 4.4: The Free Flow Turbine of Fishflow innovations (Fishflow innovations, n.d.).

Considering the second factor, many aspects influence the final design. From linear wave theory, it is known that the wave action reaches a depth equal to half the wavelength (Bosboom & Stive, 2021). However, the wave action does not have to be dissipated fully, but enough to mitigate possible damages. This also depends on the strength of the turbine components and the wave load the turbine can bear. Considering that the wavelength, wave action and specific turbine strength properties are not known at this stage, there are too many unknowns to accurately calculate the turbine depth requirement. Therefore, the wave action factor will not be taken into account in the initial design, but the turbines will be positioned to be always submerged (also under wave conditions). Please keep in mind that in a detailed design, the wave effect has to be studied and the turbine position adjusted accordingly.

Caisson dimensions
First, the required height, width and length of the caisson design are determined. The height is the difference between the Top of Structure (ToS) and the Bottom of Structure (BoS). The BoS depends on the bottom depth and will thus be scalable in the design. The ToS is dependent on the minimum required turbine height (10 m) and the following hydraulic boundary conditions: (Voorendt et al., 2011)

Hydraulic boundary conditions

- Astronomical tide
  Since the tidal range is not known, some range has to be assumed. According to Hulsbergen et al., 2008, DTP could initiate a tidal range of 6m. Therefore a conservative large tidal range of 6m is assumed, which corresponds to a tidal amplitude of 3m.
- (Wind) wave height
  To determine the wave height, an analysis of the global wave heights versus depth is performed. For this analysis, a significant wave height dataset is used that is based on historical satellite measurements in the period of September 2009 to December 2019 (Noveltis et al., 2019). From this dataset, the maximum significant wave height is derived for each grid cell and plotted against the depth using a global bathymetry database (Group, 2022). The result of this analysis is shown in figure 4.5, where it can be seen that for depths in the range of -40 to 0, the bandwidth between the upper and lower quartiles lies between 4.8m and 2.3m. At a depth of -20 meters, the median wave height is 3 meters. Therefore for simplicity, a design wave height of 3 meters will be taken into account. Since it concerns a general design without a known specific location, this general approach suffices in the current design phase.
- Wind set-up
- Refraction, shoaling, breaking, reflection and diffraction of wind waves
- Overtopping

No roads or facilities are built on the dam in this general design, eliminating the need to consider overtopping. However, the height of the dam should be sufficient to contain the water level difference;

therefore, the astronomical tide and the wind wave height are taken into account. The other phenomena are neglected in this design stage since they are location-specific. Additionally, since the basic design does not include a road or other facilities on the dam, overtopping is not taken into account in detail.

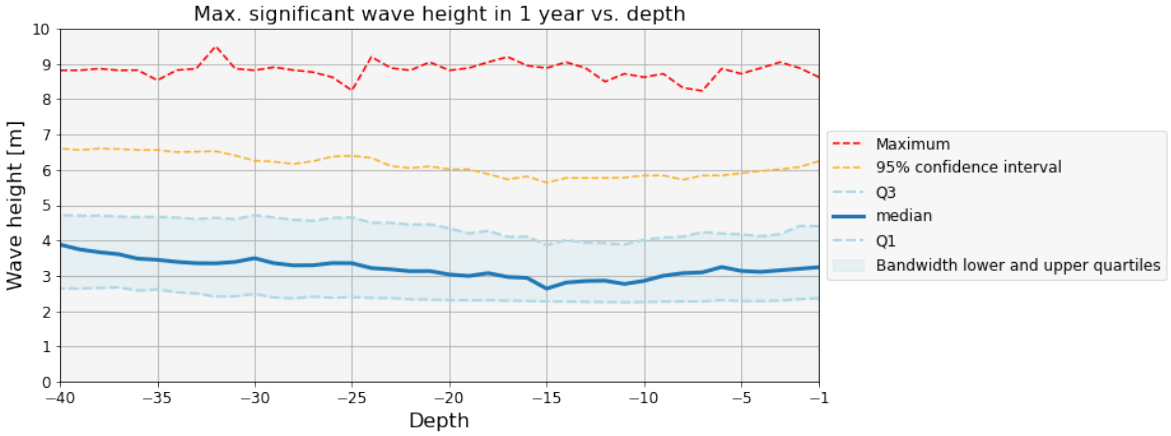

Figure 4.5: Global analysis of the maximum significant wave height occurring in the period of September 2009 to December 2019 plotted against the depth, using databases of (Noveltis et al., 2019) and (Group, 2022).

Caisson height

The hydraulic boundary conditions determine the minimum ToS. The ToS must be set at a sufficient height to accommodate the Highest Astronomical Tide (HAT) of +3 meters and a wave amplitude of +1.5 meters. Additionally, a small crown wall with a height of 1 meter is constructed to block small overtopping water volumes. For simplicity, the wall thickness is set to 1 meter for all outer walls. Therefore, the ToS is established at an elevation of +5.5 meters above Mean Sea Level (MSL). If desired, these parameters can be adjusted based on the assessed location. In this study these values are used for all hydraulic model results.

The BoS needs to be situated low enough to provide the necessary clearance for the turbine. The turbine should be submerged beneath the waves to minimize wave impact. Hence, the top of the turbine is positioned at a minimum of -4.5 meters below MSL (below the lowest astronomical tide (LAT) and the waves with an amplitude of 1.5m). The turbine height is 10 meters; therefore, the BoS is located -14.5 meters below MSL. If the depth increases, the design will be scaled, and the volume of concrete will scale with the depth accordingly. Figure 4.6a shows the cross-section of the caisson design, including dimensions and water levels.

Caisson width, length and wall thickness

Width

The caisson needs to accommodate the turbines. The Free Flow Turbine of Fishflow innovations (Fishflow innovations, n.d.) is about 26 meters long. Accounting for the turbine spoiler inlets and outlets with a 1:7 angle, 7 meters is added at both sides. This results in a total width of 40 meters.

The width also determines the strength and stiffness of the caisson and the float conditions during transport (weight = buoyance force, influences draught). Since no specific location is known, there are no draught requirements. Concerning the strength and stiffness, a wall thicknesses of 0.50 m and a bottom plate thickness of 1.00 m have proven to be reasonable start values (Voorendt et al., 2011). However, the design needs to be applicable for larger depths, thus to be conservative, a wall thickness of 1 m will be applied.

Length

Concerning the strength, a rule of thumb is to apply a length-height ratio of 1:2 (Voorendt et al., 2011) for caissons without internal walls. However, since this design has internal walls in between the turbine compartments, the length can be increased. Increasing the length is beneficial in terms of costs and reduces immersion risk (since fewer immersions are needed). Regarding navigation of the caisson, a rule of thumb is to use a minimum width-length ratio of 1:3. Applying this, the length could be approximately 120 meters.

Since the turbine in- and outlets have a width of 10 meters and the walls in between the compartments a width of 1 meter, caissons of 111 meters can be constructed that facilitate space for 10 turbines. This complies with the earlier-mentioned requirements.

A 3D illustration of the final design is shown in figure 4.3. The final caisson dimensions are shown in figure 4.6.

Bed protection
Concerning the foundation and bed protection, the caissons are positioned on the quarry run to provide stability. Higher flow velocities occur at the in- and outlet locations of the turbines, where concrete blocks are applied. The quarry run is protected by an armour layer of 3-6 T and a filter layer of 300 - 1000kg. The designed armour layer thickness is 2.4 m, and the filter layer thickness is 1.3 m, corresponding to the guidelines of the rock manual (CIRIA, 2007).

To mitigate scour and eventually possible undermining of the foundation, extensive bottom protection needs to be applied, which is not shown in figure 4.6a. For comparison, the Eastern Scheldt barrier in the Netherlands counts a total length of 500-600 meters of bed protection, including an armour layer of 6-10 T instead of the now designed 3-6 T (Witteveen+Bos, 2017), see figure I.1. However, the turbine type included in the design will induce lower flow velocities. Therefore, it is expected that smaller armour layer stones can be used and a bed protection of 400 meters will be applied on both sides, which is shorter than the 500 meters used at the Eastern Scheldt barrier.

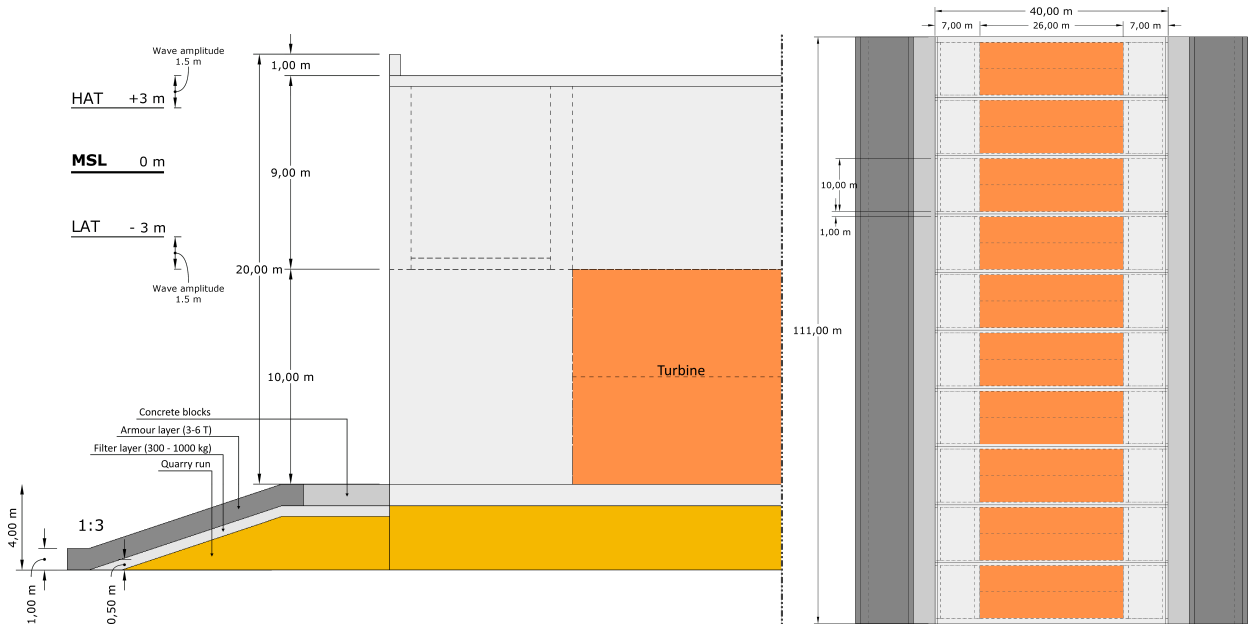

(a) Cross-section caisson design (one side), including dimensions and water levels

(b) Top view of the caisson design including dimensions

Figure 4.6: Final caisson design, suitable for water depths of 18.5 m (caisson height (14.5m) + sill height (4m))

4.3.2. Dam design costs

To be able to compare different locations with each other, the design of the dam should be linked to the corresponding costs. Please note that the cost estimates provided are based on assumptions and should not be interpreted as precise or definitive figures. Rather, these estimates are intended to serve as a comparative tool to assess the relative costs of different locations.

Caisson costs

The caisson construction costs are determined by multiplying the material volumes by a concrete volume price, see table 4.3. For simplicity, the branch and main dam are considered to have the same caisson design. Therefore, the costs for a branch or main dam part are the same (except for the installed turbines).

Concerning the concrete price, this price includes all costs related to the construction of the caisson (except for the construction dock and immersion works). Tutuarima and d'Angremond, 1998 indicated a price of 385 €/m^3 (corrected for inflation and currency rate). A DTP dam reference project indicated a concrete price of 540 €/m^3 (Tidal Bridge bv, 2020). The cost department of Witteveen+Bos reflected on these prices and suggested adding an additional 300 €/m^3 since it is reinforced concrete. The concrete price is therefore set on 800 €/m^3 to be conservative.

	Base design		**Additional height**	
Volume	173	[m^3/m]	8	[m^3/m^2]
Cost	140,000	[€/m]	6,000	[€/m^2]

Table 4.3: Caisson volumes and costs, using a concrete unit price of 800 €/m^3

Sill and bed protection costs

The sill material volumes, unit prices and costs can be found in table 4.4. The material unit prices include production, placement and transportation costs and are based on literature (Tutuarima & d'Angremond, 1998) and (DMC, 2022), corrected for inflation and currency rate. Transportation costs are assumed to be 14.4 €/t (0.19 €/t per km) for stone sizes below 300kg and 23.1 €/t (0.31 €/t per km) for stone sizes above 300kg, as found in the paper of Tutuarima and d'Angremond, 1998. A rock density of 2.5 t/m^3 is assumed to determine the prices in € / m^3. A quarry distance of 75 km is assumed, which is kept the same as in the papers of Tutuarima and d'Angremond, 1998 and Hauer et al., 1995. The quarry distance can deviate significantly for different locations; therefore, this assumption contains a big uncertainty. It is important to keep this uncertainty in mind when analysing the model results. The paper of Tutuarima and d'Angremond, 1998 does not differentiate between the costs of the armour and filter layers; therefore, the armour and filter costs were approximated using a different source (DMC, 2022). The bed protection mainly consists of block mats, so a total length of 800 meters of block mats will be applied with a price of 70 € / m^2 (GW Rotterdam, 2005).

Sill & bed protection materials	**Layer thickness [m]**	**Volume [m^3 / m]**	**Price [€ / m^3]**	**Cost [€ / m]**
Concrete blocks (not reinforced)	1	4	500	2,000
Armour (3 - 6 T)	2.4	50	135	6,800
Filter (300 - 1000kg)	1.3	26	100	2,600
Core (Quarry run)	3	313	35	11,000
Bed protection (block mats)	-	2 x 400 [m^2/m]	70 [€/m^2]	20,000
			Total	**42,400**

Table 4.4: Sill and bed protection material costs (Tutuarima & d'Angremond, 1998), (DMC, 2022) and (GW Rotterdam, 2005). Corrected for inflation and currency rate

Additional costs

Electronics

To estimate the electronics cost, two sources were found. The first source (cost of DTP paper) indicates a cost of 100 million per MW (interview with Kees Hulsbergen and Rob Steijn (TNO, 2020)). The second source is the reference project in Oman, which estimated a total electronics cost of 570 million. The projected power output is 0.76 MW, resulting in a cost of 750 million per MW. These results show a significant difference. To be conservative, the highest value of €750 million per MW is used. The electronic costs exclude the costs for optional batteries.

Construction dock and immersion works

The oman reference project (Tidal Bridge bv, 2020) estimates a total cost of €100 million for the construction dock to build 7.2 km of caissons. This results in approximately 15,000 € per meter, which is included in the costs. An additional €11.000 per meter is included for the immersion works, based on Tidal Bridge bv, 2020. Please note that these are simplified approximations; these numbers can deviate significantly based on the location and design requirements.

Total costs

The total costs are shown in table 4.5, including a comparison with literature. What can be seen is that the estimated costs per km deviate significantly between literature sources. W. Walraven estimated a cost of 400 M €/km for the main dam and 40 M €/km for the closed-T dam. The reference project of Oman estimated a cost of 200 M €/km for the caisson part, including turbines. K. Hulsbergen and R. Steijn estimated a significant cost of 140 M €/km (excluding turbines and depth not specified). The determined costs in this study deviate but are in the same order of magnitude. For a water depth of 20m, the costs are higher (330 M €/km including turbines, 250 M €/km excluding turbines) than the costs of two out of three other studies (250 M €/km including turbines, 140 M €/km excluding turbines). This is probably due to the conservative design and costs determination approach; the caisson wall thickness is large (1 m) for both internal and external walls, reinforced concrete is used, and conservative material prices are applied,

This study	Depth			**Literature**		
	20 m	30 m	40 m		Depth	Source
Incl. turbines (10% permeability)	**330**	**435**	**540**	**400** **250**	Not specified 15 m	W. Walraven (DTP Netherlands, n.d.) (Tidal Bridge bv, 2020)
Excl turbines	**250**	**315**	**380**	**140**	Not specified	Hulsbergen and R. Steijn (TNO, 2020)

Table 4.5: Total costs [Million € / km] compared to literature

5

Model set-up

5.1. Hydraulic model

5.1.1. Theoretical Framework

Equations and derivations

At the background information, chapter 2, the maximum hydraulic head was derived; see equation 2.1. This equation will be used in the hydraulic model. Now, to calculate the energy generation by the turbines when the hydraulic head difference is known, Bernoulli's equation can be used. This is a simplified form of the law of conservation of energy, where the energy density along a streamline stays constant. It is only applicable to non-viscous fluids that are also non-compressible.

Presuming conservation of energy along the streamline depicted in figure 5.1, the energy level before inflow (H_1) should be equal to the outflow energy level (H_2) minus the energy losses and turbine energy absorption. Point 2 (H_2) is taken just behind the outflow point of the turbine, which has the advantage that here only the atmospheric pressure has to be considered.

The energy balance can be seen in equation 5.1. Applying this to a streamline in the cross-shore direction of a DTP dam (see figure 5.1) results in equation 5.2.

$$\begin{aligned} H_{in} &= H_{out} \\ H_1 &= H_2 + \Delta H_t + H_{loss} \end{aligned} \tag{5.1}$$

$$\frac{P_a}{\rho g} + \frac{V_1^2}{2g} + h_1 = \frac{P_a}{\rho g} + \frac{V_2^2}{2g} + h_2 + \Delta H_t + C\frac{V_2^2}{2g} \tag{5.2}$$

where:

P_a = Atmospheric pressure [N/m^2]
ρ = Specific water mass [kg/m3]
g = gravitational acceleration [m/s^2]
V_1 = Flow velocity at point 1 [m/s]
h_1 = Water height at point 1 [m]
V_2 = Flow velocity at point 2 [m/s]
h_2 = Water height at point 2 [m]
C = Loss coefficient [-]
ΔH_t = Energy gain of turbine [m]

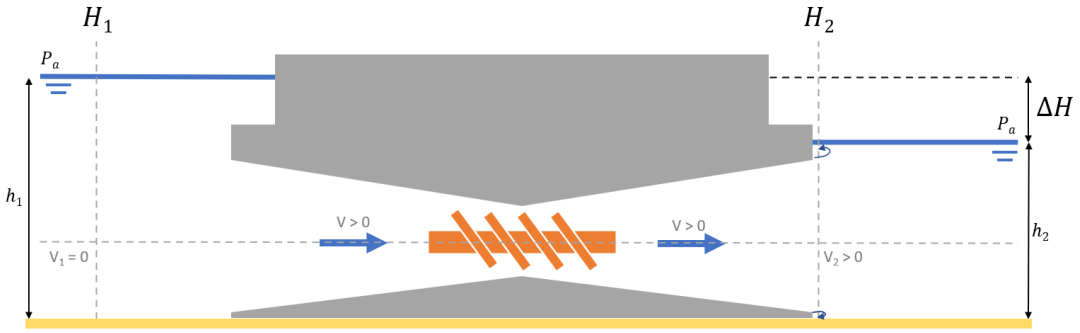

Figure 5.1: Cross subsection DTP dam with flow stream to apply Bernoulli's equation

The outflow velocity at point 2 (H_2) can be found by subsiding the hydraulic head ($\Delta h = h_1 - h_2$)) into equation 5.2, which results in equation 5.3.

$$V_{out} = \frac{\sqrt{2g(\Delta h - \Delta H_t)}}{1 + C} \tag{5.3}$$

As can also be seen in figure 5.1, the turbines have "spoilers" that converge the flow from a larger inlet area (A_{in}) towards the turbine rotor area (A_t). It depends on the turbine design and how large these areas are in relation to the turbine areas. For a bi-directional tidal turbine, the inflow and outflow surfaces are assumed to be the same size. The inflow area of the turbine relative to the turbine rotor area can be described by equation 5.4, which will be used in further calculations. The angle of the spoilers influences the energy losses of the turbine. A greater angle results in more flow separation during outflow, which increases the loss coefficient. See chapter 5.1.2 for more information about the theory behind these energy losses and the derivation of the used loss-coefficient C.

$$\gamma_s = \frac{A_t}{A_{in}} \tag{5.4}$$

The energy balance (equation 5.1) includes a turbine energy gain (ΔH_t). To be able to calculate this turbine energy gain, a new factor is introduced that expresses the fraction of the hydraulic head that is being used to generate power by the turbine, defined in equation 5.5. As is derived in appendix D.4, maximum power generation is achieved for $a = 2/3$. This is also shown by Anteagroup, 2018, based on the optimization of a similar analytical model. Please see appendix D.4 for additional explanation on this parameter and its physical meaning.

$$a * \Delta h = \Delta H_t \tag{5.5}$$

Flow rate Q and power output P

The flow rate Q can then be found by combing equations 5.3, 5.4 and 5.5, which results in equation 5.6.

$$Q_{in} = Q_{out} = A_{out} V_{out} = \gamma_s * A_t \frac{\sqrt{2g(1-a)\Delta h}}{1 + C} \tag{5.6}$$

Using the earlier derived flow rate equation 5.6 ,the maximum hydraulic power can be expressed with equation 5.7.

$$P_{t,max} = \eta \rho g \Delta H_t Q_{in} = \eta \rho g a \Delta h_{max} Q_{in} = \eta \rho g a \gamma_s A_t \frac{\sqrt{2g(1-a)\Delta h_{max}^3}}{1 + C} \tag{5.7}$$

where:

$P_{t,max}$ = Maximum hydraulic power output [kW]
η = Installation efficiency [-]
ρ = Specific water mass [kg/m3]
g = gravitational acceleration [m/s^2]
ΔH_t = Energy gain of turbine [m]
a = fraction of the hydraulic head used for energy generation [-]
C = Loss coefficient [-]
γ_s = fraction between rotor and inflow area [-]
A_t = Turbine opening [m^2]
Δh_{max} = Maximum hydraulic head difference between both sides of the dam [m]

Partly-permeable DTP dam
Equation 5.7 calculates the maximum power output, considering the maximum head difference. In this equation permeability of the dam is not taken into account. Increasing the permeability of the dam increases the flow rate and reduces the hydraulic head difference. Therefore, the permeability is fairly important for the power output and has to be taken into account.

If the dam is fully permeable, the maximum undisturbed flow through the imaginary dam can be described using equation 5.8.

$$Q_{dam,open} = A_{dam} * V_{max} \tag{5.8}$$

The hydraulic head will change relatively with the difference in flow rate through the dam. Therefore this can be approximated by using equation 5.9, where the change in the hydraulic head is related to the disturbed (Q°_{max}) and undisturbed (Q_{dam}) flow rate through the dam. The formulation of equation 5.9 can be observed in appendix D.2.

$$\Delta h^{\circ}_{max} = \Delta h_{max}[1 - (\frac{Q^{\circ}_{max}}{Q_{dam}})^2] \tag{5.9}$$

The permeability of the dam can be described by introducing a factor b, which is the quotient of the total flow area of the turbine rotors and the total surface area of the dam. This is shown in equation 5.10.

$$b = \frac{A_0}{A_{dam}} \tag{5.10}$$

Now the flow rate through a partially permeable dam can be derived using equations 2.1, 5.6, 5.8, 5.9 and 5.10. This results in equation 5.11. A comprehensive derivation of equation 5.11 can be found in appendix D.3. The corresponding theoretical power output is shown in equation 5.12.

$$Q^{\circ}_{max} = A_{dam}V_{max} * [1 + (\frac{\Delta h_{max} g}{2\omega L b \gamma_{model}})^2 \frac{1 + C}{\gamma_s^2 * 2g(1 - a)\Delta h_{max}})]^{-\frac{1}{2}} \tag{5.11}$$

$$P^{\circ}_{max} = \eta \rho g a \Delta h^{\circ}_{max} Q^{\circ}_{max} \tag{5.12}$$

where:

Q°_{max} = Maximum flow rate when partly permeable [m^3/s]
P°_{max} = Maximum hydraulic power output when partly permeable[kW]
Δh°_{max} = Maximum hydraulic head difference when partly permeable [m]

All the equations derived above are based on or with the help of the following papers: (Talstra & Pak, 2020), (Anteagroup, 2018), (Tidal Bridge bv, 2020) and (Swamee, 1992). Please consult these for additional information.

5.1.2. Energy losses

The loss coefficient C in the energy balance (5.1) summarizes all flow energy losses (see equation 5.14). There are four main types of losses: induced turbulence from the turbine ($k_{turbine}$), inflow flow contraction (k_{inlet}), outflow flow separation (k_{outlet}), and friction against the turbine walls (($k_{friction}$). These will be addressed and approximated using the FishFlow innovations turbine as a base case.

Turbine losses

Hydropower turbines generally have high efficiency. Fishflow Innovations claims that their free flow turbine has a turbine efficiency of 85%, which means that 85% of the energy head can be converted to electricity and 15% is considered as energy loss. Recalculating this loss in terms of a turbine loss coefficient as defined in equation 5.14 gives $k_{turbine} \approx 0.38$.

$$H_{loss} = C * \frac{v^2}{2g} \tag{5.13}$$

$$C = k_{turbine} + k_{inlet} + k_{outlet} + k_{friction} \tag{5.14}$$

5

Gradual contraction

The inlet of the turbine consists of a gradual contraction part. The streamlines are contracted and focused towards the smaller rotor diameter of the turbine (Diameter gradually decreases from 11m to 8m). The loss coefficient of this gradual contraction is derived by Crane (equation 5.15), which is valid for $\phi < 45°$ (*Crane Technical Paper 410: Flow of Fluids Through Valves, Fittings and Pipe*, 1982). Applying this formula for the FishFlow turbine results in a contraction coefficient of $k_{inlet} = 0.094$.

$$k_{inlet} = \frac{0.8 * \sin\frac{\phi}{2}(1-\beta^2)}{\beta^4} = \frac{0.8 * \sin\frac{8}{2}(1-0.72^2)}{0.72^4} = 0.094 \tag{5.15}$$

where:

ϕ = Half top angle of inlet [°]
$\beta = \frac{D_1}{D_2}$ = Smallest and widest diameters of inlet [–]

Gradual enlargement

The turbine outlet gradually increases in diameter. The corresponding losses are described by the gradual enlargement coefficient derived by Crane (equation 5.16), which is valid for $\phi < 45°$ (*Crane Technical Paper 410: Flow of Fluids Through Valves, Fittings and Pipe*, 1982). This results in $k_{outlet} = 0.14$ for the FishFlow innovations turbine. The enlargement coefficient is relatively low. This is because almost no flow separation occurs for an angle of 8 degrees (at angles below 7° the flow separation is zero) (Chandavari, 2014).

$$k_{outlet} = \frac{2.6 * \sin\frac{\phi}{2}(1-\beta^2)^2}{\beta^4} = \frac{2.6 * \sin\frac{8}{2}(1-0.72^2)^2}{0.72^4} = 0.14 \tag{5.16}$$

where:

ϕ = Half top angle of inlet [°]
$\beta = \frac{D_1}{D_2}$ = Smallest and widest diameters of inlet [m]

Friction

The friction can be calculated using the Colebrook-White equation, shown in equation 5.17. As relative pipe roughness, we use forged steel which has an internal roughness (ϵ) of approximately 0.025. Using a diameter of 8m, the relative pipe roughness is 0.00313.

Inside the turbine, there will be some turbulence. However, FishFlow innovations claim that there is relatively low turbulence present due to the slow rotations and ergonomic shape. If there is turbulence, the Reynolds number will be approximated at $1 * 10^7$, which gives a friction factor (f) of 0.026. If there were low turbulence (transition region between laminar and turbulent flow), the friction factor (f) would be 0.051. To be conservative, the highest factor will be taken into account, thus $f = 0.05$.

Darcy's formula can be used to calculate the corresponding friction coefficient $k_{friction}$, as shown in equation 5.18 (*Crane Technical Paper 410: Flow of Fluids Through Valves, Fittings and Pipe*, 1982). Here, the weighted length (L) and diameter (D) of the FishFlow turbine is used. This results in a friction coefficient of $k_{friction} = 0.15$.

$$\frac{1}{\sqrt{f}} = -2\log\left(\frac{\epsilon}{3.7D_h} + \frac{2.51}{Re\sqrt{f}}\right) \tag{5.17}$$

$$k_{friction} = f * \frac{L}{D} = 0.05 * \frac{26.6}{8.75} = 0.15 \tag{5.18}$$

Total Loss coefficient C

Finally, all friction coefficients need to be summarized (equation 5.14) to find the loss coefficient C. This gives $C = 0.38 + 0.09 + 0.14 + 0.15 = 0.76$. This friction coefficient corresponds to the friction coefficient found in literature, where also the FishFlow turbines are addressed in a design for a DTP dam in Oman (Tidal Bridge bv, 2020). Their friction coefficient is defined differently. Recalculating gives $C = \sqrt{\frac{1}{1.85}} = 0.73$, which is very close to the $C = 0.76$ found above.

5.1.3. Overview

Figure 5.2 shows an overview of the hydraulic model. Yellow-coloured blocks represent input values, orange blocks represent calculations, and the blue block shows temporary hydraulic model outputs. Combining these outputs with the costs and finding the optimum results in the black block where the final output results are gathered.

It can be noticed that in figure 5.2, the first orange block shows two parameters that are not introduced yet. Firstly, there is a distinction made between the total length (effective length) and dam length. In a standard DTP dam situation, these parameters are equal because the dam that needs to be built is the same length as the total length it blocks. However, when the natural coastline or an island is used, the effective blockage length could be greater than the dam length. This could greatly increase the energy potential and/or reduce the construction costs. Therefore, the hydraulics calculations use the effective length (L_{eff}) while the costs calculations use the dam length (L_{dam}). See figure 2.10 for an illustration of the use of the natural coastline.

Secondly, a Branch parameter is introduced. When this parameter is equal to 0, equations of a normal DTP dam without a branch are used. When the Branch parameter is equal to 1, the model requires the additional input parameters: branch length and branch angle.

Concerning the flow velocity signal, a simplified tidal signal can be used (for example, an artificial M2 using a simple cosine curve) or a custom signal for a specific region. Providing a latitude and longitude, the tidal signal of the closest available grid cell is used for the desired time period.

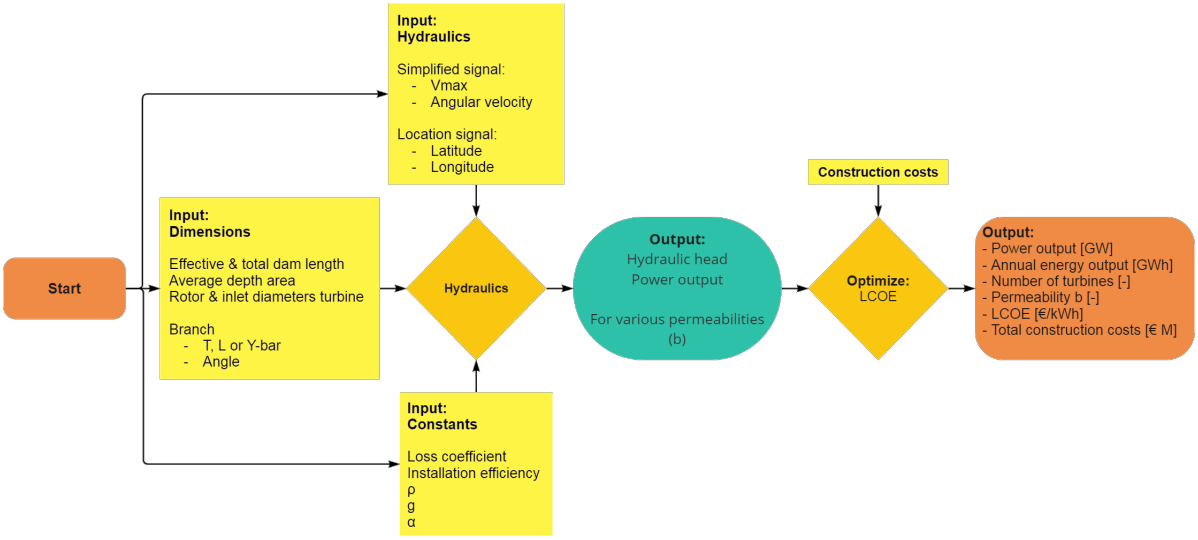

Figure 5.2: hydraulic model steps

5.2. Spatial model

The spatial model performs a Multi Criteria Weighted Overlay Analysis (MCWOA) using GIS software, which will include several data-sets that correspond to the feasibility study (chapter 4) decision criteria, which can be seen at table 5.1. The spatial model uses several steps, which are shown at figure 5.3. The model is parametric and flexible, since the thresholds and weighting criteria can be easily adjusted, map constraints such as protected areas can be included or excluded in the analysis and also multiple linkage opportunities can be included. This flexibility helps at possible future research projects.

Feasibility criteria	
Technical	Secondary
Natural tidal current speed Water depth	Energy market capacity Resource availability Shipping Environmental impact Area development Linkage opportunities
Chapter 5.2.2	Chapter 5.2.4

Table 5.1: Feasibility criteria derived at feasibility chapter 4.

5.2.1. MCWOA method

Spatial model steps

Step 1: Identify and map criteria influential on DTP potential
- a) Map criteria values
- b) Apply thresholds / constraints
- c) Normalize values from 0 - 1 (Unsuitable (0) - Highly suitable (1))

Step 2: Create Potential Index (PI) map
- a) Determine weighting factors
- b) Combine weighted criteria, using MCWOA method, determine PI for technical and secondary criteria

$$PI = \sum_{j=1}^{m} w_j * C_j, \quad w_j, C_j \in [0,1] \tag{5.19}$$

- c) Combine PI technical (PI_t) and PI secondary (PI_s), using:

$$PI_{total} = w_t * PI_t + w_s * PI_s \tag{5.20}$$

Step 3: Identify and map constraints (protected areas)
- a) Identify protected areas
- b) Substract protected areas from PI map

Step 4: Apply filter (minimum population size or energy usage)
- a) Discard locations where filter conditions do not comply

Step 5: Add linkage opportunities on PI map
- a) Identify linkage opportunities
- b) Highlight linkage opportunities locations corresponding with PI map locations

Result: Final PI map

Max. normalized values producing final PI values ranging from >0.0 - 1.0 (highest potential)

Figure 5.3: Spatial model steps and final PI head map, an elaboration is given on the next page.

Elaboration on figure 5.3
Potential Index (PI)
The potential Index (PI) ranks each grid cell for its potential to apply DTP, based on the other normalized datasets and their corresponding weighting factors. For the calculation of the PI, see equation 5.19

$$PI = \sum_{j=1}^{m} w_j * C_j, \quad w_j, C_j \in [0, 1] \tag{5.19}$$

where:

PI = Potential Index [-]
w_j = Weighting factor [-]
C_j = Normalized criteria value [-]

To add model flexibility, the potential index is calculated separately for the technical PI_t and secondary PI_s criteria and then combined using weighting factors to determine the total potential PI_{total}.

$$PI_{total} = w_t * PI_t + w_s * PI_s \tag{5.20}$$

where:

PI_{total} = Total potential index [-]
PI_t = Potential index of technical criteria [-]
PI_s = Potential index of secondary criteria [-]
w_t = Weighting factor of technical criteria [-]
w_s = Weighting factor of secondary criteria [-]

Weighting factors
The weighting factors need to comply with condition 5.21 (Kaymak & van Nauta Lemke, 1998). This means that all weighting factors should be between 0 and 1 and the sum of all weighting factors should be equal to 1. Applying this conditions ensures that the PI value also lies between the limits of 0 and 1.

$$\sum_{j=1}^{m} w_j = 1, \quad w_j \in [0, 1] \tag{5.21}$$

5.2.2. Technical criteria

The technical feasibility analysis involves the natural tidal current speed and the water depth. Considering the natural tidal current speed, a global dataset is required derived from an accurate tidal model. The second criterion requires a global bathymetry dataset.

Global tidal currents dataset
First, the natural tidal current speed dataset will be established. The currently most accurate model in terms of assessing the tidal current on a global scale is the FES2014 Finite Element Solution model, developed, implemented and validated by the LEGOS, NOVELTIS and CLS, within a CNES funded project (Noveltis et al., 2016). The model includes the amplitude and phase of 34 tidal constituents distributed on 1/16° grids (≈ 7x7 km grid size at the equator). Using this model, a database with tidal current information can be established.

Equations 5.22a and 5.22b describe how tidal velocities in u (eastward or x-direction) and v (northward or y-direction) can be calculated, using the different amplitude, angular speed and phase difference of each constituent (Xu, 2002). The magnitude of the tidal velocity is then determined by using equation 5.23, which combines the vectors in u and v direction and finds the magnitude of the residual vector. Using the FES2014 model and these equations, the tidal signal can be calculated for each grid cell.

$$u = \sum_{i=1}^{i=N} A_{i,u} \cos\left(\omega_{i,u} t - \theta_{i,u}\right) \tag{5.22a}$$

$$v = \sum_{i=1}^{i=N} A_{i,v} \cos\left(\omega_{i,v} t - \theta_{i,v}\right) \tag{5.22b}$$

$$w = \sqrt{u^2 + v^2} \tag{5.23}$$

Figure 5.5 shows an example of the tidal signal calculated at one grid cell for one month time, including the calculated mean, standard deviation and corresponding histogram (exact location shown at figure 5.4). To acquire a valid and complete dataset of the tidal currents worldwide, this calculation is repeated for each individual grid cell, and the mean and maximum velocity of the tidal signal is derived and stored in a dataset. This resulted in a global tidal current speed dataset, from which figure F.2 was created.

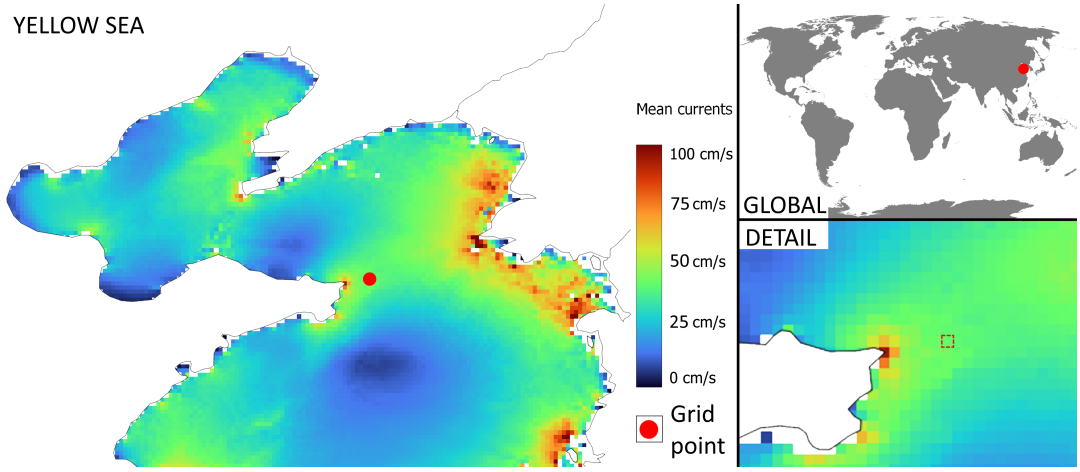

Figure 5.4: Location of grid-cell corresponding to the China1 dam described in the paper of Hulsbergen et al., 2008. The right top figure shows the location on a global map. The right low figure shows the detailed grid cells and, in red, the grid cell that is assessed. Latitude and Longitude, respectively (37.5, 123.0). The tidal mean current database generated using the FES2014 model (Noveltis et al., 2016).

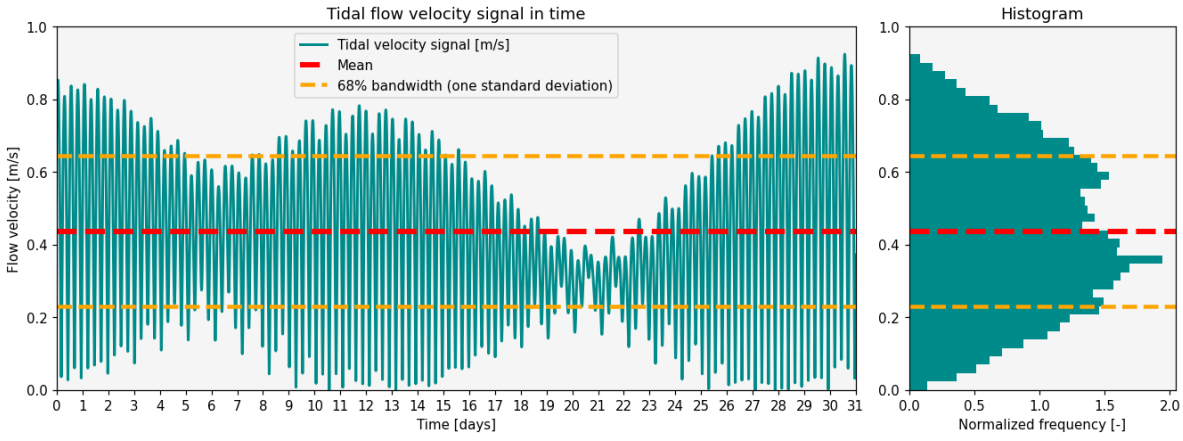

Figure 5.5: Tidal velocity signal output for one month and the corresponding histogram. Grid cell location is shown at figure 5.4, latitude and Longitude respectively (37.5, 123.0)

Discussion computation time tidal signal
To optimize computational efficiency, the tidal signal calculation and storage for each grid cell require careful consideration of the time span. It should be long enough to ensure representative values with low error, yet not too long to avoid excessive computation. The top 5 most potential locations were analyzed by calculating the mean and maximum values for time spans up to one year. The results of this analysis can be found in Appendix F.1. It was found that computing the mean tidal current velocity using a time span of 1 month gives an error between 2% and 2.5%. Since DTP is investigated on a broad global scale, an error of 2.5% is small compared to other model uncertainties. Therefore, the mean tidal flow velocity values that were computed using a 1 month time span are used in the spatial model and analysis. This results in a global mean tidal currents dataset as shown in figure F.2, where the mean tidal current flow velocities are approximated, using a 1/16°x1/16° grid resolution.

Bathymetry dataset
For the initial analysis, the water depth and, thus, the bathymetry is required on a global scale. The GEBCO (General Bathymetry Chart of the Oceans) data set includes accurate and publicly available bathymetry data worldwide. It is based on a combination of ship-based soundings, satellite-derived gravity data, and digital terrain models. Elevation data is provided in meters on a 15 arc-second interval grid (Group, 2022).

Overview technical criteria datasets

Parameters	Dataset	Name	Description	Type	Resolution	Source
Water depth	Bathymetry	GEBCO Gridded Bathymetry Data	Global terrain model providing elevation data	Raster	1/4'x1/4' grid	(Group, 2022)
Natural tidal flow speed	Dataset produced using Global tide model	FES2014	Tidal signals can be calculated for each grid cell	Raster	1/16°x1/16° grid	(Noveltis et al., 2016)

Table 5.2: Overview of technical criteria datasets

5.2.3. Discussion correlation technical datasets
There is a correlation between the bathymetry and tidal currents datasets since the depth and shape of the sea bottom have a significant influence on the tidal currents see appendixes A.3 and A.4). This is also illustrated in figure 5.6, where the mean tidal current speed is represented against the water depth. The following observations can be made based on figure 5.6:

- *Depth:*-40 till -22.5
  The flow velocities are small for water deeper than -22.5, with mean flow velocities around 0.1 m/s. The maximum flow velocity does not exceed 0.75 m/s.
- *Depth:* -22.5 till -15
  The natural tidal current speeds are significantly higher than for depths deeper than -20 meters. This shows that the area from 0 to -20 is most interesting to assess during the spatial model.
- *Depth:* -15 till -5
  For shallow water regimes with depths < 15m, the flow velocities decrease (median, Q3 and 95% confidence interval). As described in appendix A.4, this is because the inertia effect is small and the velocity is mainly governed by the balance of the alongshore water level gradient and friction.
- *Depth:* -5 till 0
  The median flow velocities are low, but an increase in the maximum and 95% confidence interval can be seen. There are two possibilities for this increase. The first explanation is that the tidal model has a large spatial resolution and is, therefore, inaccurate for locations located close to the coastline. Since these locations have smaller water depths, the model inaccuracy is larger. Secondly, with local properties such as flow contractions and sudden increases in depth, the flow speed could still be fairly high. Please note that although it is not possible to install turbines at this depth, this depth can be blocked by a normal and less expensive dam construction, which helps with the blockage of the progressive tide. The same dam should reach deeper waters as well to be able to install turbines.

To conclude, the highest flow velocities are found in depths between -22.5 till 0. Therefore, the analysis of the simplified hydraulic model will focus on this depth region.

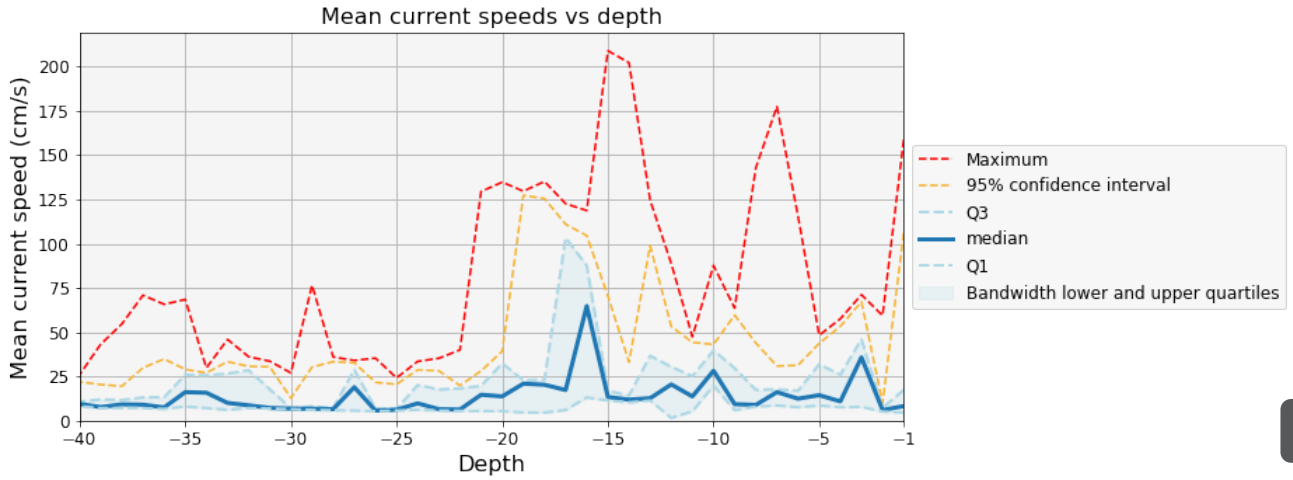

Figure 5.6: Mean current speed versus depth of the currents dataset (FES2014)

5.2.4. Secondary criteria

To include the secondary feasibility criteria (see table 5.1) in the spatial analysis, datasets that represent the criteria are included in the spatial model. Four criteria (Energy market capacity, shipping, environmental impact and linkage opportunities) are included in the spatial analysis directly. Two criteria (Resource availability and area development) could not be included because no suitable datasets were found. These criteria have to be evaluated manually when locations with high potential are found and assessed in more detail, which could be done in further research. An overiew of all datasets included in the secondary criteria spatial analysis is shown at table 5.3.

Secondary criteria		Dataset	Implementation	Source
Shipping		Global shipping traffic density	Criteria in MCWOA	(Cerdeiro et al., 2020)
Energy market	Capacity	Population count & Energy usage per capita	Criteria in MCWOA	(CIESIN, 2020) & (Bolt & van Zanden, 2020)
	Replace existing power plants	Global Power Plant	Manual assessment	(World Resources Institute, 2021)
Environment: protected areas		Global protected marine areas	Map constrain	(UNEP-WCMC & IUCN, 2023)
Linkage opportunities	Islands	Global coastlines	Automatic identification	(Patterson & Kelso, 2023)
	Port expansion	International ports	Manual assessment	(The World Bank, 2020)

Table 5.3: Overview: Secondary criteria datasets used

Shipping

Shipping was taken into account with the use of a global shipping traffic density dataset (Cerdeiro et al., 2020). The dataset describes the total number of AIS positions reported by vessels for each grid cell (dimensions 0.005°x 0.005°, approx. 500m x 500m grid at the Equador) in the period between January 2015 and February 2021. The AIS positions were transmitted by both moving and stationary ships; therefore, it describes the general shipping activity. Figure F.4 in appendix F.3 shows the plotted data of the shipping density dataset.

Energy market

Capacity

The include the energy market capacity, the following method is applied. First, a radius is selected around each site, within which the number of persons is calculated. Subsequently, the energy consumption per capita in that specific location is determined by adopting the energy consumption per

capita of the nearest country. Finally, these values are multiplied to derive the overall energy utilization in that area. The population size is determined using the population count dataset of CIESIN, 2020, shown in figure F.5. The energy consumption per capita is determined the dataset of Bolt and van Zanden, 2020, shown in figure F.6. Interestingly but not surprisingly, the energy consumption per person is significantly higher for northern countries than for countries close to the equator (with the exception of the Middle East).

Replacing fossil fuels
The replacement of oil and gas power plants can be analysed manually in the spatial analysis, after locations of interest are identified. A global power plant database is available, that provides the existing power plants location, type and energy capacity (World Resources Institute, 2021).

Environment: protected areas
As described in chapter 4.1, the environmental impact of DTP is not known yet and differs greatly for each location. To spatially include the environmental impact in the spatial analysis, the protected areas are taken into account. This is done using a global protected areas database (shapefiles) (UNEP-WCMC & IUCN, 2023), which is the most comprehensive global database of marine and terrestrial protected areas. An impression of the protected areas dataset used is shown in figure F.8.

Linkage opportunities
Considering the linkage opportunities described at chapter 2.7, not all linkage opportunities are included in the spatial model. Table 5.3 shows the linkage opportunities that were included in the spatial model and in what form. The usage of an island (to combine a bridge with a DTP dam) is included in the spatial model directly by automatic identification of islands close to the mainland that comply with all technical feasibility criteria. The port expansion linkage opportunity is analysed manually for regions with high potential with the help of global datasets.

6

Model results & analysis

6.1. Hydraulic model

6.1.1. Location assessment

To demonstrate the capabilities of the hydraulic model, the energy yield, construction costs, and energy LCOE are approximated at the location with the highest potential for DTP, which is a location near Mawlamyine, Myanmar (as found in the spatial analysis, see chapter 6.2.4).

First, a brief analysis of the area is conducted, followed by selecting the location and orientation of the dam. Subsequently, the dam length is determined through several iterations of the model, and the final results for this location are presented.

Area examination

The population size in the area is large (4.4 M people in a radius of 1 spatial degree), but the energy usage per person is low (3.2 MWh per person). In the case of economic growth of the area, the energy usage per person will probably rise. This increases the energy demand in the future, giving this location a higher potential to apply DTP. Figures 6.1 show the PI score per grid cell, the mean tidal current speeds, bathymetry and shipping intensity in the area. At the Eastern bank, the highest flow velocities occur, in combination with the lowest shipping intensity. Therefore, the dam is designed to be connected to the Eastern bank.

Input

The depth in the area is relatively shallow, with an average depth of -18 meters that slowly declines towards deeper waters. Therefore, it is possible to construct a long dam. The input values used are stated in table 6.1. By iteration of the hydraulic model at this specific location, a dam length of 50 km resulted in an LCOE of 0.066 €/kWh (see table 6.2). This is different for each location, especially because an increase in dam length generally means that the mean depth increases as well (due to a sloping sea bed).

Input parameters		
Latitude	16.0	Latidue of grid cell with highest potential
Longitude	97.5625	Longitude of grid cell with highest potential
L	50	Dam length [km]
z	18	Mean water depth [m]
D_{in}	11	Inlet diameter
D	8	Turbine rotor diameter

Table 6.1: hydraulic model example input values

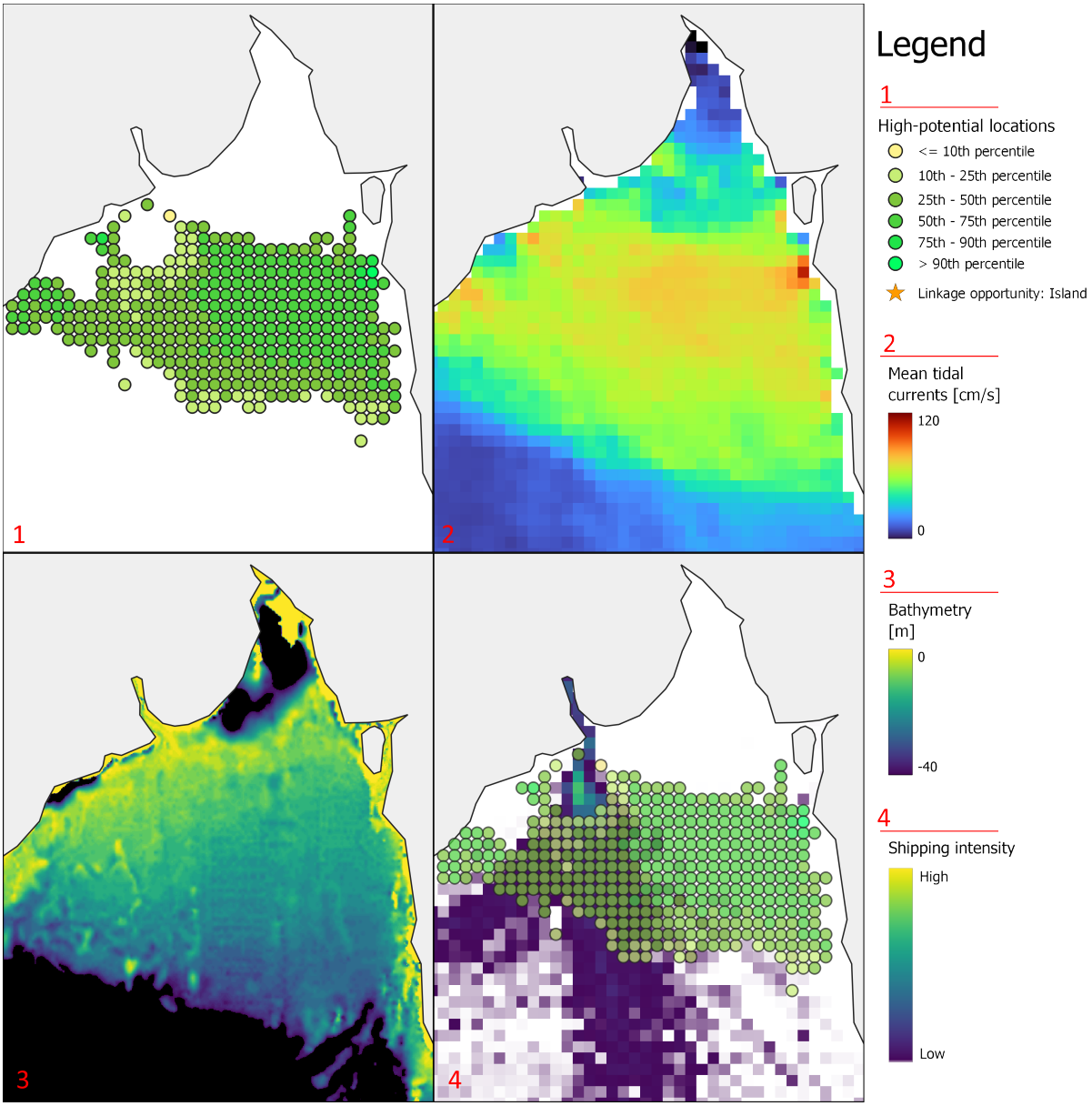

Figure 6.1: Potential location near Mawlamyine, Myanmar.

Output

The simplified hydraulic model gives the output results for various permeability factors (b) and indicates the permeability factor that gives the most optimal LCOE possible. Figure 6.2 shows the tidal current velocity and figure 6.3 the power output for a time span of one month. Figure 6.4 shows the hydraulic head, power output and LCOE for permeability factors between 0% and 16% permeability. The final output is stated in table 6.2.

	Parameter		Output	
Maximum	P	Power	4.59	[GW]
	b	Permeability	0.17	[-]
	n	Number of turbines	3382	[#]
	E	Annual energy production	16.53	[TWh]
	LCOE	Levelized cost of electricity	0.068	[€/kWh]
Optimum LCOE	P	Power	4.38	[GW]
	b	Permeability	0.13	[-]
	n	Number of turbines	2586	[#]
	E	Annual energy production	15.78	[TWh]
	LCOE	Levelized cost of electricity	0.066	[€/kWh]

Table 6.2: hydraulic model output results

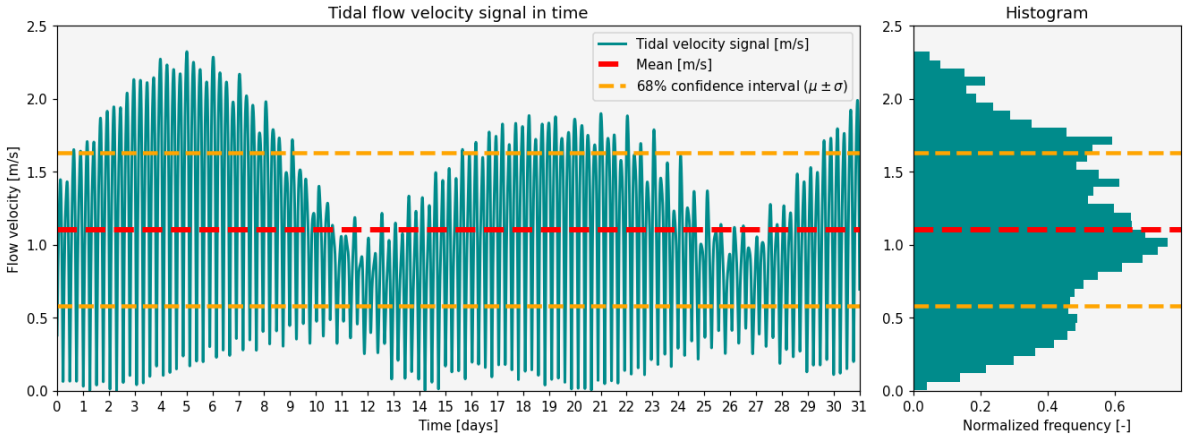

Figure 6.2: Tidal current flow velocity for a time span of one month at location (16, 97.56), Mawlamyine, Myanmar.

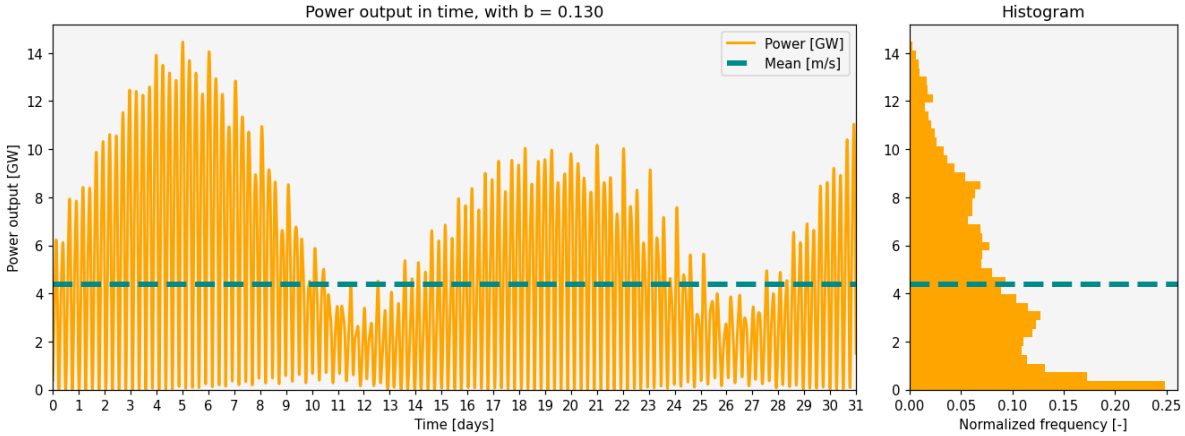

Figure 6.3: DTP dam power output for a time span of one month at location (16, 97.56), Mawlamyine, Myanmar.

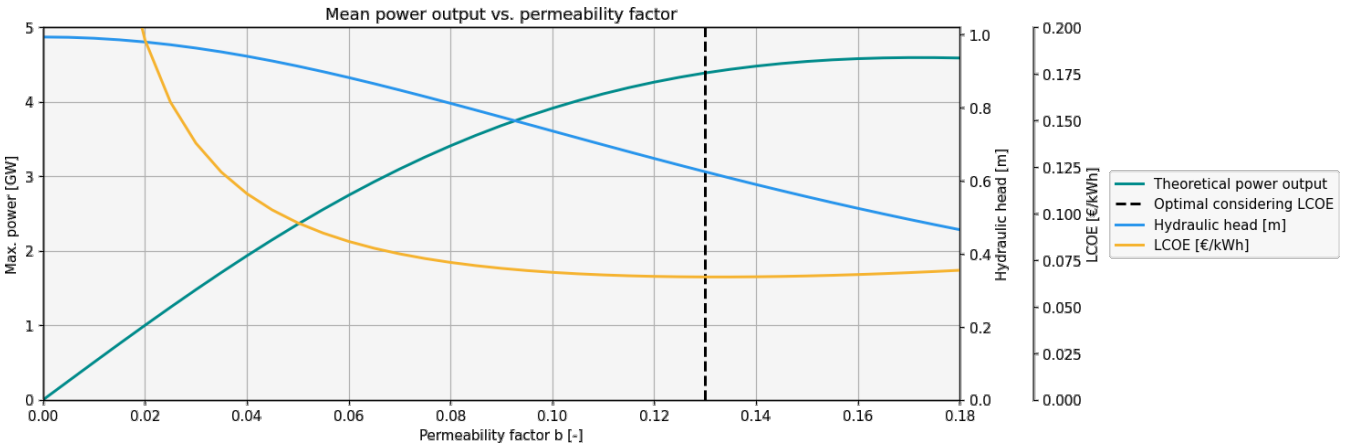

Figure 6.4: Hydraulic model result: Power output, permeability, hydraulic head and LCOE at location (16, 97.56), Mawlamyine, Myanmar. See chapter 5 for the hydraulic model set-up and the used equations.

Elaboration figure 6.4

It can be observed that as the permeability (b) increases, the power output initially rises until it reaches its maximum at $b = 0.16$. During this increase in permeability, the hydraulic head decreases. Eventually, the hydraulic head decreases to a point where further increases in permeability would lead to a decrease in power output. This represents the tipping point where adding more turbines no longer translates into higher power output. This result corresponds to the background information theory that is described in chapter 2.3.2. However, please note that the exact values at this example is case-dependend. The dam permeability, power curve, induced hydraulic head and LCOE are all different for other locations.

The optimum LCOE (€/kWh) was determined to be at a permeability of $b = 0.13$. However, it can be seen that the LCOE stays approximately constant between permeabilities of 0.1 and 0.16. Therefore, it depends on the budget available for the project and the targeted energy production to determine the desired number of turbines.

6.1.2. Threshold analysis

The threshold analysis forms the basis for the spatial analysis; it defines the thresholds of the most important criteria to be applied in the spatial model. The technical, economical and social-ecological feasibility (described in chapter 4) determine the total feasibility. The social-ecological feasibility will be discarded in the threshold analysis since this feasibility is not included in the simplified hydraulic model. Therefore the threshold analysis will include the technical and economical feasibility.

Inclusion of technical feasibility

As was determined in chapter 4.2, the technical feasibility is determined by the tidal flow velocity, the water depth and the dam design. The tidal flow velocity and water depth are both parameters directly included in the threshold analysis; the dam design is included in the simplified hydraulic model and determines the total project costs.

The discussion of the technical datasets in chapter 5.2.2 showed that the highest flow velocities are found at depths between -22.5 and -15m. Therefore, the threshold analysis will focus on a water depth of -20m.

Inclusion of economic feasibility

To measure the performance of these criteria, the levelised costs of electricity (LCOE) in €/kWh is included in the analysis. This indicates the economic feasibility, by combining the energy production criteria with the total construction costs. For DTP to be competitive in the energy market, the energy price should be competitive with other renewable energy sources. To not exclude potentially feasible locations beforehand, the upper limit LCOE of 0.1 €/kWh will be targeted in the threshold analysis. The mean flow velocity threshold will be included in the spatial analysis to identify potentially feasible locations. Further case-studies at these locations should determine the actual feasibility at the detailed locations, this is out of the scope of this study.

Results

Figure 6.5 shows the effective dam length against the mean flow velocity for a constant mean depth of -20m, for which an energy price of 0.07 €/kWh can be achieved. If a combination of criteria lies above the plotted lines, the energy can be generated for a price lower than 0.1 €/kWh. If a combination of criteria lies below the plotted lines, the price is above 0.1 €/kWh.

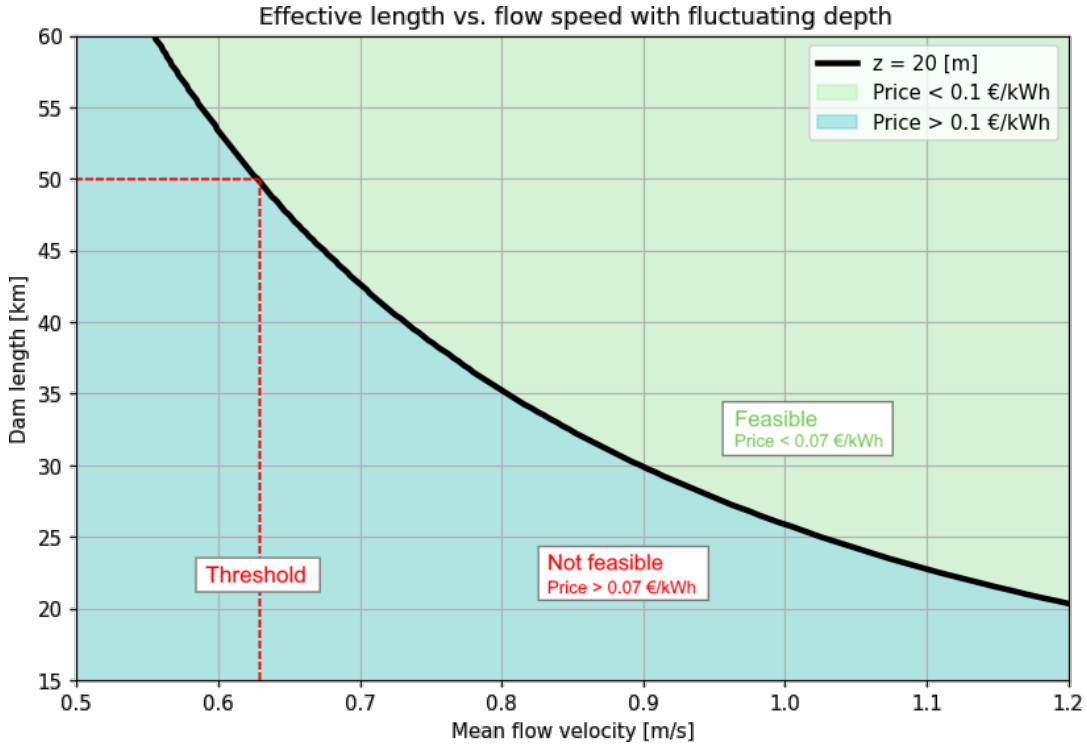

Figure 6.5: Effective length and mean flow velocity required to generate energy for 0.1 €/kWh

The maximum dam length in the analysis is set to 50 km, based on the following considerations:

- Smaller dam lengths correspond to lower project costs and, thus, a higher chance to be initiated and to attract investors. Considering that currently no DTP dam has ever been built, the focus of this research lies in having a dam design that has a chance to be implemented as the first DTP project in the world. Dam lengths longer than 50 km will need a large initial capital investment.
- The effects of a DTP dam on the environment is largely unknown, especially for very large dams. Therefore, first the focus will be on dam lengths shorter than 50 km.
- In the hydraulic model, the bottom depth and dam length parameters are not dependent on each other. However, in reality a sloping sea bed is present. Therefore, an increase in dam length will increase the mean water depth at most locations, increasing the construction costs. Due to this increase in construction costs and additional technical challenges, a maximum length of 50km is assumed.

As can be seen in figure 6.5, a maximum dam length of 50km corresponds to a mean flow velocity of 0.63 m/s, which is the threshold used in the spatial analysis.

Effect of linkage opportunity: island

Connecting the dam to an existing island extends the effective blockage length. The effect of this extension is shown for multiple island and construction dam lengths in figure 6.6. As can be seen, the usage of an island can reduce the required mean flow velocity significantly. Using a maximum dam length of 50 km, the minimum required mean flow velocities are stated in table 6.3.

Threshold incl. linkage opportunity: Island						
Island length [km]	5	10	15	20	25	30
Min. mean flow velocity [m/s]	0.57	0.53	0.48	0.45	0.42	0.39

Table 6.3: Minimum required mean flow velocity in combination with an island to achieve an energy price of 0.10 €/kWh.

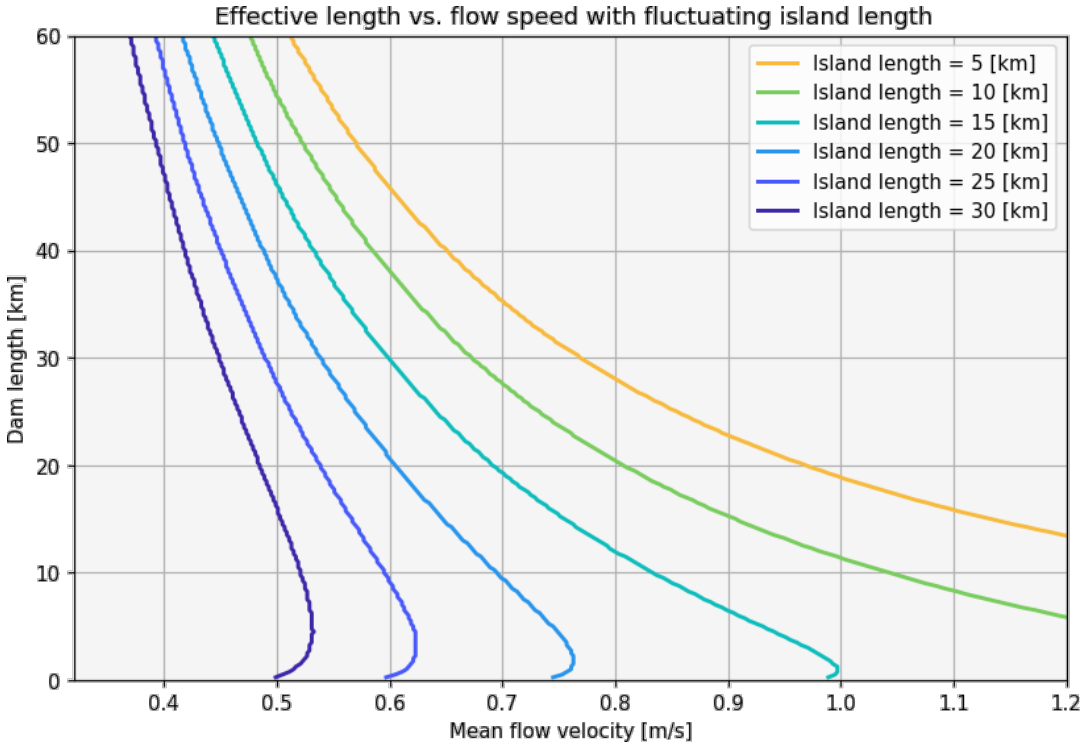

Figure 6.6: Effective length and mean flow velocity required to generate energy for 0.1 €/kWh. Plotted for the island linkage opportunity, using different island lengths. Total effective length = dam length + island length.

Influence of target LCOE in threshold analysis

Figure 6.7 shows the effect of different LCOE targets on the threshold analysis. Decreasing the target LCOE results in an increase in the required dam length or mean flow velocity. This effect shows to have a significant influence. Using the same approach to determine the minimum mean flow velocity threshold (maximum dam length of 50 km) results in the mean flow velocity thresholds shown in table 6.4. The LCOE range is based on the lowest and highest LCOEs found globally in 2021; for more information see section 2.5.3.

Threshold analysis for different LCOE targets

LCOE €/kWh	0.04	0.06	0.08	0.10	0.12	0.14
Min. mean flow velocity [m/s]	1.07	0.85	0.72	0.63	0.57	0.52

Table 6.4: Minimum required mean flow velocity for different LCOE targets

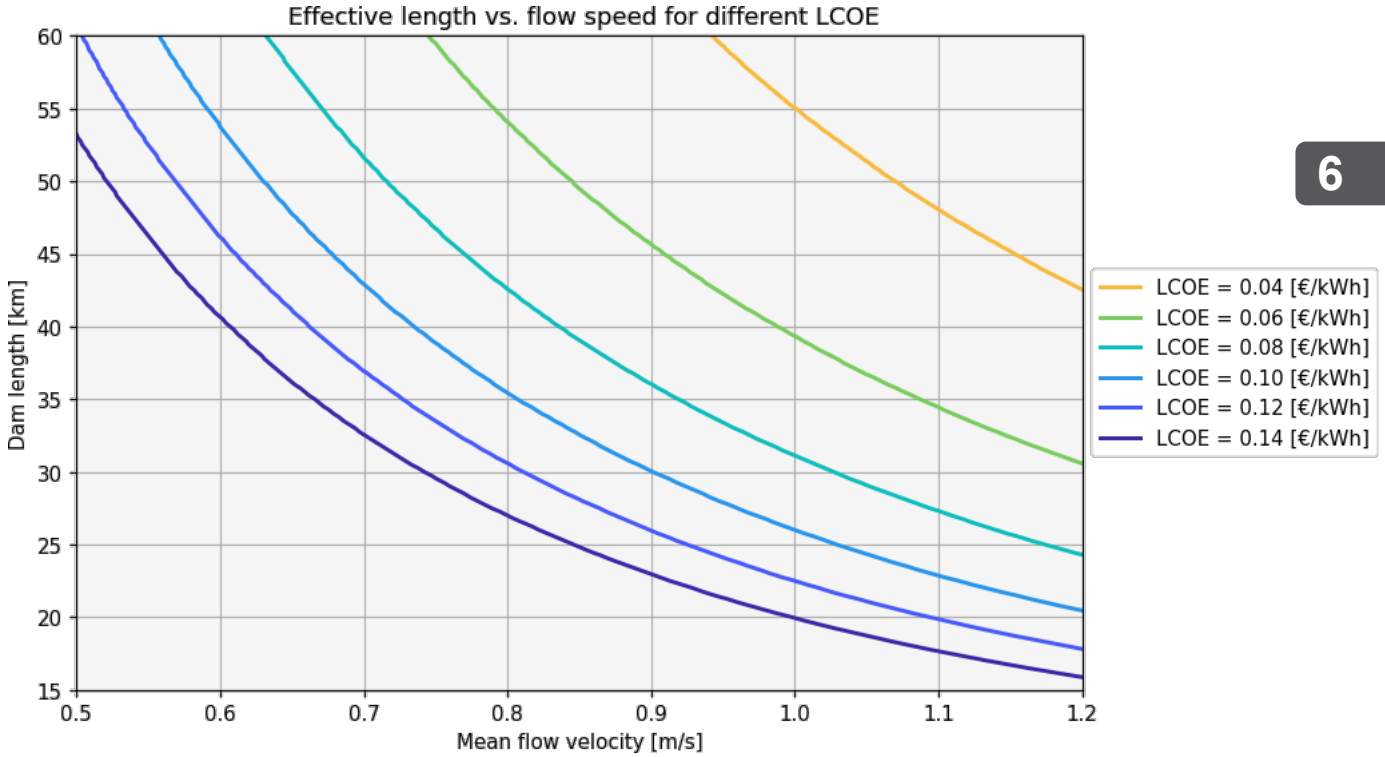

Figure 6.7: Effective length and mean flow velocity corresponding to different LCOE.

Influence of depth in threshold analysis

Appendix H.1 shows the threshold analysis using multiple depths (between 10 and -40 meters). As can be seen, the threshold analysis curve does not change at depths deeper than 10 meters. This effect is explained in more detail in appendix H.1.

6.1.3. Sensitivity analysis

The sensitivity analysis investigates the influence of the input parameters to determine the weighting factors to be used in the spatial model. The range of the sensitivity analysis is adapted to the threshold analysis results; the mean flow velocity is analysed between 0.6 m/s to 1.4 m/s, the depth is adjusted to correspond to the same input difference in %, thus between 12 m and 28 m.

Figure 6.8 shows the influence of a change in the mean flow velocity or depth on the energy production and total construction costs. The following observations can be made:

Energy production

- The slope of the mean flow velocity curve is approximately twice as steep (slope: ≈ +1.9) as the depth curve (slope: ≈ +1). This means that an increase in mean flow velocity has a two times larger positive effect on the energy production than a similar increase in bottom depth.
- The curve of the mean flow velocity is slightly exponential, while the depth curve is fully linear.

Total construction costs

- The depth linearly influences the total construction costs, with a slope of +3/4 (an increase in depth of 40% increases the total construction costs by 30%). In reality, the costs significantly rise with increasing depth. This is because greater depths would require additional design adjustments, such as thicker walls, increased concrete armouring and other aspects, such as larger construction pits, resulting in higher costs.
- The mean flow velocity has little influence on the total construction costs. A higher flow velocity results in an increased hydraulic head difference, allowing for the installation of more turbines and yielding greater energy production. Consequently, the costs rise due to the additional turbines being installed.

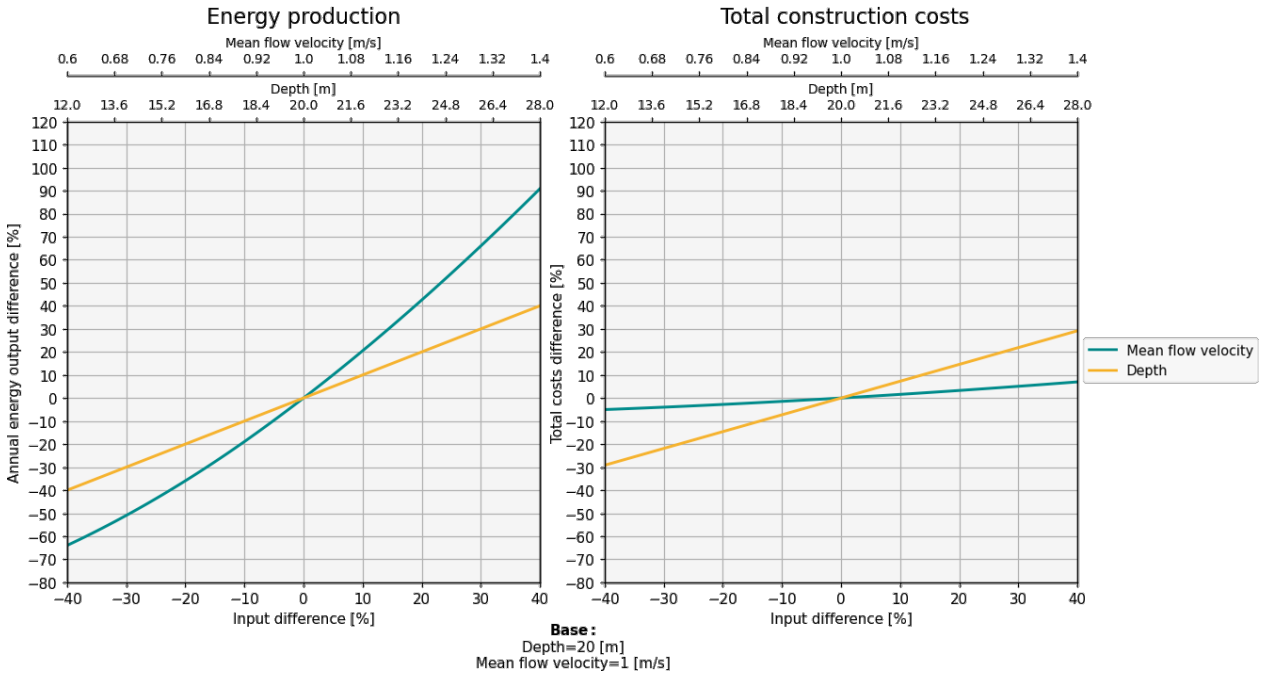

Figure 6.8: Influence of the depth and mean flow velocity on the energy output and total costs in percentages

Final technical weighting factors

To include both the energy production and the total construction costs in the analysis, the Levelized Cost Of Electricity (LCOE) (€/kWh) is included in the analysis; see figure 6.9. The technical weighting factors will be based on this sensitivity analysis, since the price includes both the energy production and the construction costs in one analysis. The following observations can be made in figure 6.9:

LCOE

- The mean flow velocity is of severe importance to the LCOE, describing an exponential curve; an increase in mean flow velocity results in a decrease in LCOE (slope: ≈ -2.25).
- The depth shows little influence on the LCOE, indicated by a slope of approximately +0.35. Surprisingly, an increase in depth leads to a decrease in the LCOE. This can be explained by examining the sensitivity of energy production and construction costs, as depicted in Figure 6.8. With increasing depth, energy production rises while construction costs also increase. These factors balance out, resulting in a moderately declining LCOE influence curve. However, if the construction costs were incorporated exponentially, it is likely that the LCOE would increase with greater depth. To realistically include the depth in the spatial analysis of section 6.2, the depth was negatively incorporated in the spatial analysis; the depth was normalized from -20 till -40, giving scores of 1 and 0 respectively. This assumption should be examined in future studies, by incorporating the construction costs fully in the hydraulic model, including realistic scaling with increasing depth.

The slope of the mean flow velocity curve is approximately -2.25, and the slope of the depth is approximately -0.35. The weighting factors should comply with equation 5.21, as shown in chapter 5.2. This gives the weighting factors $w_{currents} = \frac{-2.25}{-2.25-0.35} = 0.87$ and $w_{depth} = \frac{-0.35}{-2.25-0.35} = 0.13$, shown in table 6.5.

Criteria	Weighting factor
Tidal current velocity	0.87
Bottom depth	0.13

Table 6.5: Technical criteria weighting factors

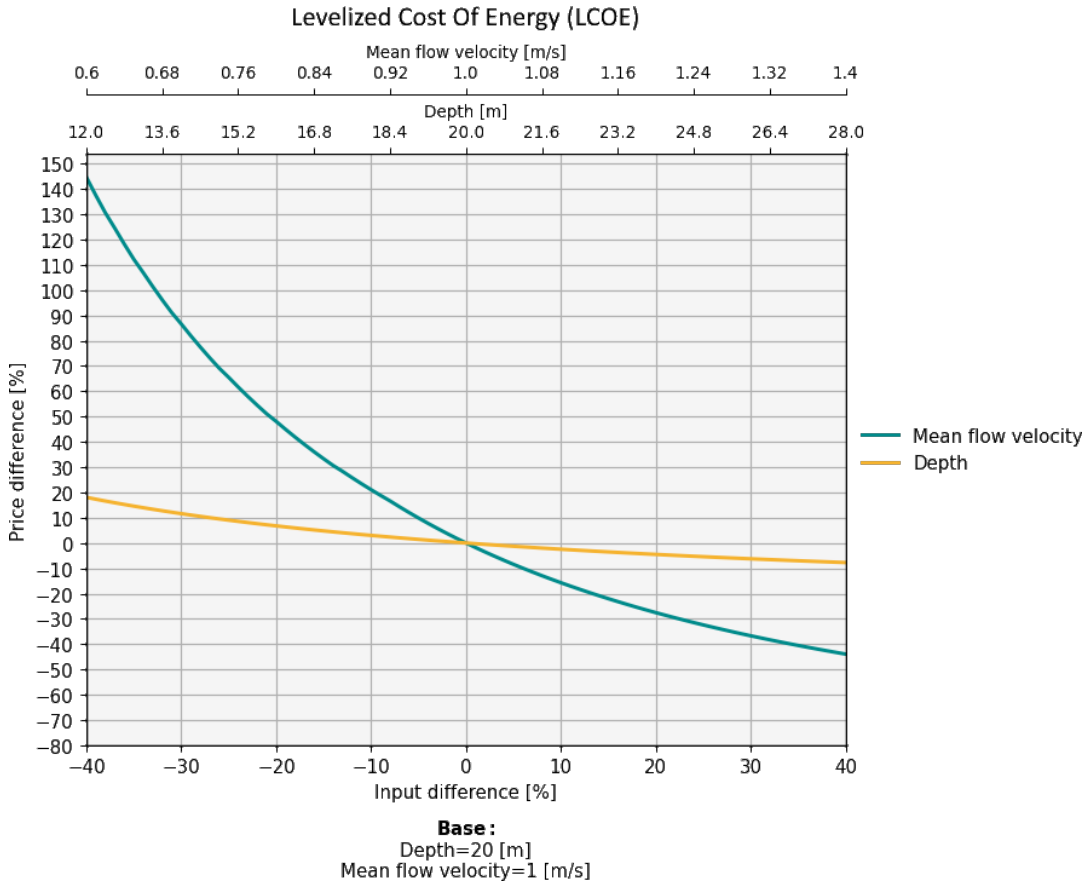

Figure 6.9: Influence of input parameters depth and mean flow velocity on the LCOE (€/kWh), with respect to a base case

6.2. Spatial analysis

6.2.1. Input

The criteria, weighting factor, ranges (thresholds) and optional spatial radius used in the spatial model analysis are stated in table 6.6. Since the spatial model is parametric, the chosen weighting factors and ranges can be adjusted depending on the user's preferences. The chosen values for this study are shown in table 6.6; an elaboration can be found below.

Category	Criteria	Effect	Weighting factor	Range	Radius
Technical criteria			0.7	-	-
	Tidal current velocity	*Positive*	0.87	[0.63; ∞] m/s	-
	Bottom depth	*Negative*	0.13	[−40; 0] m	-
Secondary criteria			0.3	-	-
	Shipping intensity	*Negative*	0.50	[0; $2 * 10^7$] AIS positions	0.15625° (≈ 17.4km at the equator)
	Population size	*Positive*	0.25	-	1.5° (≈ 167 km at the equator)
	Energy usage	*Positive*	0.25	[5; ∞] TWh	1.5 deg (≈ 167 km at the equator)
Linkage opportunity	Islands: minimum distance between islands and main land: 0.494∘ (≈ $50km$ at the equator))				

Table 6.6: Spatial model input: weighting factors, ranges, and radius for each criterion

Elaboration on table 6.6

To combine the technical and secondary criteria, weighting factors are applied for both categories. A 70% to 30% balance was set between the technical and secondary criteria since the main focus lies on the technical feasibility. However, the secondary criteria are still of big importance, especially since the energy and shipping intensity filters are applied that keeps or discards locations.

Technical criteria

The weighting factors and ranges of the technical criteria were determined in chapters 6.1.2 and 6.1.3, respectively.

Secondary criteria

The shipping intensity, population size and energy usage are taken into account. As can be seen, the shipping weighting factor is higher (0.50) than for the other two (both 0.25). This has the following reasons:

- Disrupting shipping has a significant impact on a country's trade and, thus, economy. This makes the shipping intensity an important factor. The upper limit of normalization of the shipping intensity can be adjusted based on the user's preference. In this study, locations above 10,000,000 AIS positions were assigned a 1, which corresponds to the shipping intensity at the port of Belém (Brazil).
- Energy consumption has a significant influence by filtering the locations. If a location passes this filter, the location is feasible considering the energy usage. The population size is partly taken into account since the energy usage is determined using the population size and energy usage per person.
- The normalized population size and energy consumption together account for 0.5 of the secondary criteria. Both are included separately in the analysis due to differences in locations. Some locations have a low population size but high energy usage per person (northern countries, due to the cold climate conditions). Other locations have a high population size but low energy usage per person (for example India and Myanmar). It is possible that the locations that currently have a low energy usage per person need more energy capacity in the future due to economic growth; this could be an opportunity for DTP. Therefore, both the population size and energy usage are included as separate criteria in the analysis.

Energy filter
A filter is applied that includes locations with a minimum energy usage of 5 TWh in a radius of 1.5 spatial degrees (≈ 167km). The exact settings can be adjusted based on the user's preference. The range of 1.5 spatial degrees was chosen based on manual assessment. The minimum energy usage in an area was set to be approximately 5 times the energy production of one DTP dam (> 1 TWh); this has the following reasons (based on figure 4.2 in chapter 4.1):

- As can be seen in figure 4.2, in the case of sufficient energy capacity in the area, replacement of existing fossil fuel power plants is possible. Since DTP could not replace all energy sources in an area (an energy mix is always required), the threshold was set to replace a maximum of $\frac{1}{5}$ of the full energy production. Therefore, if one DTP dam generally produces around 1 TWh, an area with an energy usage of at least 5TWh is required.
- The energy threshold of 5TWh in a range of 1.5 spatial degrees is relatively modest (a standard DTP dam could have a capacity of 3 TWh). This conservative threshold removes all remote and low-population size locations but keeps the most potentially interesting locations in the analysis. A range of 1.5 spatial degrees combined with an average energy consumption of 21,000 kWh/person corresponds to 240,000 people in a range of 1.5 spatial degrees, which is a modest range.

An example that was found in the manual assessment of the energy filter is the island group (archipelago) Faeröer, which has a small population size of 50.000 people and uses 75.0000 kWh/person, resulting in an energy consumption of 4.125 TWh. The economy of this archipelago is not expected to grow rapidly; thus, additional power in the order of 1TWh is not expected to be needed in the future. Islands like Faeroöer are excluded from the analysis using the energy filter threshold values described above.

Shipping filter
A shipping filter is included in the spatial model, discarding all locations that lie within a high shipping intensity area. Locations that had 20,000,000 AIS positions were filtered out of the analysis. These were main marine routes, such as the English Channel, Strait of Malacca and routes towards major seaports such as Shanghai and Hongkong.

6.2.2. Results

Global overview of results

In total 66 suitable locations are found, shown in figure 6.10. The impact of the energy and shipping filters is addressed in section 6.2.3. All locations are classified into geographical regions (red squares in figure 6.10), and each region is analysed manually in more detail in section 6.2.4. At section 6.2.5, the results of the manual assessment of all 66 potential locations are summarized and analysed. Finally, at section 6.2.6, the conclusions of the spatial analysis are stated and elaborated on.

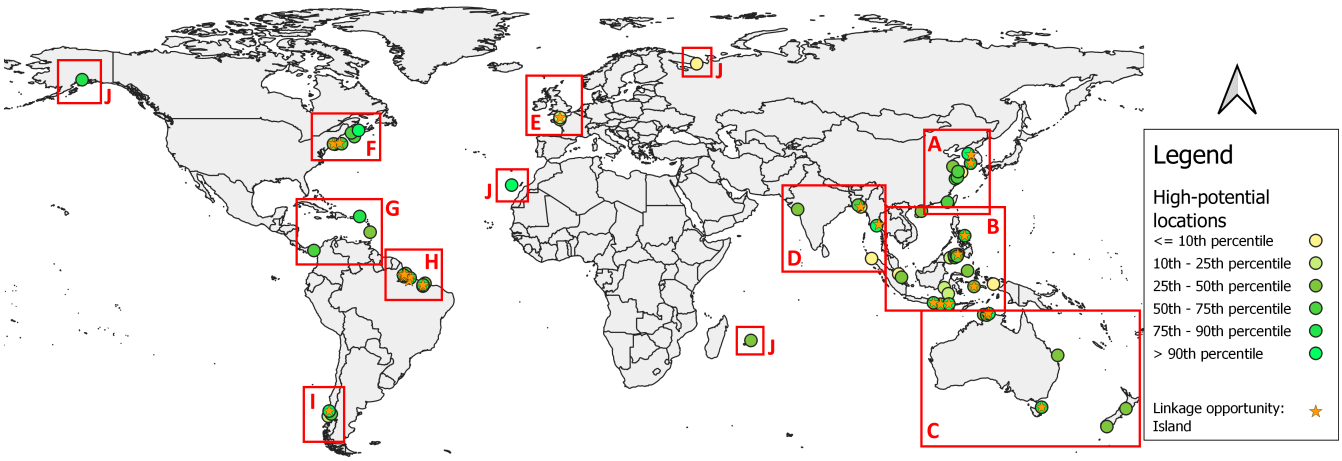

Figure 6.10: Spatial model result: 66 potential locations including potential island linkage opportunity. 10 regions are defined, marked A till J, that are analysed in detail in chapter 6.2.4. From yellow to green dots the lowest till highest potential, see table 6.7 for the Potential Index (PI) score per percentile class.

PI score	Percentile range
> 0.76	>90th percentile
0.53 - 0.76	75th - 90th percentile
0.37 - 0.53	50th - 75th percentile
0.28 - 0.37	25th - 50th percentile
0.19 - 0.28	10th - 25th percentile
< 0.19	< 10th percentile

Table 6.7: Potential Index (PI) scores and corresponding percentiles.

6.2.3. Model steps

The model steps and the number of potential locations in the analysis after each step are shown in table 6.8. Two filters are applied; a minimum energy usage filter and a maximum shipping intensity filter. Due to these filters, in total 223 locations are discarded. Excluding protected marine areas leaves a total of 66 potentially feasible locations. Of these locations, 25 are suitable to combine the island linkage opportunity.

Most locations removed by the shipping filter are located in Europe, the Yellow Sea and around Japan. The energy filter discards all locations that have an energy usage below 5 TWh, using a radius of 1.5° (≈ 167km). As can be seen in figure 6.11, a significant amount of remote locations are removed, especially in Hudson Bay, the Bering Sea, the Gulf of Alaska, the Argentine Sea, the coastline of Australia and the Sea of Okhotsk.

Step	Number of locations
Initial PI map	300
Filters: Energy & Shipping	77
Map constraint: Protected marine areas	66
Linkage opportunity: Island	25

Table 6.8: Number of locations still in the analysis after each model step

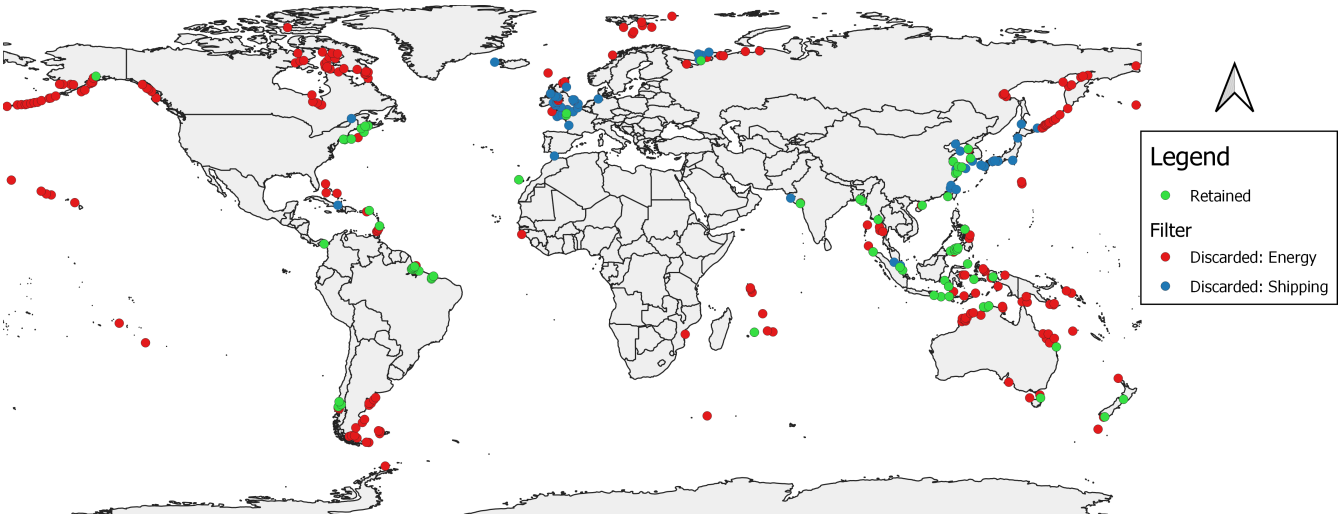

Figure 6.11: Spatial model filters. Discarded locations due to energy or shipping filters.

Sensitivity energy filter
As seen in figure 6.11, the minimum energy filter discards most locations. The influence of changing the energy filter parameters on the number of potential locations found is assessed, the results are summarized in tables 6.9 and 6.10.

As can be seen, a decrease in the energy threshold or an increase in the energy radius (radius in which the energy usage is calculated) results in an increase in potentially feasible locations found. The effect of increasing the energy radius parameter is stronger than decreasing the energy threshold by the same amount.

Energy threshold	Locations [-]	Increase [%]
Basis (5 TWh)	66	-
Decrease 20% (4TWh)	72	9%
Decrease 50% (2.5TWh)	87	32%

Table 6.9: Effect of decreasing the energy threshold on the number of potential locations

Energy radius	Locations [-]	Increase [%]
Basis (1.5 deg)	66	-
Increase 25% (1.87 deg)	79	20%
Increase 100% (3 deg)	93	41%

Table 6.10: Effect of increasing the energy radius on the number of potential locations

Island linkage opportunity
The threshold analysis showed that using islands as linkage opportunities reduces the required average flow velocity (Table 6.3). If this is taken into account in the spatial analysis, focusing only on linkage opportunities, the required mean flow velocity threshold can be lowered. Manual assessment will then determine whether there are indeed feasible linkage sites. The spatial model was run several times, lowering the required mean flow velocity threshold. The number of potential locations found is summarized in table 6.11.

Table 6.11 shows that by lowering the mean flow velocity threshold, more potential island linkage opportunities are found. For example, an island length of 20 km yields nearly twice as many potential linkage opportunity locations. It is recommended to take these locations into account in future studies.

Island length [km]	0	10	20	30
Mean flow velocity [m/s]	**0.63**	**0.53**	**0.45**	**0.39**
General [-]	66	89	122	157
Island linkage opportunities [-]	25	37	46	57

Table 6.11: Number of potentially feasible locations identified for different mean flow velocities, corresponding to the island linkage opportunity thresholds derived in chapter 6.1.2.

6.2.4. Regional analysis
The regions shown in figure 6.10 are analysed manually. All locations with a PI score above the 75th percentile (PI score > 0.53) are addressed in more detail. Additionally, several other locations are included in the analysis to provide additional interesting observations. For each region, the mean tidal currents (figure F.2) and bathymetry (figure F.3) maps are shown to provide additional information.

A: Yellow Sea

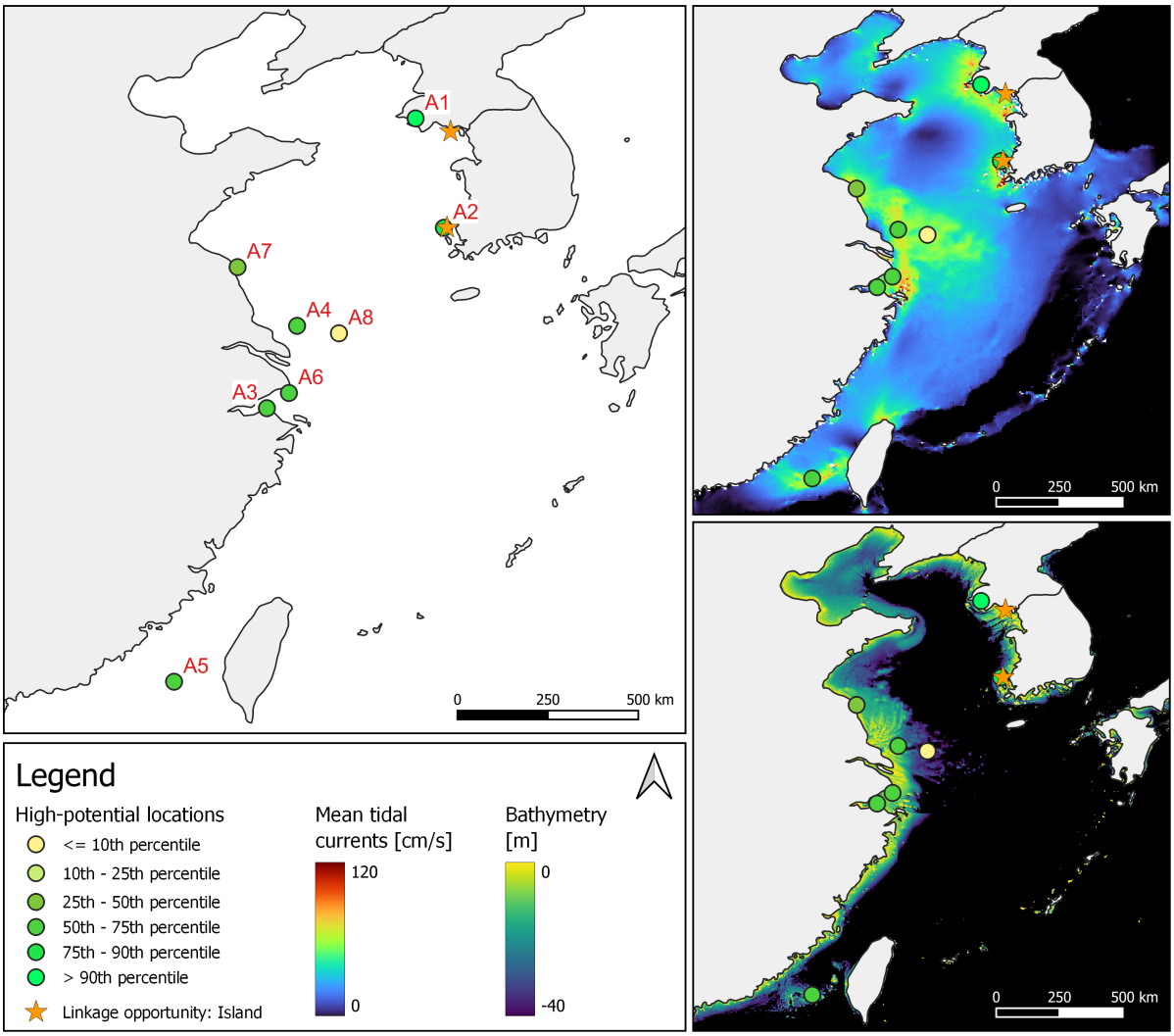

Figure 6.12: Potential locations in the Yellow Sea

General

The Yellow Sea experiences high tidal flow velocities and has a relatively shallow water depth. Due to these properties, most literature studies that examine Dynamic Tidal Power are focussed on the Yellow Sea (e.g. (Hulsbergen et al., 2008), (Park, 2018), (Dai et al., 2018), (Shao et al., 2017)). These studies only examined the technical aspects of a DTP dam, the shipping intensity and energy usage are not taken into account. The shipping intensity is shown in figure 6.13. Near the coastline of China, the shipping intensity is severe. The total PI score of locations near the coastline of China is degraded (locations A3, A4, A6, A7 & A8) and some locations are excluded by the shipping filter. At the east coast (coastline of North Korea and South Korea), the shipping intensity is less; therefore, the PI score of locations A1 and A2 is higher. In the north of the Yellow Sea Hulsbergen

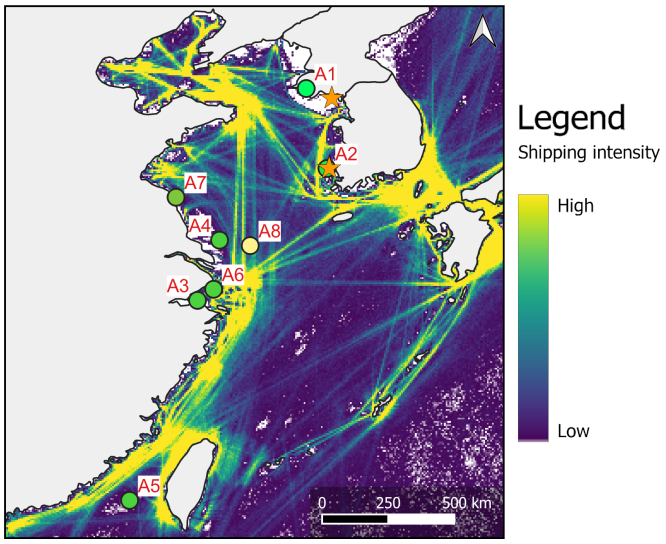

Figure 6.13: Shipping intensity in the Yellow Sea

et al., 2008 indicated three dam location possibilities. Figure 6.13 shows that the shipping is more intense in the north of the Yellow Sea; therefore, the locations in the north were not found to be feasible in this spatial analysis.

	A			Velocity [m/s]	
	Location	Rank	PI	Mean	Max
A1	Yellow Sea, North-Korea	1	0.89	1.3	2.9
A2	Yellow Sea, South-Korea	16	0.53	1.1	2.2

Table 6.12: High potential locations with PI score above 0.53 found in the Yellow Sea. Values are the maximum values found at these locations.

High potential: A1
At the coast of North Korea, large tidal flow velocities occur. This, in combination with the low shipping intensity and many island linkage opportunities, results in a high PI score of 0.89, placing it at the first rank of high potential to apply DTP. Additionally, the population size is large (5.4M people in a radius of 1.5°). At this moment, the energy usage per person is low (3.6 MW/person in 2019 (Bolt & van Zanden, 2020)). Therefore, this location could possibly benefit from a DTP dam in the future if the energy usage per person increases.

High potential: A2
The coast of South Korea is very suitable due to the high tidal flow velocities in the area; the location currently found is located in the north of the tip of South Korea. However, at the tip of South Korea, significantly higher flow velocities can be found (an average of 1.5 m/s and a maximum of 3 m/s). This location is currently discarded due to the high shipping intensity since the vessels sail around the tip (see figure 6.13). Placing the dam at the tip could generate significantly more energy; it is recommended to investigate this in a detailed case study.

Observation: A3, A4, A6, A7 & A8
The East-coast of China experiences high tidal flow velocities, especially in the south of Shanghai. However, due to the large shipping intensity (the seaport of Shanghai), the PI index is severely downgraded. The north of Shanghai experiences less shipping; therefore, this could be better suitable for DTP. Another possibility is to connect some of the southern islands of Shanghai. The Jintang Bridge currently connects the southern islands (Zhoushan). If a dam were constructed and connected with the southern island, an effective blockage length of at least 30km could be achieved, with a significantly lower construction length (≈10 - 15 km). However, it is highly debatable whether this is acceptable due to the blockage of shipping.

Observation: A5
This location is positioned in the middle of the strait between China and Taiwan; the distances between the shores of China and Taiwan are too large ($\pm$ 150 km). Therefore, this location would be better suited for constructing a detached DTP dam possibly.

B: Southeast Asia

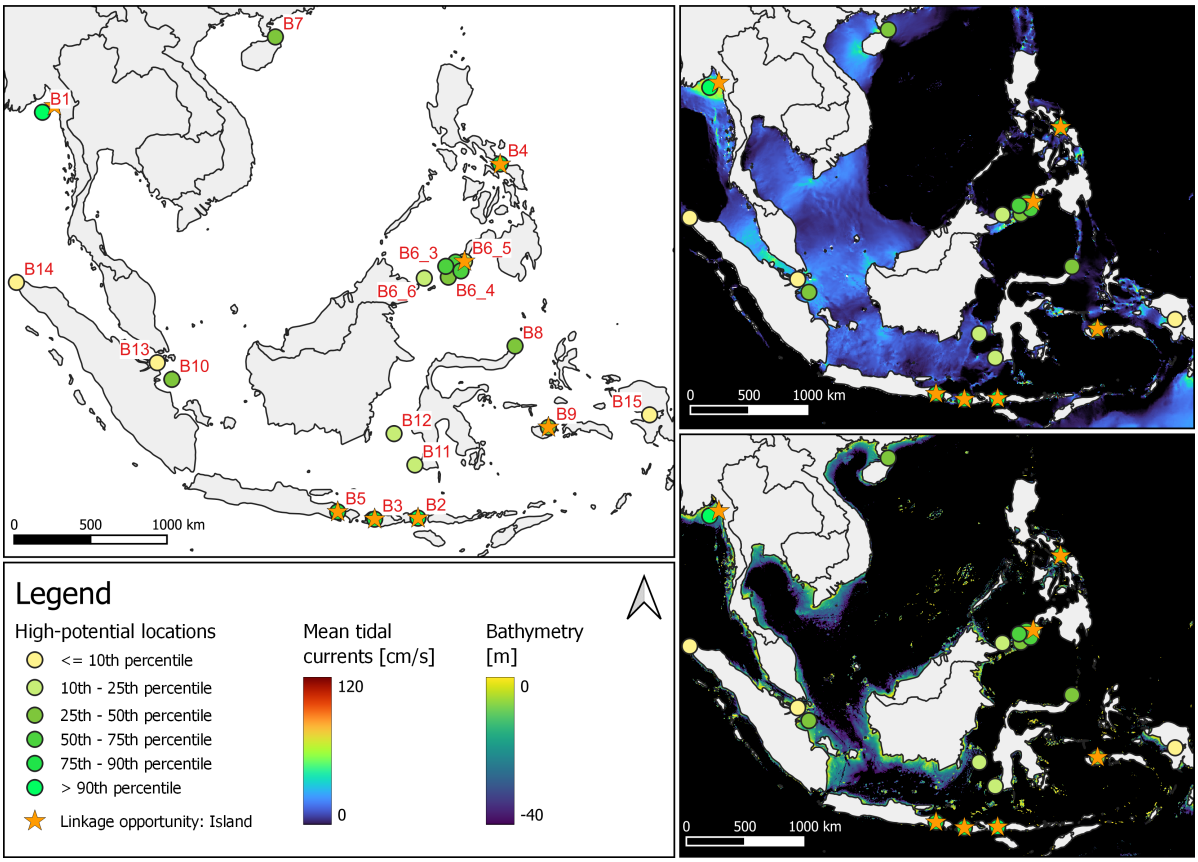

Figure 6.14: Potential locations in Southeast Asia

B: General

Southeast Asia counts numerous islands, many of which experience strong currents both around and between them. Potential locations are mostly identified in straits, where strong tidal currents and shallower water depths are found. One of the most important trade routes can be found in the strait of Malakka (Locations B10, B13 % B14).

	B			Velocity [m/s]	
	Location	Rank	PI	Mean	Max
B1	Andaman Sea, Myanmar	4	0.81	1.1	2.3
B2	Lintah Strait	5	0.79	2.3	5.5
B3	Alas Strait	12	0.64	1.2	2.7
B4	San Bernardino Strait	14	0.55	1.1	2.6
B5	Bali Strait	17	0.53	0.9	2

Table 6.13: High potential locations with PI score above 0.53 found in Southeast Asia. Values are the maximum values found at these locations.

High potential: B1

This location in Myanmar is assessed in more detail in chapter 6.1.1. It showed to be a location with high potential because of the shallow depth, high flow velocities, large population size and low shipping intensity.

High potential: B2, B3 & B5
These locations are positioned in three straits of Indonesia (Bali Strait, Alas Strait and Lintah Strait). High flow velocities are present, possibly higher than currently identified. This is because of the large grid size ($\approx 7x7$ km) compared to the strait width (Bali: 2.3 km, Alas: 14km and Lintah: 21km). In the straits of Alas and Lintah, a large water depth is found in the middle of the straits (> 70m deep). Therefore, it is challenging to construct large dam lengths, making these locations less suitable. The strait of Bali has a shallow water depth (≈20-30 m), but the strait has a small width. Therefore, these three locations are probably more suitable for applying the tidal stream method than the DTP method to extract tidal energy.

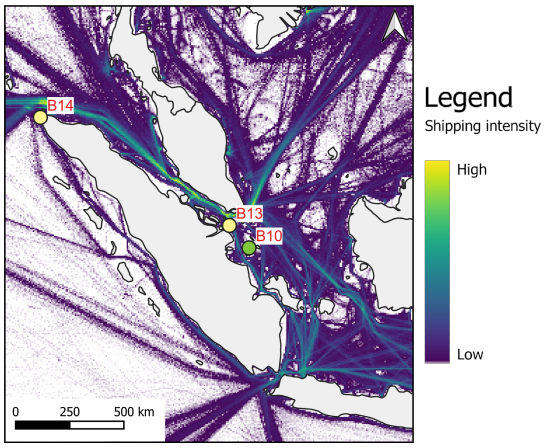

Figure 6.15: Shipping intensity in the strait of Malakka, generated using: (Cerdeiro et al., 2020)

High potential: B4
In the San Bernardino strait, high flow velocities occur, but the bathymetry shows a fast-increasing water depth towards a maximum depth of -140 m. Therefore, this location is possibly better suited to apply the tidal stream method or a combination between the tidal stream method and a partial blockage.

Observation: B10, B13 & B14
In the strait of Malakka and Singapore, some locations were found, but the PI index is below 0.4 because of the high shipping intensity. This is a desired outcome of the model since there is most likely no support to block a part of this important shipping strait with a DTP dam.

Observation: B6
This cluster of possible locations is located at the Sulu Archipelago, which is formed by tectonic tilting of the sea bottom. Due to this, the water depth of the Sulu Archipelago is relatively shallow (0m to -60m with a maximum depth of -200m) while the surrounding Sulu and Celebes seas are deep (≈ -5000m). This is beneficial for a DTP dam since the large ocean water mass induces a large inertia, possibly increasing the hydraulic head difference significantly and, thus, the DTP dam power output. This involves complex processes, detailed studies and the use of numerical models are required to retrieve a first understanding of the impact of a DTP dam in this area.

Observation: B12
This location is positioned in the middle of the Makassar Strait, 120km from the shore. This location would be better suited to apply a detached DTP dam. However, due to the significant distance towards the shore, the energy transmission cables will be costly. Therefore this location is probably not feasible.

Observation: Model identification of straits
As shown in figure 6.16, not all straits are included in the tidal currents dataset due to the low model resolution. The most Western strait of the eastern Lesser Sunda Islands has the smallest width of 700m, making this strait undetectable with the used tidal current dataset grid sizes ($\approx 7x7$ km at the equator).

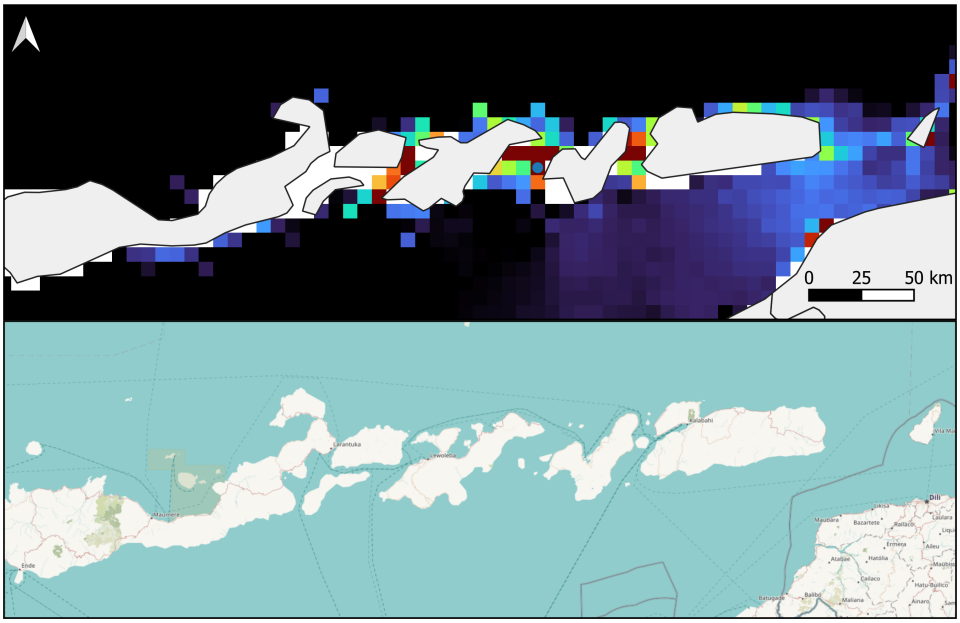

Figure 6.16: Example of the tidal currents model resolution in the straits of the eastern Lesser Sunda Islands.

C: Oceania

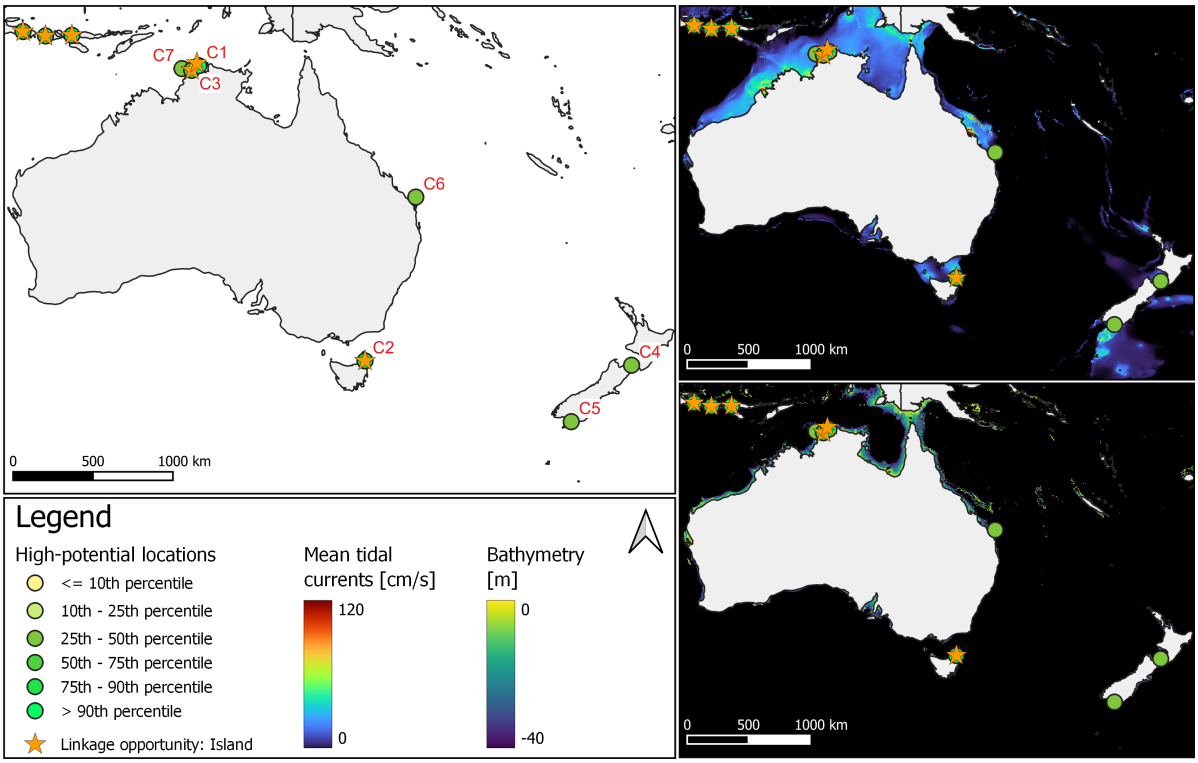

Figure 6.17: Potential locations in Oceania

C: General

Oceania has several regions where high flow velocities occur, in Australia mainly in the Timor Sea (C1, C3 & C7), the Bass Strait (C2) and the Great Barrier Reef (above C6). New Sealand experiences high flow velocities in the Cook Strait (C4) and at the south of the Island (C5). The Great Barrier Reef is a protected marine area; therefore, these locations are filtered out of the analysis.

	C			Velocity [m/s]	
	Location	Rank	PI	Mean	Max
C1	Australia	6	0.78	1.4	2.7
C2	Australia	11	0.67	1.1	2.2

Table 6.14: High potential locations with PI score above 0.53 found in Oceania. Values are the maximum values found at these locations.

High potential: C1, C3 & C7

Location C1 is located near the city of Darwin in Australia. One large linkage opportunity is present, several small islands can be connected to each other and the Tiwi islands. The dam would need to be 25km long, and this would allow for an effective length of up to 130km. However, there are several large constraints; firstly, the Tiwi Islands are a protected land area so the DTP dam should not impact this protected area in any negative way. Secondly, the impact of a dam of such size would be severe; a detailed study of the effects on the hydrology, morphology and ecology should be performed. It is highly debatable if this is desired. Possibly a smaller dam could be initiated that has less impact on the local hydrology, morphology and ecology.

High potential: C2

In the north of Tasmania, the flow velocities are high, and the water depth is relatively shallow (0 to -40m). This is a low-populated area (normalized population score of 0.01), but the benefits are low

shipping intensity and several linkage opportunities using islands. An effective length of 120 km could be achieved by constructing a 40km dam connecting three islands. There is also the option to construct a 30km long dam to achieve a 50km effective length, connecting two islands. These are both potentially feasible options.

Observation: North of C6
Several locations with high potential were found in the great barrier reef, which is a protected area. Therefore, these locations are automatically removed from the potential locations.

Observation: West of C1, C3 & C7
The northwest of Australia shows to have the highest tidal currents and sufficient bottom depth. However, these are low-populated areas, and therefore, these locations were removed. A follow-up study could be performed to investigate the costs of electricity transmission lines and whether these locations could still be feasible.

D: India & Bangladesh

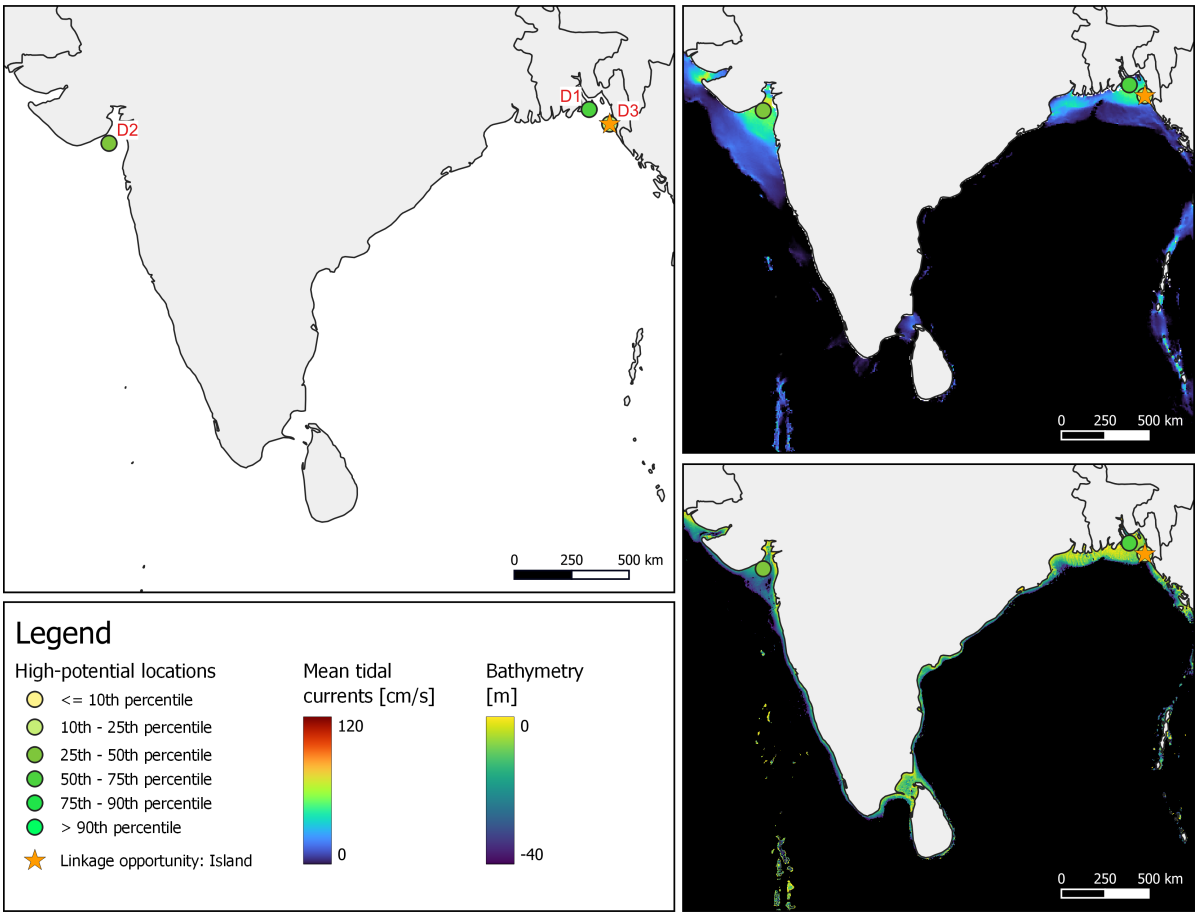

Figure 6.18: Potential locations in India & Bangladesh

D: General

In India and Bangladesh, several regions with high tidal flow velocities are present, shown in figure 6.18. What is especially interesting in these two countries is the population size. Both countries are densely populated, especially near the coast (see figure 6.19). Considering the population size of India and Bangladesh in relation to the prospected economic growth, the energy need in the future could be significant. Currently, the energy consumption per person in India and Bangladesh are 7,000 kWh and 2,700 kWh, respectively, which is quite low compared to more developed neighbouring countries (china, for example, consumed 31,000 kWh per person in 2021 (Bolt & van Zanden, 2020)). If India indeed experiences economic growth, significantly more energy is needed, giving a good opportunity for a DTP dam.

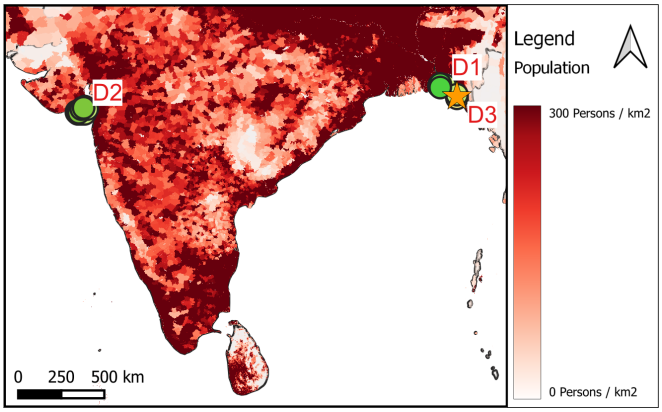

Figure 6.19: Population density in India, generated using: (CIESIN, 2020)

Observation: D1

This location is located in Bangladesh at the Ganges Delta. The flow velocities are lower than for other locations (mean: 0.7 m/s); therefore, the technical potential is low (0.23). The secondary potential is high (0.75) due to the large population size and low shipping intensity (the seaport of Chittagong is

located 100km eastward, and no shipping passes location D1). Since the energy usage per person is currently low (2.7 MWh/person in 2021 (Bolt & van Zanden, 2020)), an increase in future energy needs could be an opportunity for a DTP dam.

Observation: D2
The shipping ports Kandla and Hazira (Surat) are located nearby, so the dam possibly blocks these shipping lanes. Although the shipping intensity, a dam could be connected to the northern coastline (vessels should sail around the dam in this case). The population size is large, and there is moderate energy usage (7 MWh/person in 2021 (Bolt & van Zanden, 2020)), so the energy demand is probably sufficient.

E: Europe

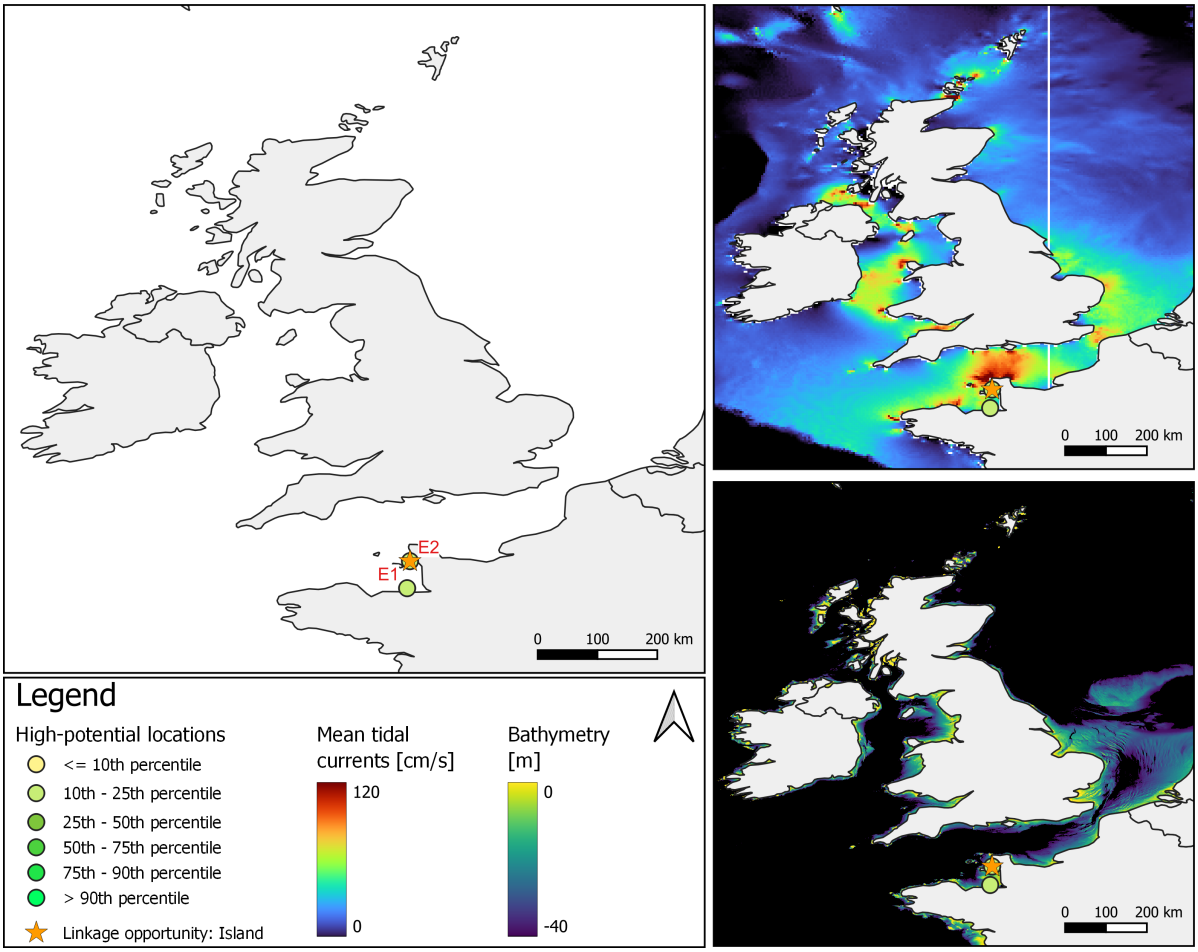

Figure 6.20: Potential locations in Europe

E: General

The tidal flow velocities are strong around the United Kingdom and Ireland, especially in the English Channel, the Irish Sea and near the Orkney Islands. However, due to the high shipping intensity, many locations were discarded, leaving only two possible locations E1 and E2. E1 is located near Saint-Malo, with an average flow velocity of 0.73 m/s. E2 is located near Jersey, with a higher average flow velocity of 1.1 m/s. A linkage opportunity is possible by connecting Jersey with the mainland (construction length ≈ 22km, effective length ≈ 38 km). Currently, the tidal wave that propagates through the English Channel propagates through this bay and induces high tidal amplitudes (at Saint-Malo tidal range of 13m possible). A DTP dam could increase the tidal range in the bay more, increasing the flood risk in the area. This complex system should be investigated in more detail.

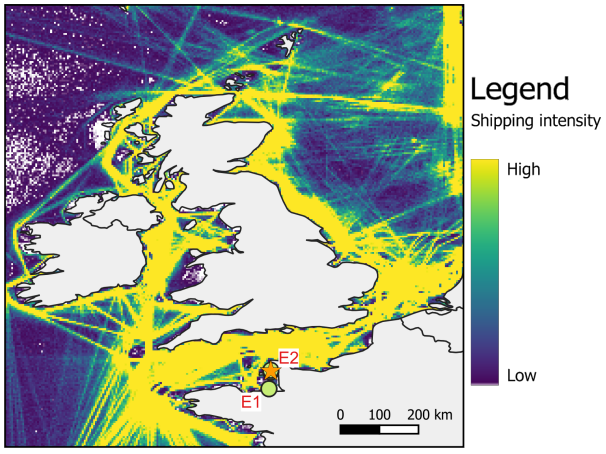

Figure 6.21: Shipping intensity in Europe

Observation: shipping

As can be seen in figure 6.21, there is a significant amount of marine traffic. Due to this, many locations in Europe were discarded because of the shipping density. It is recommended to investigate the marine traffic at the discarded locations. The additional sailing distance and the corresponding (economic) impact should be examined. Possible options are to accept the additional sailing distance or to construct a ship passage in the dam. This study will not go further into details on the discarded locations due to the shipping intensity filter.

F: North-America - U.S. & Canada

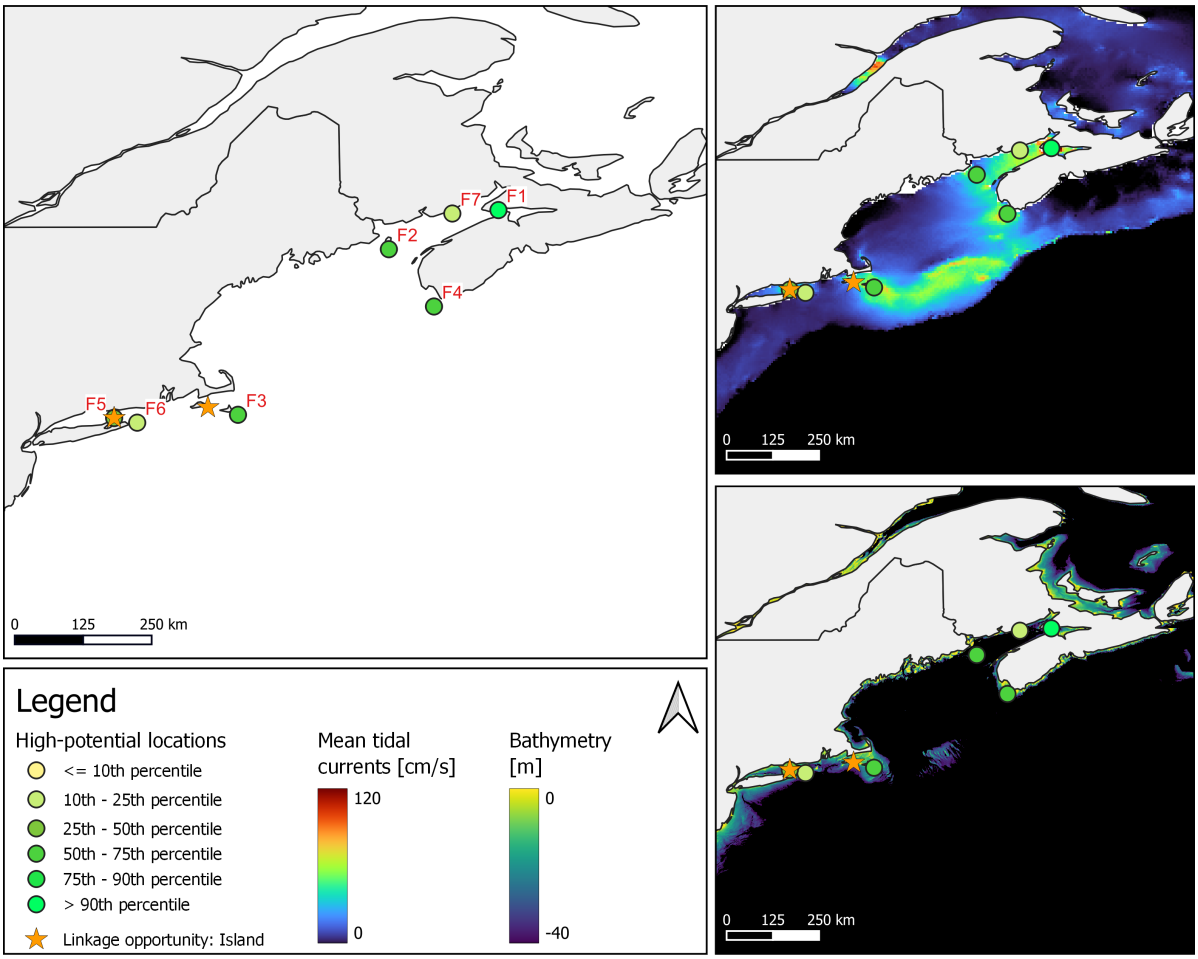

Figure 6.22: Potential locations in the U.S. & Canada

F: General

It is interesting to note that the location with the highest PI score is location F1, which is located the furthest inside the Bay of Fundy. Here, the tidal basin method is probably better suited to apply than DTP, since a high tidal amplitude of up to 12 m is present (NASA Earth Observatory, 2019).

Locations F2 and F4 are located at the Bay mouth and have a PI score of 0.45 and 0.38, respectively. At location F2, the DTP dam can be attached to the island Grand Manan, which lies in the middle of the bay mouth. Location F4 can be attached to the southern tip of Nova Scotia. Lastly, location F3 appears to be highly suitable for DTP. An island linkage opportunity is present since the water depth between the islands Nantucket and Dukes County is shallow.

	F			Velocity [m/s]	
	Location	Rank	PI	Mean	Max
F1	Canada	3	0.82	2.4	6

Table 6.15: Location with PI score above 0.53 found in North America. Values are the maximum values found at these locations.

G: Caribbean Islands and Central America

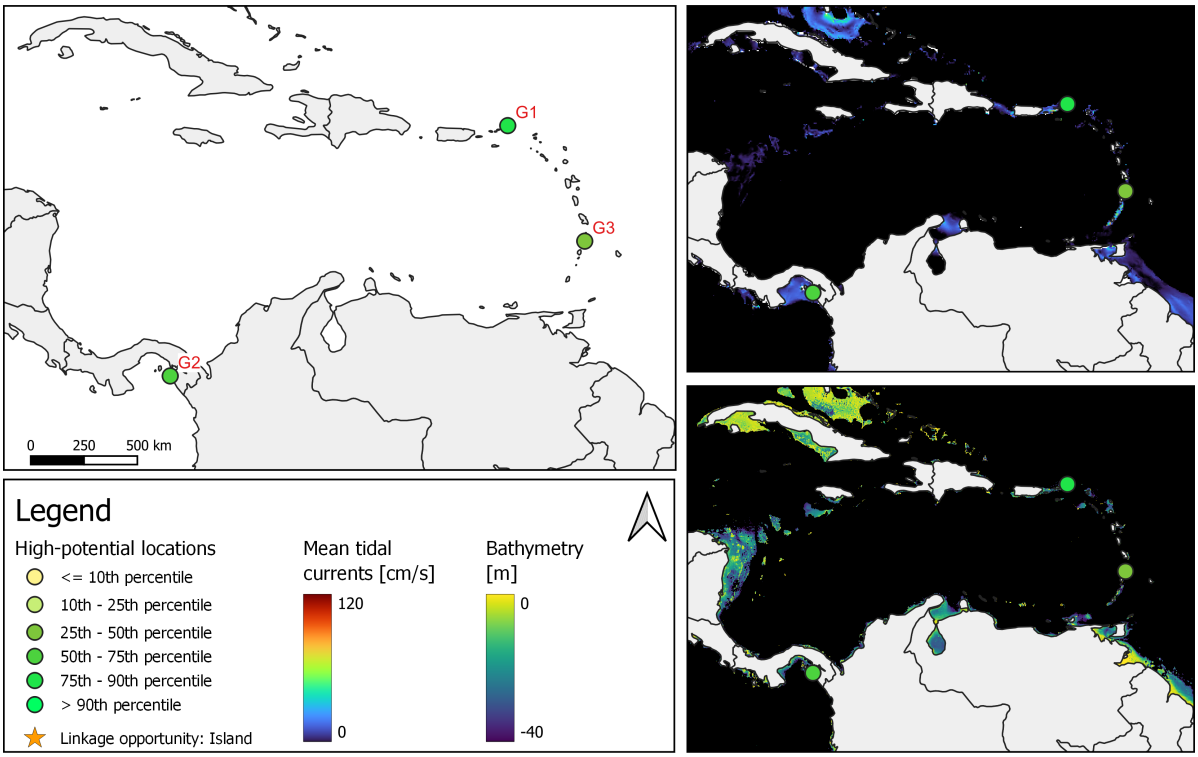

Figure 6.23: Potential locations at the Caribbean Islands and Central America

G: General
Locations G1 and G3 are positioned at the Caribbean Islands. Location G1 is positioned at the British Virgin Islands. The bathymetry shows that the water depth is relatively shallow in between the islands (smaller than -40m). Although the spatial model did not identify linkage opportunities at this location, it is possible to connect several islands. Therefore, this location indeed has the potential to apply DTP. This could be an attached or detached DTP dam based on the designed attachment point and orientation. At location G3, the depth increases quickly for longer dam lengths, towards deep water depths of more than -1000m. As a result, it is not possible to construct a dam longer than 6 km at location G3, making this location probably unfeasible to apply DTP. Location G2 is positioned in the Gulf of Panama. A depth of -60 meters is approached quickly, making this location less suitable for DTP as well due to high construction costs.

	G			Velocity [m/s]	
	Location	Rank	PI	Mean	Max
G1	British Virgin Islands	15	0.54	0.9	1.75

Table 6.16: High potential locations with PI score above 0.53 found in North America. Values are the maximum values found at these locations.

H: North-America - Brazil

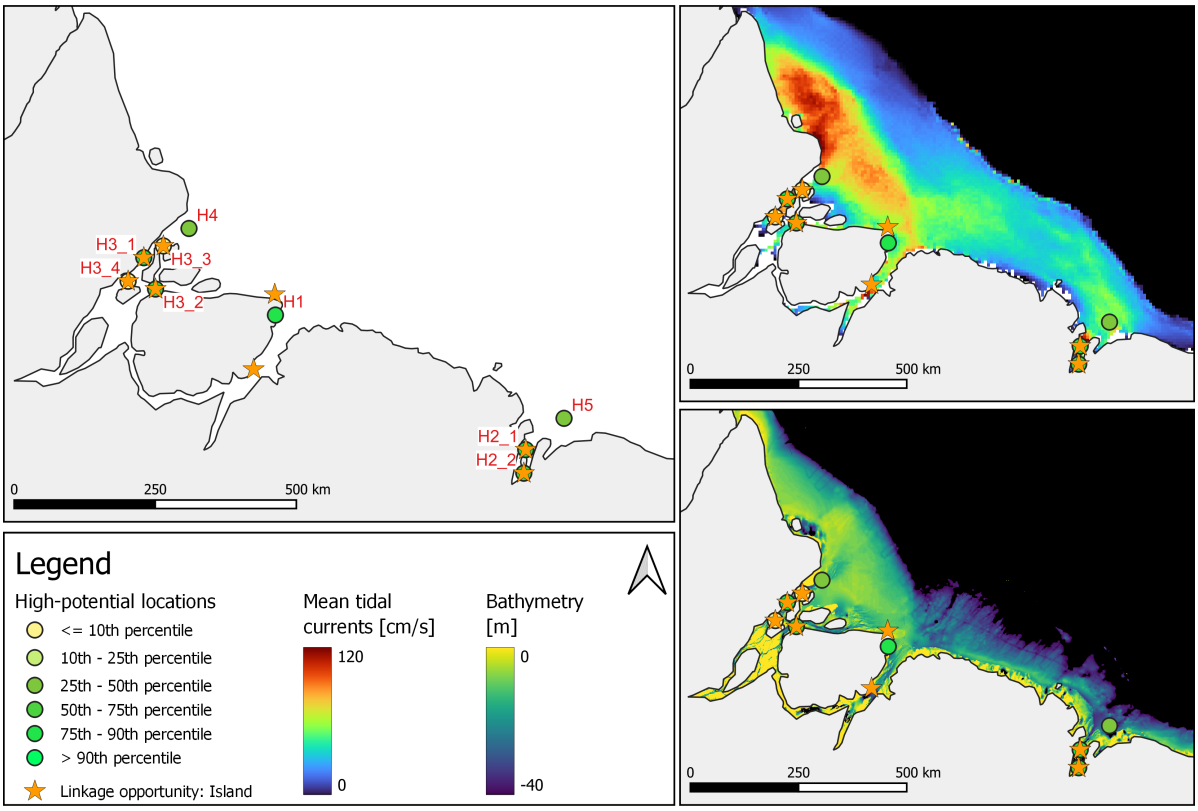

Figure 6.24: Potential locations in Brazil

H: General

Located in the Amazon Delta, this region is highly complex. The discharge of the amazon river is approximately 230,000 m^3/s, representing 20% of the global riverine discharge to the ocean (Moura et al., 2016). Figure 6.24 shows that high tidal current velocities are present at the coastline, especially in the north (Brazilian state Amapá). The water depth is generally shallow, with a slowly declining sea bed.

The high tidal current velocities in the north (Amapá) and the shallow water depth seem highly favourable to applying DTP, but no locations are identified in that region. The reason for this is the low population size and, thus, energy consumption in that area. It is advisable the investigate the possibility of transmitting energy over longer distances (several 1000km) using UHVDC (Ultra High Voltage Direct Current, see chapter ...). Taking longer distances into account, the energy filter radius can be increased, which probably also includes these remote northern locations in the analysis.

	H			Velocity [m/s]	
	Location	Rank	PI	Mean	Max
H1	Baía de Marajó, Brazil	9	0.71	0.85	1.95
H2	Baía de São Marcos, Brazil	10	0.67	1.3	2.55
H3	Amazone, Brazil	13	0.63	1.1	2.1

Table 6.17: High potential locations with PI score above 0.53 found in Brazil. Values are the maximum values found at these locations.

High potential: H1
H1 is located north of Baía de Marajó. Here, the shipping intensity is low. The grid cell that has the highest potential (0.71) corresponds to a mean flow velocity of 1 m/s. However, this grid cell is positioned inside the bay area, making this cell not representative of applying DTP. Outside of the bay area, the flow velocities are lower, reaching a mean of 0.8 m/s and a maximum of 2 m/s. These flow velocities are still sufficient, making location H1 a location with potential to apply DTP.

High potential: H2 & H5
Location H2 seems highly favourable, but when examining more closely, the high flow velocities are located in the Baía de São Marcos, which is no suitable location to apply DTP. At location H2, the tidal stream method is more suitable. Outside of the bay, location H5 is found with a PI index of 0.34. Although the PI index is lower, this location could be feasible to apply DTP.

High potential: H3 & H4
This cluster of locations is positioned at the main outflow area of the Amazon River, making it a highly complex system. Since the cluster of locations H3 are located inland in the delta, the tidal stream method is better suitable. Location H4 is suitable for applying DTP. However, please keep in mind that this is a complex region due to the large water discharge of the Amazon River, which also involves high sedimentation transport. The construction of a large dam at the outlet of the river will have large effects on the whole Amazon Delta, which should be investigated in detail and with high caution.

I: South-America - Chile

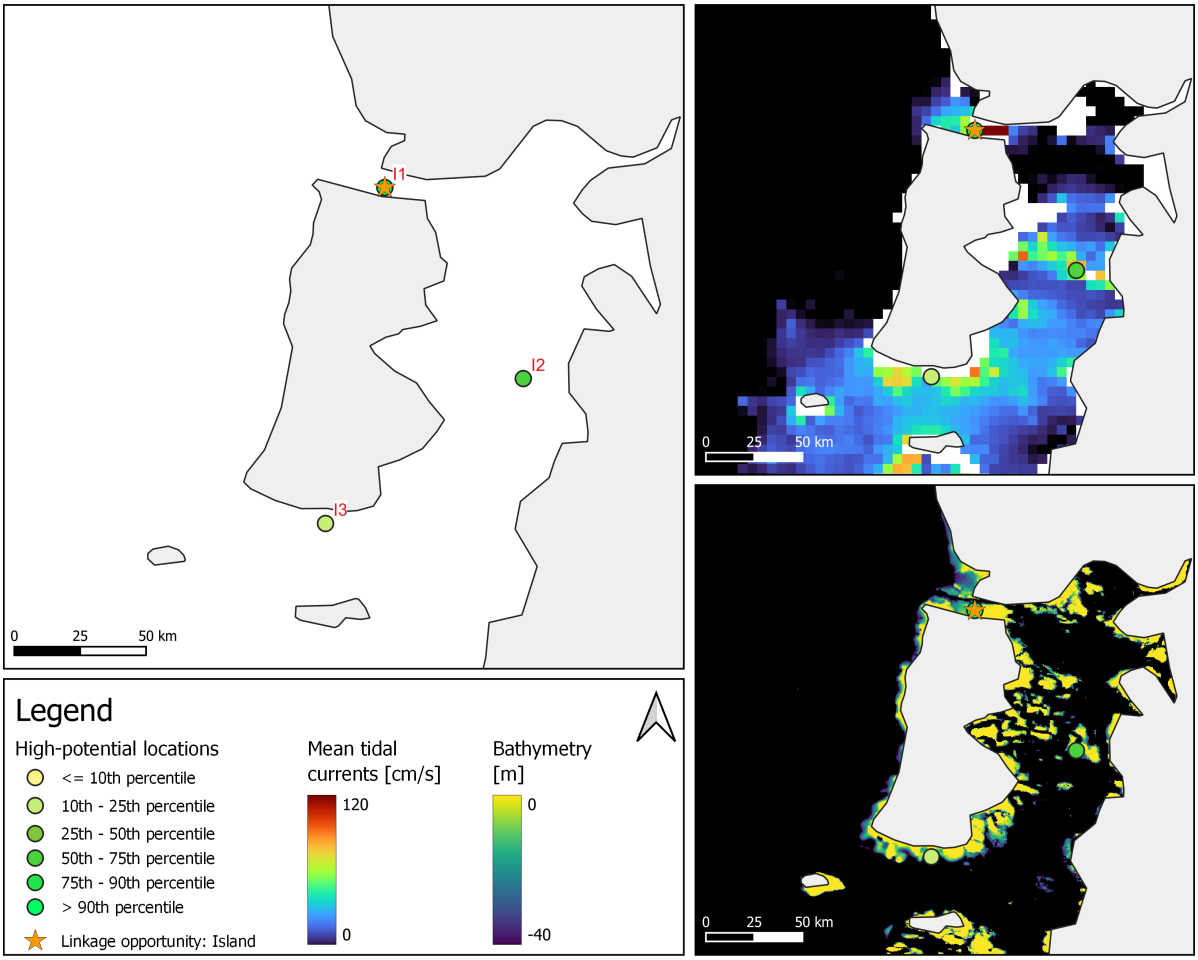

Figure 6.25: Potential locations in Chile

	I		Velocity [m/s]	
Location	Rank	PI	Mean	Max
I1	2	0.87	1.5	3.4

Table 6.18: Locations with PI score above 0.53 found in South-America. Values are the maximum values found at these locations.

High potential: I1

This location seems highly favourable (ranked 2nd) due to the high currents, low water depth and low shipping intensity. However, the location is positioned in a channel with a width of only 2 km, making this location favourable for applying the tidal stream method instead of DTP. Currently, the Puente Chacao bridge is constructed that connects Chiloé Island with the mainland of Chile, crossing the Chacao Channel. This bridge could be combined with tidal stream turbines.

Surprisingly, although the grid cell has a width of 7x7km, the mean flow velocities correspond well with real measurements at this location. Measurements conducted by Guerra et al., 2017 showed a mean flow velocity of approximately 1.4 m/s and a maximum flow velocity that exceeds 4 m/s. Guerra et al., 2017 also studied the potential power output using the tidal stream method and found a maximum annual energy production of 2.8 GWh.

Observation: remote locations South-America

The east coast of South America has several technically feasible locations, but due to their remote location, they are excluded from the analysis by the energy usage filter (see figure 6.26). Transmitting electricity from these remote regions to populated areas would induce high costs; therefore, these are considered not feasible in this analysis.

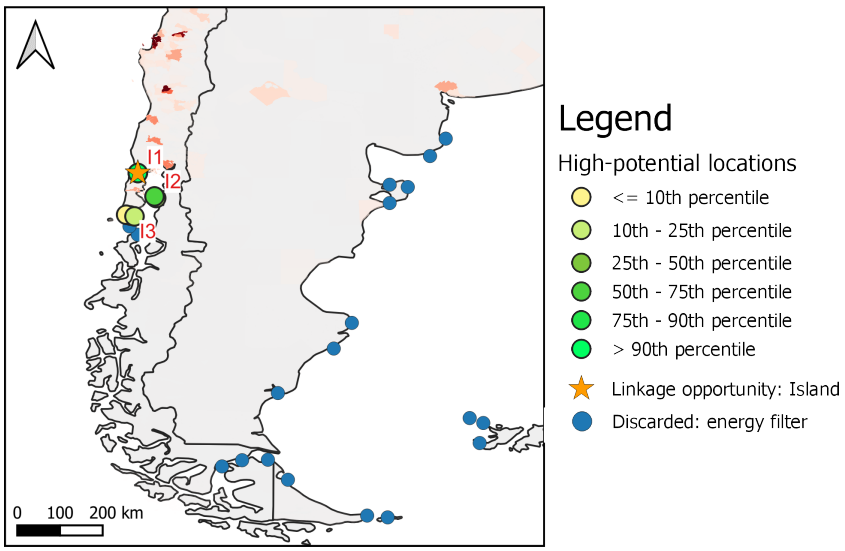

Figure 6.26: South America including the East-coast. The blue dots indicate the removed locations due to the energy filter. Population density is plotted to show the populated and remote locations.

6.2.5. Manual assessment of potential locations

All potential locations are assessed manually to validate the amount of correctly identified potentially feasible locations by the model. This manual assessment was done using the same criteria: mean tidal currents, bathymetry, shipping intensity, energy usage, future energy usage potential, linkage opportunities and other factors, if relevant.

Table H.1 shows the results of the manual assessment. Please note that this is no detailed assessment or case study; the locations are only checked to be potentially feasible or not feasible. If feasible for tidal power, the most suitable tidal extraction method is stated. If not feasible, the reason is stated. The manual assessment gives an indication of potentially feasible locations for tidal poewer but it is no exact assessment.

General results

The results are summarized in three pie charts, which can be seen in figure 6.27. Of all 66 potential locations, 55 (83%) are also identified as potentially feasible for tidal power in the manual assessment. Of these feasible locations, 41 (75%) were most suitable for DTP, 11 (20%) for the tidal stream method and 3 (5%) for the tidal basin method. Concluding, of all 66 potential locations, DTP is applicable at 41 locations (62%).

Reasons not feasible

The main reason for a location to be not feasible was a steep sloping sea bed. In most cases, one or two grid cells did suffice all criteria, but the surrounding cells were not suitable due to a water depth deeper than -40 m. Since one grid cell is approximately 7x7km at the equator, no long dam lengths can be constructed at these locations. Therefore, these locations were wrongly identified as feasible locations. An improvement of the model is possible in several ways. Firstly, a model requirement can be introduced: at least 3 adjacent grid cells need to match the criteria. Although this requirement would help exclude these steep sloping sea bed locations, it would also exclude other feasible locations, such as the tidal stream method (mostly identified by only one grid cell) or feasible DTP locations that match the model requirements on only one grid cell. Therefore, for further research, it is recommended to introduce a bed slope model criteria: if the bed slope between three grid cells is steep and only one grid cell matches the criteria, the location is excluded. The shipping intensity was only insufficient at one location, which shows the efficiency of the shipping filter in the model.

Linkage opportunity: Island

Remarkably, at 24 of 55 feasible locations (44%) the island linkage opportunity was available. This is higher than the initial 19 island linkage opportunities identified by the spatial model.

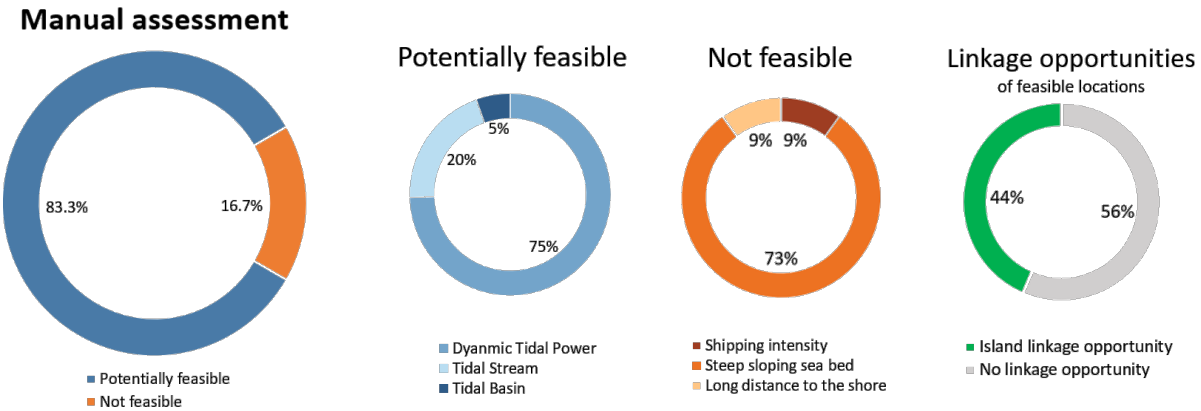

Figure 6.27: Pie charts summarizing the manual assessment of all potential locations

6.2.6. Conclusions spatial analysis

The main conclusions from the detailed analysis of regions (section 6.2.4) and the full manual assessment (section 6.2.5) are summarized below:

Tidal extraction methods

The manual assessment of all locations (section 6.2.5) showed that of all feasible locations, 75% were suitable for DTP, 20% for the tidal stream method and 5% for the tidal basin method. Since this research is focused on finding potentially feasible locations for DTP, the high proportion of locations suitable for DTP (75%) is a desired outcome.

The tidal stream method accounts for 20% of the potentially feasible locations. This is still a remarkably high percentage since the tidal currents dataset used has a low resolution (1/16°x1/16° or ≈ 7x7 km grid at the equator). This grid size is large compared to narrow straits where the tidal stream method is mostly applicable. Figure 6.16 in section 6.2.4 showed that not all straits are included in the tidal currents dataset and thus the analysis. Therefore, it is expected that many locations suitable for the tidal stream method are undetected. Additionally, due to the low resolution, the magnitude of the tidal currents is most likely not accurate. Concluding, the spatial model does identify several suitable locations for the tidal stream method, but it is not suitable to detect all tidal stream locations correctly. This is a desired outcome since the main focus lies in identifying suitable DTP locations.

The tidal basin method was suitable at only three locations (5%), all positioned in large bay areas. The limited number of tidal basin locations can be attributed to the setup of the spatial model; it is limited to the coastline and does not involve smaller bays, estuaries or basins. The resolution is too low to include all possible basin locations. However, also this is a desired outcome since the focus lies on locations where DTP is applicable. Nevertheless, it should be kept in mind that the model is not suitable to specifically use for finding the tidal basin method; the set-up of the spatial model should be adjusted if studying this is desired.

Steep sloping sea bed

Of all locations that were marked as not feasible in the manual assessment, 73% did have a steep sloping sea bed. Due to this, the bed level decreases rapidly to depths where a DTP dam is costly (deeper than 40m) or technically not possible to construct (deeper than 100m). Therefore, this rapid decrease in bed level prevents the possibility of constructing a long dam. At most of these locations, a maximum dam length of 7 to 14 km could be constructed, which is too short to induce a sufficient hydraulic head. As mentioned in section 6.2.5, this model limitation could be mitigated by introducing a bed slope model criteria to filter these locations out of the analysis.

Island linkage opportunities

A relatively high share of island linkage opportunities was found; at 44% of all feasible locations. An explanation is that islands form an obstruction; tidal currents need to flow around the islands (where the water depth is shallower as well). This causes flow contraction and, thus, higher flow velocities. The combination of high flow velocities and shallower water depths are the main technical criteria for DTP. This explains the high share of island linkage opportunities.

As shown in table 6.11, lowering the mean flow velocity threshold results in more potentially feasible island linkage opportunities. If an island length of 20km is assumed, the flow velocity threshold becomes 0.45, which results in 45 potential island linkage opportunities, almost two times as much as the initial analysis found (25). These locations should be assessed manually to check if an additional effective blockage length of 20km can be achieved. This could be an interesting result to investigate in further studies.

Remote locations

As seen in table 6.8, an initial set of 300 potential locations was identified. However, a significant number of these locations (223 locations) were discarded due to insufficient energy needs in the direct area. These remote locations could have a high technical potential, but the generated energy cannot be used. Therefore, the possibility of transmitting energy over long distances should be studied. This could be done using Ultra High Voltage Direct Current (UHVDC) transmission lines, which can transfer energy over distances of more than 1000 km. If the benefit of electricity production outweighs the costs of construction and energy transmission, it may be economically beneficial to build a dam in a remote

location. Therefore, an additional study on remote locations should be performed, including the costs of energy transmission.

6.2.7. Result: top 10 highest potential locations

The 10 locations with the highest potential for the DTP method are shown in table 6.19, including the normalized values for each criterion. The locations consist of multiple (clustered) grid cells; the number of grid cells at that location is also shown in the table.

For all location results, including potential locations suitable for the tidal stream or tidal basin methods, see table H.1.

Rank	Location	Country	Coordinates		Potential			Normalized score					Number of cells	Island: Linkage Opp.
			Longitude	latitude	Total	Technical	Secondary	Currents	Bathymetry	Shipping	Population	Energy		
1	A1	North Korea	125.2221	38.07597	0.89	1.00	0.65	1.00	1.00	0.80	1.00	0.008	112	✓
2	B1	Myanmar	96.71593	15.72637	0.81	0.85	0.73	0.82	1.00	0.96	1.00	0.005	397	-
3	C1	Australia	131.7126	-11.5841	0.78	0.94	0.41	0.93	1.00	0.81	0.01	0.003	33	✓
4	H1	Brazil	-48.4937	-0.50239	0.71	0.69	0.75	0.64	1.00	0.99	1.00	0.027	213	✓
5	C2	Australia	148.09	-40.6565	0.67	0.75	0.49	0.80	0.40	0.98	0.01	0.003	15	✓
6	G1	British Virgin Islands	-64.2187	18.59871	0.54	0.59	0.41	0.54	0.95	0.78	0.07	0.002	1	✓
7	A2	South Korea	125.9783	35.1542	0.53	0.61	0.36	0.55	1.00	0.17	1.00	0.115	15	✓
8	B6_1	Philippines	121.789	6.225616	0.52	0.47	0.65	0.49	0.35	0.97	0.65	0.004	7	✓
9	C3	Australia	131.0156	-12.0365	0.49	0.53	0.40	0.46	1.00	0.79	0.01	0.003	17	✓
10	B6_2	Philippines	121.4709	6.750662	0.47	0.40	0.64	0.31	1.00	0.97	0.62	0.003	3	✓

Table 6.19: Spatial analysis result: top 10 highest potential locations suitable for DTP

7

Discussion

This study focused on finding locations that have the highest potential to implement the Dynamic Tidal Power concept. The feasibility of DTP was investigated by identifying key criteria and finding the influence of these criteria on energy production, costs and energy price. These findings were used to find geographic regions with high potential for DTP. Additionally, linkage opportunities were identified, assessed and mapped to possibly improve the feasibility of DTP. This chapter reflects on the research findings, the implications and the limitations.

Based on a sustainable feasibility study framework, the key aspects can be categorized into three main categories; technical, economic and social-ecological feasibility. The literature study found that for DTP to be economically competitive, the upper limit of the Levelized Cost of Energy (LCOE) is approximately 0.1 €/kWh. Using this LCOE limit, the threshold analysis found that a mean flow velocity of at least 0.63 m/s is required to be technical and economically feasible (under the conditions of a maximum dam length of 50km and a depth of -20 m). The tidal flow velocity proved to be more influential on the feasibility than the depth, finding weighting factors of 0.87 and 0.13, respectively. These findings were included in the spatial model in combination with secondary criteria. Using a Multi-Criteria Weighted Overlay Analysis (MCWOA) approach, 66 potential locations were identified. The geographic regions with the most potential were found to be the Yellow Sea, the seas in Southeast Asia, and the seas of Oceania. The Yellow Sea was designated as a high-potential area by previous literature (Hulsbergen et al., 2008), (Dai et al., 2018).
The island linkage opportunity proved to be highly valuable. Connecting an island increases the effective blockage length, resulting in a hydraulic head and power output increase with approximately the same dam construction costs. The threshold analysis showed that using an island as a linkage opportunity lowered the mean tidal current speed required for achieving an LCOE of 0.1 €/kWh from 0.63 to 0.39 - 0.57 m/s, dependent on the island length. In the manual assessment of the spatial analysis, a high share of islands was found at all feasible locations (44%).

The hydraulic model formed the basis of the threshold and sensitivity analysis. The analytical equations used to determine the hydraulic head are based on the papers of Talstra and Pak, 2020, Anteagroup, 2018, Tidal Bridge bv, 2020 and Swamee, 1992. Several studies found a higher hydraulic head using a numerical model compared to analytical equations (Hulsbergen et al., 2008) and (Dai et al., 2018). A higher hydraulic head would have a significant impact on the results of the threshold and sensitivity analysis. Since this study is focused on the general feasibility and finding suitable locations, no exact location is known. Therefore, the basic analytical equations are used, which probably underpredicts the actual hydraulic head.

The design and associated construction costs integrated into the hydraulic model follow a conservative approach for shallow water depths. The caisson wall thickness is large (1 m) for both internal and external walls, reinforced concrete is used, and conservative material prices are applied. As was seen in the comparison of the total costs with literature, for a water depth of 20m, the costs were higher

(330 M€/km including turbines, 250 M€/km excluding turbines) than the costs of two out of three reference projects (250 M€/km including turbines, 140 M€/km excluding turbines). The design scales linearly with increasing depth by increasing the caisson height. However, the caisson dimensions, wall thickness and additional construction costs (larger construction dock needed) do not increase with increasing depth. Since deeper depths require significant strengthening of the caissons, it is expected that the model will underestimate the construction costs at greater depths ($\approx -40m$). Concluding, the hydraulic model probably overpredicts construction costs for shallow water depths and underpredicts costs for deep waters. The model could be improved by scaling the full design and corresponding costs with increasing depth, which will result in a more exponential growth in costs. This limitation in the construction costs calculation affects the threshold and sensitivity analysis and, thus, the spatial analysis.

The threshold analysis is based on a relatively shallow water depth of -20m, which is the depth where globally the highest flow velocities occur (chapter 5.2.3). As described above, at this depth the costs are probably overpredicted. Taking into account that the hydraulic head is determined by equations that probably underpredict the actual hydraulic head, the actual energy generation is possibly higher. This means that the LCOE determined by the hydraulic model is probably an underprediction of the actual LCOE. However, the target LCOE used was 0.1 €/kWh, which is the upper limit. Dependent on the energy market prices in an area, it is possible that the LCOE should be lower to be feasible. Concluding, the actual LCOE is probably lower than currently determined by the hydraulic model, but at an actual location, the target LCOE could also be lower. The actual feasibility at a location should be determined by using numerical models, making a detailed design at that specific location and analysing the local energy market to determine the required LCOE.
Since the costs are underpredicted for deeper water, the required mean flow velocities are possibly higher to compensate for higher real construction costs. This, in combination with the smaller tidal current speeds found in deeper waters (section 5.2.3), results in low feasibility in deep waters.

Considering the sensitivity analysis, surprisingly, the LCOE showed to decrease with increasing water depth. This effect is explainable since an increase in depth increases both energy production and construction costs. However, if the construction costs were included more realistically (exponential increase in costs with increasing depth), it is likely that the LCOE would increase with increasing water depth. Therefore, the depth was negatively incorporated in the spatial analysis; the depth was normalized from -20 to -40 with scores between 1 and 0, respectively. This assumption is debatable and should be investigated in more detail by improving the scaling of the design and construction costs for increasing depth in the hydraulic model.

Since this study assesses no specific location, it approaches a general design and corresponding costs. Location-specific labour prices, material availability, or other factors could significantly influence construction costs. This, in combination with the possible underprediction of the hydraulic head, comes with uncertainties regarding the hydraulic model results. Therefore the hydraulic model can be used as a first approximation of the feasibility, but a detailed case study is required in order to exclude a potential location definitively.

The target LCOE, it was set to the upper limit (0.1 €/kWh) not to exclude feasible locations beforehand. However, doing this requires additional assessments of the actual feasibility of detailed locations.
Concerning the total Potential Index (PI) score in the spatial analysis, it relies on two criteria: the technical PI and secondary PI, each assigned weighting factors of 70% and 30%, respectively. This ratio is used since the technical feasibility is considered more important for an initial assessment. However, it's important to note that these values lack an exact supporting theory and should be treated as rough assumptions rather than precise values.

Although the secondary weighting factor is lower, the secondary criteria proved to be highly valuable. The energy and shipping filters had a significant impact by discarding all remote, low-energy usage and high-shipping intensity locations, keeping only 77 out of 300 technically suitable locations.
The applied magnitude and range of the energy filter are debatable. The energy capacity threshold (5TWh) was based on replacing a maximum of 1/5 of the current energy production in an area and the range (1.5°) by manual assessment of the retrieved locations. These values are not exact and should be adjusted according to user preference. As seen in tables 6.9 and 6.10, lowering the energy filter thresholds increases the number of potentially feasible locations, providing more locations but simul-

taneously increasing the workload for the manual assessment.

Considering linkage opportunities, the usage of an island to increase the effective dam length has a significant impact on the technical feasibility of DTP. It was advantageous that a relatively high share of island linkage opportunities (44%) was found. The main explanation is that areas with high currents are typically associated with shallow water depth regions with narrowing land boundaries or islands, which create additional flow contractions. Therefore, naturally, more locations with islands are found. The island linkage opportunity requires a lower mean flow velocity threshold to be feasible, dependent on the island length. Assuming an island length of 20km resulted in 45 potential island linkage opportunity locations (table 6.11), which is almost twice the number of islands the initial spatial analysis showed (25). It is interesting to investigate this in future studies.

The manual assessment of potential locations (chapter 6.2.5) showed that of all 66 potential locations, 55 (83%) are identified as potentially feasible for tidal power. Of these feasible locations, 41 (75%) were most suitable for DTP, 11 (20%) for the tidal stream method and 3 (5%) for the tidal basin method. Since DTP uses substantial dam lengths above 30 km, the grid cell dimensions used in the spatial model (1/16° ≈ 7.5x7.5km at the equator) are sufficient to identify suitable locations for DTP (one dam spans at least four grid cells or more). However, it is important to note that local flow velocities close to the coastline or shallow areas can be substantially different.
Although the spatial model did find locations that are more suitable to apply the tidal stream method, the grid cell dimensions are too large to identify these locations accurately. Additionally, this low model resolution cannot accurately predict the magnitude of the tidal currents in small straits. This is no issue for this research since the focus lies on identifying DTP locations. The tidal basin method was applicable at three locations, all positioned in large bay areas. The reason for finding only three locations is the setup of the spatial model; it is limited to the coastline and does not involve smaller bays, estuaries or basins. This is desired for this research since the focus lies on DTP.
The main reason for a location to be unfeasible was a steep sloping sea bed. At these locations, the bed level decreases rapidly to depths where a DTP dam is costly (depth > 40m), making it expensive to construct longer dam lengths. Therefore, these locations were marked unfeasible manually. This model limitation could be mitigated by introducing a bed slope model criteria to filter these locations out of the analysis.
At one location, the actual shipping intensity was too high, making that location unfeasible. Since this only was one location, it can be concluded that the shipping filter was effective. This is mostly due to a model improvement made; the shipping radius determines the shipping intensity using multiple neighbouring grid cells. This was a valuable model improvement.

As stated in section 4.1.3, the impact on the ecology was partially included in the study by discarding locations that lie in protected marine areas from the spatial analysis. However, the ecological impact on all potential locations is widely unknown. DTP actively changes hydrological current patterns, the tidal range and thus also the morphodynamic and ecological evolution in an area. At this moment, only one study is conducted on the social-ecological effects of a DTP dam (Berlee et al., n.d.). Since the ecological impact is of severe importance, more detailed studies should be conducted on the actual impact of a DTP dam. Possible solutions to mitigate negative effects on the ecology and adjustments to improve the ecology in the area should be examined. This is a crucial but understudied part of the feasibility of DTP.

The LCOE was included to determine the economic feasibility. However, the financing of a project is another important economic factor. The total construction costs of a DTP dam are high (in the order of € billions). Since no DTP dam has ever been built, the technology is not empirically proven. This probably makes the attraction of investors in a DPT project challenging. Considering the substantial capital investment required, this is an important aspect.
With respect to sea level rise and the increase in population size in flood-prone areas (Tellman et al., 2021), flood risks are highly important to take into account. A DTP dam increases the tidal range at both sides of the dam, meaning that the tidal range in the surrounding area will increase. This increase in tidal range could increase flood risks in an area. This effect can be examined in a detailed case study. Another option is to expand the current spatial analysis, including an additional flood risk dataset as secondary criteria. By doing this, flood-prone areas could be excluded from the study or the PI score

in these areas lowered.

Despite the limitations of the model, this study provides an initial assessment and mapping of potential locations for DTP. Considering the feasibility of DTP, the impact of many factors are still uncertain. The impact of a DTP dam on the ecology, morphology, hydrodynamics and flood risks is largely unknown. Looking at the technical feasibility, it is possible to construct a DTP dam with current technologies. However, since a DTP project requires a large capital investment, financing will be challenging. Lastly, DTP can only be applied at specific locations where the tidal currents, bathymetry and secondary factors suffice. Therefore, the identified 66 locations in this study should be examined in more detail to assess the actual global feasibility of DTP. The island linkage opportunity proved to be highly valuable, these 25 locations should be studied in more detail.

Concluding, Dynamic Tidal Power has the potential to be feasible, but many aspects should be studied in more detail. The impact of a DTP dam on the ecology, morphology, hydrodynamics and flood risks should be examined extensively. The potentially feasible locations identified in this study provide a first step for detailed studies to investigate the potential for DTP at specific locations. Possibly this will result in the construction of the first DTP dam in the future.

8

Conclusion

The main objective of this study was to identify locations that have the highest potential to implement the Dynamic Tidal Power concept. By investigating the feasibility criteria and their influence and translating these criteria to a spatial analysis, geographic regions with high potential were identified. Additionally, linkage opportunities were assessed and identified.

The geographic regions with the highest potential to implement DTP are the Yellow Sea, the seas in Southeast Asia, and the seas of Oceania. This is due to a combination of high tidal current velocities, relatively modest water depths and a good combination of secondary criteria (energy usage, population size and limited shipping disruption).

Based on a sustainable feasibility study framework, the key aspects can be categorized into three main categories; technical, economic and social-ecological feasibility. For DTP to be economically competitive, the upper limit of the LCOE is approximately 0.1 €/kWh. Using this LCOE limit, the threshold analysis determined that a mean flow velocity of at least 0.63 m/s is required for DTP to be technical and economically feasible (under the conditions of a maximum dam length of 50km and a depth of -20m). The tidal flow velocity proved to be more influential on the feasibility than the depth, with weighting factors of 0.87 and 0.13, respectively.
Additionally, the island linkage opportunity proved to be highly valuable. The threshold analysis showed that using an island as a linkage opportunity lowered the mean tidal current speed required for achieving an LCOE of 0.1 €/kWh from 0.63 to 0.39 - 0.57 m/s, dependent on the island length.

These findings were included in the spatial model in combination with secondary criteria. Using a Multi-Criteria Weighted Overlay Analysis (MCWOA) approach, datasets and weighting factors were combined for each criterion, and a Potential Index (PI) score was defined. In total 66 potential locations were identified. Manual assessment showed that 55 (83%) locations are potentially feasible for tidal power. Of these feasible locations, 41 (75%) were most suitable for DTP, 11 (20%) for the tidal stream method and 3 (5%) for the tidal basin method. To conclude, DTP is potentially feasible at 41 of the 66 identified locations (62%)

The manual assessment of the spatial analysis identified a relatively high share of island linkage opportunities (44%). An explanation is that areas with high currents are typically found in shallow water depth regions and narrowing land boundaries (islands). These areas create flow contraction, resulting in high flow velocity currents. Therefore, naturally, more locations with islands are found.
Since the island linkage opportunity requires a lower mean flow velocity threshold to be feasible, the flow velocity threshold can be lowered in the spatial analysis if only island linkage opportunities are considered. This increases the number of island linkage opportunities identified (from 25 to 45 locations with an island length of 20km). It is advised to investigate this in future studies since this could provide additional feasible locations.

Initially, 300 potential locations were identified. A significant number of these locations (223) were

discarded, mostly due to insufficient energy needs in the area. However, the technical potential of these locations could be high, so it is recommended to examine the possibility of transmitting the generated energy over long distances using Ultra High Voltage Direct Current (UHVDC) transmission lines.

DTP has the potential to be feasible, but the impact of a DTP dam on the ecology, morphology, hydrodynamics and flood risks is still largely unknown and should be examined extensively.

This study assessed the feasibility of Dynamic Tidal Power and identified that the Yellow Sea, the seas in Southeast Asia, and the seas of Oceania have the highest potential for a DTP project. Additionally, it provided new insights regarding the influence and thresholds of certain influential criteria. Furthermore, it presents a hydraulic model and GIS tool that can be adjusted based on the preference of the user, which could be useful in future research on the DTP concept.

9

Recommendations

Based on the findings, discussion, and conclusions of this research, the following recommendations are presented for future exploration and improvement:

- The island linkage opportunity requires a lower mean flow velocity threshold to be feasible, the flow velocity threshold can be lowered in the spatial analysis if only island linkage opportunities are considered. This increases the number of island linkage opportunities identified (from 25 to 45 locations with an island length of 20km). It is recommended to examine this in future research.
- The analytical equations underpredict the hydraulic head (in comparison with numerical models), it is recommended to perform a study to increase the accuracy of the analytical equations. This would help to identify more accurate threshold and sensitivity analysis results.
- Currently, the design and construction costs scale linearly with increasing depth. It is recommended to improve the scaling by including the full design and corresponding costs. It is expected that the costs will rise more exponentially with increasing depth. Doing this will improve the construction cost determination in the hydraulic model for both shallow and deep water regions.
- The weighting factors, targeted LCOE, energy filter parameters (threshold and range) and shipping filter parameters all influence the final locations found. It is valuable to experiment with different model settings and observe whether other potentially interesting DTP locations are found.
- Of all locations that were marked as not feasible in the manual assessment, 73% did have a steep sloping sea bed. It is recommended to improve the spatial model by introducing a bed slope criteria to filter out the steep sloping sea bed locations in the analysis.
- Initially 300 technically feasible locations were found, of which approximately 233 were located in remote areas. Although the direct energy need is insufficient at these locations, the possibility of transmitting the energy over long distances (several 1000km) using UHVDC (Ultra High Voltage Direct Current) should be examined. If the benefit of the electricity production outweighs the total costs of the project, it may be economically beneficial to build a dam in a remote location. Therefore, an additional study on remote locations should be performed, including the costs of energy transmission.
- The environmental, social and ecological impact of a DTP dam is largely unknown. Therefore, future research on this subject is essential, particularly considering the immense scale of a DTP dam, which makes it challenging to predict the impact fully.
- The spatial analysis could be extended by including other criteria: flood risks, resource availability, power grid connections, expected future economic growth, replacement of power plants and linkage opportunities such as port expansions, combining DTP with wind parks and (renewable) energy infrastructure.

- This study focuses on DTP dams attached to the shore. However, it is possible to modify the hydraulic and spatial models to examine the global feasibility of detached DTP dams. This could be an interesting and valuable follow-up study.

References

Abeberese, A. B. (2017). Electricity cost and firm performance: Evidence from india [Cited by: 50; All Open Access, Green Open Access]. *Review of Economics and Statistics*, *99*(5), 839–852. https://doi.org/10.1162/REST_a_00641

Allcott, H., Collard-Wexler, A., & O'Connell, S. D. (2016). How do electricity shortages affect industry? evidence from india. *American Economic Review*, *106*(3), 587–624. https://doi.org/10.1257/aer.20140389

Andersen, T. B., & Dalgaard, C.-J. (2013). Power outages and economic growth in africa. *Energy Economics*, *38*, 19–23. https://doi.org/https://doi.org/10.1016/j.eneco.2013.02.016

Anteagroup. (2018). Memo-DTP-v6.2.

Aqua-RET. (2012). Tidal stream - european resource map. https://www.aquaret.com/indexcd1b.html?option=

Arcadis. (2022). *The Arcadis International Construction Costs Index 2022* (tech. rep.).

Bause, K., Radimersky, A., Iwanicki, M., & Albers, A. (2014). Feasibility studies in the product development process [24th CIRP Design Conference]. *Procedia CIRP*, *21*, 473–478. https://doi.org/https://doi.org/10.1016/j.procir.2014.03.128

Berlee, B., Chanarin, G., Foley, S., de Jong, S., Schoonhoven, D., & Vroom, I. (n.d.). *Dynamic Tidal Power in the North Sea An exploration of ecological effects and socio-economic opportunities* (tech. rep.). www.humsterlandenergie.nl

Bluespring. (2016). Worldwide potential energy from water. https://www.bluespring.blue/post/worldwide-potential-energy-from-water

Bolt, J., & van Zanden, J. L. (2020). Maddison style estimates of the evolution of the world economy. a new 2020 update [Primary energy consumption per capita (KWH/PERSON)]. https://ourworldindata.org/grapher/per-capita-energy-use

Boon, A. D. (2020). *Drag of a surface piercing cylinder in fast current and low waves* (tech. rep.).

Borthwick, A. G. L. (1989). *PRESSURE AND FORCE MEASUREMENTS ON A CYLINDER OSCILLATED SINUSOIDALLY AT LOW AND INTERMEDIATE KEULEGAN-CARPENTER NUMBERS* (tech. rep.).

Bosboom, J., & Stive, M. J. (2021). *Coastal Dynamics*. TU Delft Open.

Brouwer, A. S., van den Broek, M., Seebregts, A., & Faaij, A. (2014). Impacts of large-scale intermittent renewable energy sources on electricity systems, and how these can be modeled. *Renewable and Sustainable Energy Reviews*, *33*, 443–466. https://doi.org/https://doi.org/10.1016/j.rser.2014.01.076

Burch, J. G. (1992). *Systems analysis, design, and implementation*. Course Technology Press.

Cerdeiro, M. D. A., Komaromi, A., Liu, Y., & Saeed, M. (2020). *World Seaborne Trade in Real Time: A Proof of Concept for Building AIS-based Nowcasts from Scratch* (IMF Working Papers No. 2020/057). International Monetary Fund. https://ideas.repec.org/p/imf/imfwpa/2020-057.html

Chandavari, V. (2014). Diffuser angle control to avoid flow separation.

CIESIN. (2020). Gridded population of the world, version 4 revision 11 (gpwv4): Population count [Center for International Earth Science Information Network - Columbia University Data retrieved from:]. https://sedac.ciesin.columbia.edu/data/collection/gpw-v4

CIRIA. (2007). *The rock manual: The use of rock in hydraulic engineering*. https://www.kennisbank-waterbouw.nl/DesignCodes/rockmanual/

Crane technical paper 410: Flow of fluids through valves, fittings and pipe. (1982). Crane Valves. https://www.researchgate.net/file.PostFileLoader.html?id=56e01ba8b0366d0ab561c315&assetKey=AS%5C%3A337709886394387%5C%401457527720082

Dai, P., Zhang, J., & Zheng, J. (2017). Tidal current and tidal energy changes imposed by a dynamic tidal power system in the Taiwan Strait, China. *Journal of Ocean University of China*, *16*(6), 953–964. https://doi.org/10.1007/s11802-017-3237-4

Dai, P., Zhang, J.-s., Zheng, J.-h., Hulsbergen, K., van Banning, G., Adema, J., & Tang, Z.-x. (2018). Numerical study of hydrodynamic mechanism of dynamic tidal power. *Water Science and Engineering*, *11*(3), 220–228. https://doi.org/https://doi.org/10.1016/j.wse.2018.09.004

de Faria, F. A., Davis, A., Severnini, E., & Jaramillo, P. (2017). The local socio-economic impacts of large hydropower plant development in a developing country. *Energy Economics*, *67*, 533–544. https://doi.org/https://doi.org/10.1016/j.eneco.2017.08.025

Dinkelman, T. (2011). The effects of rural electrification on employment: New evidence from south africa. *American Economic Review*, *101*(7), 3078–3108. https://doi.org/10.1257/aer.101.7.3078

DMC. (2022). Case study shore protection uk [Xbloc - Delta Marine Consultants]. https://b2c01drupalprdsta1.blob.core.windows.net/www-xbloc-com-public/2022-06/flood_and_coast_case_study_uk_shore_protection.pdf

DTP Netherlands. (n.d.). DTP SWOT analyse. https://www.dynamictidalpower.eu/DTP-ontwikkeling/SWOT/

Fishflow innovations. (n.d.). Fishflow innovations free flow turbine. https://fishflowinnovations.nl/en/innovations/free-flow-turbine/

Group, G. C. (2022). Gebco gridded bahymetry data. https://doi.org/doi:10.5285/e0f0bb80-ab44-2739-e053-6c86abc0289c

Guerra, M., Cienfuegos, R., Thomson, J., & Suarez, L. (2017). Tidal energy resource characterization in chacao channel, chile. *International Journal of Marine Energy*, *20*, 1–16. https://doi.org/https://doi.org/10.1016/j.ijome.2017.11.002

GW Rotterdam. (2005). Kosten en duurzaamheid van oeveren bodembeschermingsconstructies met ground consolidator. https://repository.tudelft.nl/islandora/object/uuid:02dceb2c-4cc0-4b00-9425-3d875ed575f9/datastream/OBJ/download

Hall, J. (2010). *Accounting information systems*. Cengage Learning. https://books.google.nl/books?id=Y5SrpcU7j14C

Hauer, M., den Velde, W. O., Vrijling, J. K., & Angremond, K. D. (1995). Comparison construction costs conventional rubblemound breakwaters/bermbreakwater.

Hulsbergen, K., Steijn, R., & Banning, G. (2008). Dynamic Tidal Power (DTP)-A new approach to exploit tides. *2nd International Conference on Ocean Energy (ICOE 2008)*, 1–10.

Humpert, C. (2012). Long distance transmission systems for the future electricity supply – analysis of possibilities and restrictions [6th Dubrovnik Conference on Sustainable Development of Energy Water and Environmental Systems, SDEWES 2011]. *Energy*, *48*(1), 278–283. https://doi.org/https://doi.org/10.1016/j.energy.2012.06.018

IEA. (2021). Renewables 2021 [License: CC BY 4.0]. https://www.iea.org/reports/renewables-2021

International Atomic Energy Agency. (2006). *Basic infrastructure for a nuclear power project*. https://www.iaea.org/publications/7541/basic-infrastructure-for-a-nuclear-power-project

IRENA. (2022). *Renewable power generation costs in 2021* [International Renewable Energy Agency]. https://www.irena.org/publications/2022/Jul/Renewable-Power-Generation-Costs-in-2021

Jungjohann, A., & Morris, C. (2014). The german coal conundrum. the status of coal power in germany's energy transition.

Kaymak, U., & van Nauta Lemke, H. R. (1998). A sensitivity analysis approach to introducing weight factors into decision functions in fuzzy multicriteria decision making. *Fuzzy Sets and Systems*, *97*(2), 169–182. https://doi.org/https://doi.org/10.1016/S0165-0114(96)00336-3

Lenz, L., Munyehirwe, A., Peters, J., & Sievert, M. (2017). Does large-scale infrastructure investment alleviate poverty? impacts of rwanda's electricity access roll-out program. *World Development*, *89*, 88–110. https://doi.org/https://doi.org/10.1016/j.worlddev.2016.08.003

Liu, Q., & Zhang, Y. (2014). Hydrodynamic study of phase-shift tidal power system with Y-shaped dams. *Journal of Hydraulic Research*, *52*(3), 356–365. https://doi.org/10.1080/00221686.2013.875071

Liu, X., Luo, Y., & Wang, Z. (2016). A review on fatigue damage mechanism in hydro turbines. *Renewable and Sustainable Energy Reviews*, *54*, 1–14. https://doi.org/https://doi.org/10.1016/j.rser.2015.09.025

Luijendijk, A., Ranasinghe, R., De Schipper, M., Huisman, B., Swinkels, C., Walstra, D.-J., & Stive, M. (2017). The initial morphological response of the sand engine: A process-based modelling study. *Coastal Engineering*, *119*, 1–14. https://doi.org/10.1016/j.coastaleng.2016.09.005

Martinot, E. (2016). Grid integration of renewable energy: Flexibility, innovation, and experience. *Annual Review of Environment and Resources*, *41*(1), 223–251. https://doi.org/10.1146/annurev-environ-110615-085725

Matinmikko, J., Kinnunen, S.-K., Sinkkonen, T., & Kärri, T. (2022). Towards sustainable feasibility studies for p2x investments. *Journal of Cleaner Production*, *365*, 132641. https://doi.org/https://doi.org/10.1016/j.jclepro.2022.132641

McLeod, S. (2021). Feasibility studies for novel and complex projects: Principles synthesised through an integrative review. *Project Leadership and Society*, *2*, 100022. https://doi.org/10.1016/j.plas.2021.100022

Mei, C. C. (2011). Note-on-tidal-diffraction-by-a-coastal-barrier.

Mendi, V., Rao, S., & SEELAM, J. (2016). Tidal energy: A review.

Montrone, L., Steckel, J. C., & Kalkuhl, M. (2022). The type of power capacity matters for economic development – evidence from a global panel. *Resource and Energy Economics*, *69*, 101313. https://doi.org/https://doi.org/10.1016/j.reseneeco.2022.101313

Moura, R., Amado-Filho, G., Moraes, F., Brasileiro, P., Salomon, P., Mahiques, M., Bastos, A., Almeida, M., Silva, J., Araujo, B., Brito, F., Rangel, T., Oliveira, B., Bahia, R., Paranhos, R., Dias, R., Siegle, E., Figueiredo Jr, A., Pereira, R., & Thompson, F. (2016). An extensive reef system at the amazon river mouth. *Science Advances*, *2*, e1501252. https://doi.org/10.1126/sciadv.1501252

Mourão, K. R. M., Martins Sousa Filho, P. W., José de Oliveira Alves, P., & Frédou, F. L. (2014). Priority areas for the conservation of the fish fauna of the amazon estuary in brazil: A multicriteria approach. *Ocean & Coastal Management*, *100*, 116–127. https://doi.org/https://doi.org/10.1016/j.ocecoaman.2014.08.007

Mukherjee, M., & Roy, S. (2017). Feasibility studies and important aspect of project management. *INTERNATIONAL JOURNAL OF ADVANCED ENGINEERING AND MANAGEMENT*, *2*, 98. https://doi.org/10.24999/IJOAEM/02040025

NASA Earth Observatory. (2019). Massive muddy tides in the bay of fundy. https://earthobservatory.nasa.gov/images/145784/massive-muddy-tides-in-the-bay-of-fundy#:~:text=Sediment%5C%2Drich%5C%20waters%5C%20are%5C%20a,(3%5C%20to%5C%206%5C%20feet).

Noveltis, Legos, CLS, & CNES. (2016). Fes2014, aviso+. https://www.aviso.altimetry.fr/

Noveltis, Legos, CLS, & CNES. (2019). Near-real time significant wave height, aviso+ [Data period: September 2009 - December 2019]. https://www.aviso.altimetry.fr/index.php?id=1285

Park, Y. H. (2018). The Application of Dynamic Tidal Power in Korea. *Journal of Coastal Research*, *85*, 1306–1310. https://doi.org/10.2112/SI85-262.1

Patterson, T., & Kelso, N. V. (2023). Natural earth coastline includes major islands dataset [Version 4.1.0]. https://www.naturalearthdata.com/downloads/10m-physical-vectors/10m-coastline/

Pickard, A., & Meinecke, G. (2011). The future role of fossil power generation [Siemens]. https://studylib.net/doc/10461252/the-future-role-of-fossil-power-generation

Pudjianto, D., Djapic, P., Dragovic, J., & Strbac, G. (2013). Grid integration cost of photovoltaic power generation. *Imperial College London*.

Qgis geographic information system. (n.d.). *QGIS Association*. https://www.qgis.org

Ritchie, H., Roser, M., & Rosado, P. (2022). Energy [https://ourworldindata.org/energy]. *Our World in Data*.

Shao, D., Feng, W., Feng, X., & Xu, Y. (2017). Reinvestigation of the dynamic tidal power dams and their influences on hydrodynamic environment. *IOP Conference Series: Earth and Environmental Science*, *63*(1), 012048. https://doi.org/10.1088/1755-1315/63/1/012048

Swamee, P. K. (1992). Sluice-gate discharge equations. *Journal of Irrigation and Drainage Engineering*, *118*(1), 56–60.

Talstra, H., & Pak, T. (2020). *DYNAMIC TIDAL POWER (DTP): A REVIEW OF A PROMISING TECHNIQUE FOR HARVESTING SUSTAINABLE ENERGY AT SEA* (tech. rep.).

Tellman, B., Sullivan, J. A., Kuhn, C., Kettner, A. J., Doyle, C. S., Brakenridge, G. R., Erickson, T. A., & Slayback, D. A. (2021). Satellite imaging reveals increased proportion of population exposed to floods. *Nature*, *596*(7870), 80–86. https://doi.org/10.1038/s41586-021-03695-

The World Bank. (2020). Global - international ports [Data retrieved from:]. https://datacatalog.worldbank.org/search/dataset/0038118

Tidal Bridge bv. (2020). *Project Information Memorandum Oman* (tech. rep.).

TNO. (2020). Onderzoek potentieel elektriciteitsopwekking uit water ten behoeve van de verkenning elektriciteit uit water [Factsheet energy from water]. https://www.eerstekamer.nl/overig/20210330/tno_rapport_stroom_uit_water/document

Tutuarima, W., & d'Angremond, K. (1998). Cost comparison of breakwater types. *Coastal Engineering Proceedings*, *1*(26). https://doi.org/10.9753/icce.v26

UNEP-WCMC & IUCN. (2023). Protected planet: The world database on protected areas (wdpa)[online]. https://doi.org/10.34892/6fwd-af11

United Nations, D. o. E., & Development, S. A. .-. S. (2015). Transforming our world: The 2030 agenda for sustainable development. https://sdgs.un.org/2030agenda

U.S. Energy Information Administration (EIA). (2022). Hydropower explained: Tidal power. https://www.eia.gov/energyexplained/hydropower/tidal-power.php

Voorendt, M., Molenaar, W., & Bezuyen, K. (2011). Hydraulic structures, caissons, lecture notes.

Vu, T.-D., Ni, C.-F., Li, W.-C., & Truong, M.-H. (2019). Modified index-overlay method to assess spatial–temporal variations of groundwater vulnerability and groundwater contamination risk in areas with variable activities of agriculture developments. *Water*, *11*(12). https://doi.org/10.3390/w11122492

Weidema, B. (2014). Example –temporal markets for electricity [Version: 2015-04-24]. www.consequential-lca.org

Witteveen+Bos. (2017). Integrale veiligheid oosterschelde [MIRT onderzoek - knikpunten, oplossingsrichtingen en effecten]. https://www.deltaexpertise.nl/images/5/51/RW1929-201-17-004991-rapd-IVO_nieuwe_norm.pdf

World Resources Institute. (2021). Global power plant database, a comprehensive, global, open source database of power plants [Version 1.3.0]. http://datasets.wri.org/dataset/globalpowerplantdatabase

Wu, G., Deshmukh, R., Ndhlukula, K., Radojicic, T., Reilly-Moman, J., Phadke, A., Kammen, D., & Callaway, D. (2017). Strategic siting and regional grid interconnections key to low-carbon futures in african countries. *Proceedings of the National Academy of Sciences of the United States of America*, *114*. https://doi.org/10.1073/pnas.1611845114

Xu, Z. (2002). Ellipse parameters conversion and velocity profiles for tidal currents in matlab. https://doi.org/10.13140/RG.2.1.2515.4000

Yli-Hannuksela, J. (2011). The transmission line cost calculation. https://www.theseus.fi/bitstream/handle/10024/29401/Yli-Hannuksela_Juho.pdf

A

Tidal processes on a global scale

A.1. Tidal forces

Tides are generated by the gravitational forces of the Moon, Earth and Sun. The gravitational forces pull on the ocean's water body, resulting in a rise and fall of sea levels across the earth. The rotation of the earth and the movement of the moon and sun have influence on the location of pull of gravitational forces, resulting in long tidal waves.

These influential forces can be described by tidal constituents, each constituent describing a periodic change or variation in the relative positions of the Earth, Moon and Sun. The four main important tidal constituents can be found in table A.1, including their equilibrium amplitude and period.

Tidal constituent	Name	Equilibrium Amplitude [m]	Period [h]
Principal lunar	M2	0.24	12.42
Principal Solar	S2	0.11	12.00
Lunar-solar declinational	K1	0.14	23.93
Principal lunar	O1	0.10	25.82

Table A.1: Four main tidal constituents

These long tidal waves result in tidal signals on different locations. On earth three basic tidal patterns can be distinguished; semidiurnal, diurnal and mixed semidiurnal tides. Semidiurnal tides have two high and two low tides every day, mixed semidiurnal tides also have two highs and lows, but they differ in height. Diurnal tides have one high and one low each day. See figure A.1 to see how these components are distributed across the globe. Please remark that of the earlier mentioned main tidal constituents, the M2 and S2 components are semidiurnal (period $\approx 12h$) and the K1 and O1 components are diurnal (period $\approx 24h$).

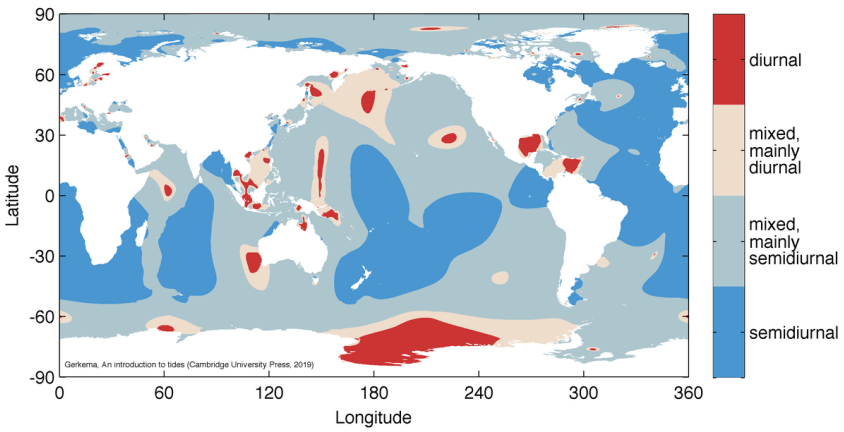

Figure A.1: Tidal classifications, generated using FES2014 database

A

A.2. Tidal oscillation

Because tidal waves can have wavelengths in the order O(1000km) in oceans and O(100km) in seas, the tidal propagation is influenced by Coriolis acceleration. Coriolis acceleration causes tidal waves to bend to the right in the Northern Hemisphere and to the left in the South Hemisphere. However, the tidal wave is also blocked by land masses. Therefore rotary movements are formed in oceans basins, bays and seas, which rotate counter-clockwise in the Northern Hemisphere and clockwise in the Southern Hemisphere. These rotary systems are called amphidromic systems, where the nodes are called amphidromic points (no vertical displacement), see figure A.3. The maximum vertical placement occurs at the edges of the basin's (land mass boundaries). An illustration of such a system can be found in figure A.2.

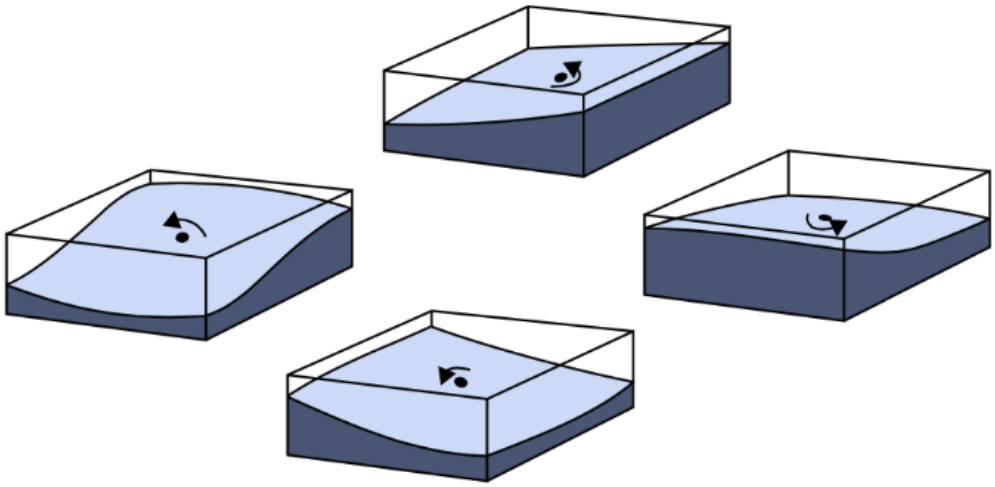

Figure A.2: Tidal oscillation of a basin in the Northern Hemisphere, Source: (Bosboom & Stive, 2021), Figure 3.29

For every constituent its influence across the globe can be calculated. As example, the height amplitudes of the M2 tidal constituent are shown in figure A.3. The tidal co-phase lines are shown as white lines. The earlier described Amphidromic points can be found where these lines coincide with each other. The change in amplitude for this specific tidal constituent is zero at these points.

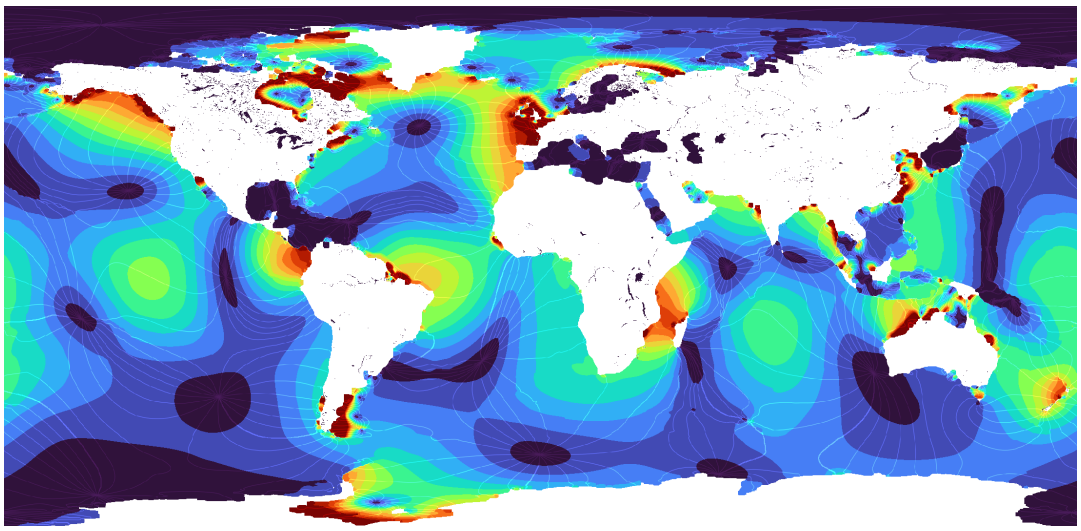

Figure A.3: Amplitudes of M2 tidal component, generated using FES2014 model (Noveltis et al., 2016). Co-phase lines (i.e., lines connecting points of equal phase) are shown in white. Amphidromic points can be at the notes of the co-phase lines, in darkblue spots.

A.3. Tidal propagation

The Airy wave theory describes the relation between frequency ω and wavenumber k (the dispersion relation), which can be found in equation A.1. The phase velocity $c = \omega/k$ is then given by equation A.2 ((Bosboom & Stive, 2021), Chapter 3.5.2).

$$\omega = \sqrt{gk \tanh kh} \tag{A.1}$$

$$c = \frac{gT}{2\pi} \tanh kh = c_0 \tanh kh \tag{A.2}$$

where:

ω = Angular velocity [1/s]
k = Wave number [m^{-1}]
h = Water depth [m]
c = Wave propogation speed [m/s]
g = gravitational acceleration [m/s^2]

Applying this relation on a typical semi-diurnal tidal wave (M2 component) results in $kh \to 0$, both for coastal and oceanic water depths. This means that the phase velocity for tidal waves can be described by the reduced dispersion relation $c = \sqrt{gh}$, because of the large wave length with the (relatively) shallow water depth.

Tidal wave progression in open oceans

For progressive tidal waves in the open oceans, the maximum velocities are found under the wave crest. The velocity amplitude is described by equation A.3 ((Bosboom & Stive, 2021), intermezzo 3.5). Here a is the wave amplitude.

$$\hat{u} = \frac{gak}{\omega} = \frac{aw}{kh} = a\sqrt{\frac{g}{h}} \tag{A.3}$$

Tidal wave progression in coastal areas

As described earlier, the amphidromic systems shown at figure A.2 include waves that propagate along the closed coastal boundaries. These waves are called Kelvin waves. At figure E.2 a definition sketch of a closed eastern boundary with a general kelvin wave in the Northern Hemisphere is shown. The main important forces are inertia, Coriolis, the pressure gradient and bed friction. Balancing these leads to the shallow water formulas at equation A.4. The first part describes the inertia, the second part the Coriolis force, the third part the pressure gradient and the last part the bed friction.

$$\frac{\delta u}{\delta t} - fv = -g\frac{\delta \eta}{\delta x} - \frac{\tau_{b,x}}{\rho h} \tag{A.4a}$$

$$\frac{\delta v}{\delta t} + fu = -g\frac{\delta \eta}{\delta y} - \frac{\tau_{b,y}}{\rho h} \tag{A.4b}$$

Neglecting friction and applying the fact that the velocity u at the closed coastal boundary is zero, gives the formulas in equation A.5.

$$-fv = -g\frac{\delta\eta}{\delta x} \tag{A.5a}$$

$$\frac{\delta v}{\delta t} = -g\frac{\delta\eta}{\delta y} \tag{A.5b}$$

$$h\frac{\delta v}{\delta y} = \frac{\delta\eta}{\delta t} \tag{A.5c}$$

Please note that the alongshore momentum balance includes the inertia in y direction and water level gradient (equation A.5b). This equation is the same for progressive shallow water waves, where the alongshore velocity is in phase with the water level (maximum velocity at crest of the wave). Equations A.5 can be further reduced to equations A.6, where the surface elevation and alongshore velocity are shown. The maximum alongshore velocity can be described by the amplitude of equation A.6b.

$$\eta(x,y,t) = \eta_0 e^{\frac{fx}{c}} \cos(\omega t - ky) \tag{A.6a}$$

$$v(x,y,t) = \frac{c}{h}\eta_0 e^{\frac{fx}{c}} \cos(\omega t - ky) \tag{A.6b}$$

A.4. Tidal currents in coastal regions

As said in chapter A.3, because $kh \ll 1$ applies for tidal waves, they propagate as a long wave in a shallow water regime. The velocity amplitude is therefore depth-uniform, and can be calculated using equation A.7. In the derivation of this formula, the reduced dispersion relation $c = \sqrt{gh}$ is used that was described in chapter A.3. The depth-uniform velocity amplitude is shown in figure A.4b, where the vertical velocity profile of tidal currents is shown.

$$\hat{u} = \frac{aw}{kh} = c\frac{a}{h} = \sqrt{gh}\frac{H}{2h} \tag{A.7}$$

Figure A.4a shows the top view of a tidal current along a shoreline. The direction of the tidal current reverses during the tidal cycle. In very shallow water regimes (approximately $h < 10m$), the inertia effect is small and the velocity is mainly governed by the balance of the alongshore water level gradient and the friction. Please note that figure A.4a describes a coastal area with a gradual increase in bottom depth. In real life the tidal current velocities could be very different due to differences in bathymetry.

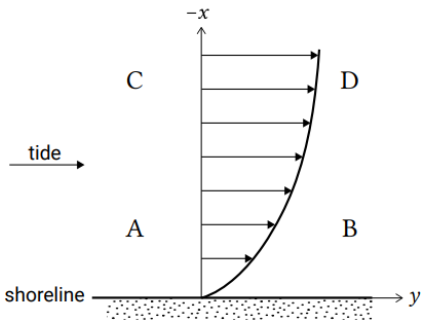

(a) Top view: Tidal current velocity along shore, source: (Bosboom & Stive, 2021), Figure 5.58

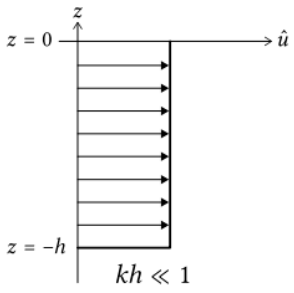

(b) Vertical profile of tidal current (both in deep and shallow waters), source: (Bosboom & Stive, 2021), Figure 5.21

Figure A.4: Top view and vertical profile of tidal currents

A.5. Tidal energy potential

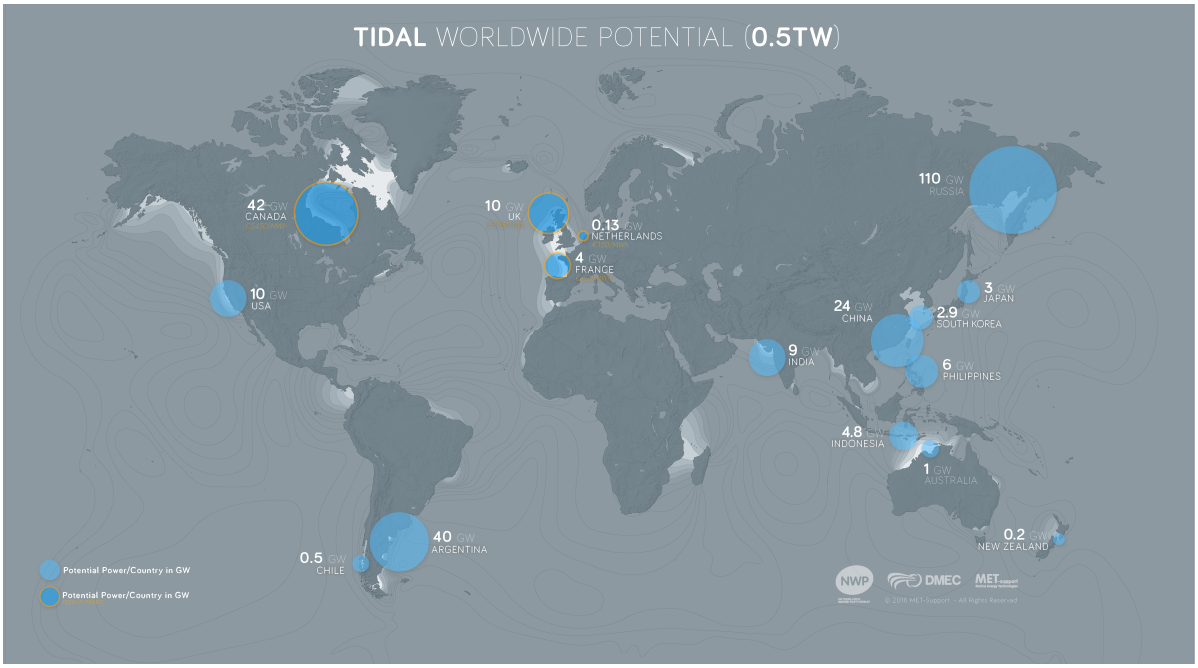

Figure A.5: Indicatino of worldwide potential of traditional tidal energy (Bluespring, 2016)

B

Theoretical proof of the DTP concept

Inertia vs drag forces
As described before, a DTP dam increases the tidal range in a coastal region where no large tidal range is normally present. This increased tidal range, in combination with the induced phase difference, results in a hydraulic head level difference between both sides of the dam. When turbines are placed inside the dam, water can flow through the turbines from one side to the other, which generates energy.

This increase in tidal range is an essential process in the functioning of DTP, because it directly relates to the potential energy output. Therefore it is important to analyse the physical processes behind this increase in tidal range and the corresponding order of magnitude. From equation A.4, it can be seen that the most important forces for a tidal wave in a coastal area are inertia, Coriolis, the pressure gradient and bed friction. The Coriolis force will mostly influence the pressure gradient in the cross-shore direction, ”trapping” the tidal wave to the coastline. The alongshore pressure gradient is mostly influenced by inertia and drag forces. This can be seen in equation B.1, where the balance of forces in alongshore direction are shown (neglecting Coriolis), see figure E.2 for a definition sketch.

$$\frac{\delta v}{\delta t} + \frac{\tau_{b,y}}{\rho h} = -g\frac{\delta \eta}{\delta y} \tag{B.1}$$

The question arises if the pressure gradient in the parallel direction is dominated by inertia, drag or a combination of these two. This will be analysed in subsection B. Additionally, the response of a system dominated by drag or inertia will be presented in subsections B and B.

Keulegan-Carpenter number
The relation between inertia and drag can be described with the Keulegan-Carpenter number (KC). This is a dimensionless number that describes the relative importance of the drag forces over inertia forces of an object in oscillatory flow. Additionally, also oscillating objects in a fluid at rest can be analysed. Because a DTP dam can be seen as an object in quasi-permanent or oscillatory flow (periodical tidal wave), the relation between inertia and drag can be analysed using this number. The KC number is defined as Equation B.2.

A first calculation with typical values can be found at the example of equation B.2, using a semi-diurnal tidal wave with a typical effective length of 40 km and a natural tidal flow velocity of 2 m/s. There is no exact threshold for the KC-number, but generally it is presumed that for KC-numbers above 5 the drag forces become dominant (see papers (Boon, 2020) and (Borthwick, 1989)). For a typical DTP dam, the KC number is generally below 5, showing the domination of inertia (see example B.2 and table B.1). Thus, it is the deceleration and acceleration of the flow, and not the velocity itself, which is governing the dynamic situation around the dam. Drag forces operate in phase with the flow velocity, while the

inertia forces operate in phase with the flow acceleration (90° out of phase with the drag forces). To conclude, an essential aspect of the functioning of a DTP dam is the domination of the inertia forces over the drag forces (Hulsbergen et al., 2008).

$$KC = \frac{V_{max} * T}{D} \qquad \text{For example} \approx \qquad \frac{2 * 12.421 * 3600}{40000} = 2.24 \tag{B.2}$$

where:

V_{max} = Maximum (tidal) flow velocity
T = (Tidal) wave period
D = Diameter of submerged object (length of dam)

Table B.1 shows multiple DTP dam situations and the corresponding KC-values. Please pay special attention to the case of a diurnal signal (23.93 h) with a high tidal flow velocity (3 m/s) and a relatively short dam length (30 km), which corresponds to a KC value of 8.61. This shows that in special cases the drag forces are the dominating factor. Especially for these cases, a numerical model could provide valuable information on the functioning of DTP.

Type	Vmax [m/s]	T [h]	D [km]	KC [-]
Semi-diurnal	1	12.42	30	1.49
	1	12.42	50	0.89
	3	12.42	30	4.47
	3	12.42	50	2.68
Diurnal	1	23.93	30	2.87
	1	23.93	50	1.72
	3	23.93	30	**8.61**
	3	23.93	50	5.17

Table B.1: Examples of DTP dam situations and their corresponding KC-values

Please remark that there is a contradictory effect in this theory. A higher flow velocity increases the importance of drag forces (and therefore possibly decreasing the hydraulic head) but it also increases the hydraulic head because of an increase of momentum (see equation 2.1). The increase of hydraulic head due to the increase of momentum is stronger than the decrease of hydraulic head due to higher drag forces. Therefore with a higher tidal flow velocity the hydraulic head will increase.

Drag dominated: Hydraulic head
Although most DTP dam situation are inertia dominated, it is important to know how a drag-dominated DTP system will respond. When drag forces are dominant, permanent flow conditions apply. The hydraulic head can then be calculated by converting kinetic energy to potential energy. Using Bernoulli's flow theory, we can find that the maximum head difference is said to be $\frac{V^2}{2g}$ (because $\frac{V^2}{2g} + h = constant$). In the case of $V_{max} = 2m/s$, this would result in a maximum hydraulic head of only 0.2 m. This hydraulic head would not be enough for DTP to be feasible, because the energy generation would be too low. However, as we said before, DTP dams are generally inertia dominated.

Inertia dominated: Hydraulic head
In the case of the domination of inertia, it is the acceleration and deceleration of the flow that causes the hydraulic head level difference across the dam. Figure 2.3 shows an illustration of a DTP dam that blocks a tidal wave. The approaching tidal wave travels in long-shore direction of the coastline and is partly blocked by the DTP dam. This blockage causes water levels to rise, because of the involved inertia of the tidal wave. On the other side, water is pulled away by the gravitational forces of the sun and moon. Therefore a head level difference occors between both sides of the dam.

The situation at figure 2.3 can also be approached by looking at the reversed situation, a oscillating plate in a fluid at rest (see figure B.1). Here the blue cylinder in figure B.1 shows the trapped water mass region that is also shown as the dark-green part in figure 2.3. By analysing an oscillating plate in a fluid at rest, the system can be analysed more easily, this method is called the macroscopic added-mass theory.

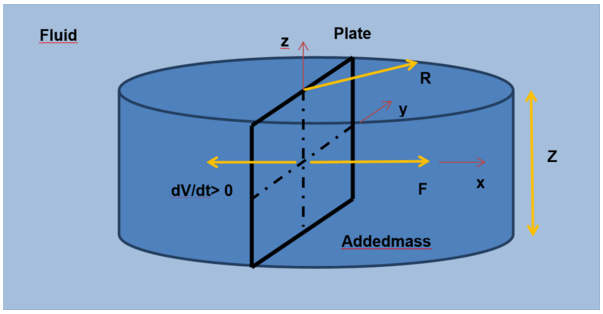

Figure B.1: Oscillating plate.

The derivation of the hydraulic head is shown in Appendix D.1. First, the maximum acceleration per tidal cycle is described. Then the forces on the oscillating plate are derived. Finally, these two derivations are combined to derive the maximum pressure on the plate, from which the maximum hydraulic head is derived. This results in equation 2.1, where the hydraulic head is expressed using the maximum tidal velocity, dam length, angular velocity and gravitational acceleration.

$$\Delta h_{max} = \frac{2\omega L V_{max}}{g} \tag{2.1}$$

where:

Δh_{max} = Maximum hydraulic head level difference [m]
V_{max} = Maximum (tidal) flow velocity [m/s]
L = Dam length [m]
ω = Angular velocity [1/s]
g = gravitational acceleration [m/s^2]

Equation 2.1 was first derived by P. Kolkman (Hulsbergen et al., 2008). Chiang C. Mei derived formula 2.1 as well, using a different approach. Chiang used Buchwald's theory on tidal diffraction by a channel to study the effects on a coastal DTP barrier (Mei, 2011). Because of some assumptions to simplify the equation, his derivation is only valid for cases where the dam length is very small compared to the tidal wave length ($L \ll \lambda$); for longer DTP dams larger-scale diffraction effects could occur. Besides this condition, it is still encouraging that both methods agree with each other in terms of the maximum hydraulic head.

The hydraulic head can also be calculated using numerical models. Several studies found that the analytically calculated hydraulic head is, in most cases, lower than the numerically calculated hydraulic head. For instance, analytical calculations of the head of a DTP dam in IJmuiden showed to be a factor 1.7 lower than the numerical calculations (Hulsbergen et al., 2008). This difference is explainable due to the tidal non-linearity. The processes behind this are, for instance, flow contraction, bottom depth fluctuations, resonance, and other shallow water influences that are not taken into account in the analytical model. A model factor can be applied to get the analytical results closer to the numerical results.

C

Background information supporting figures

C.1. Water level longitudinal profile

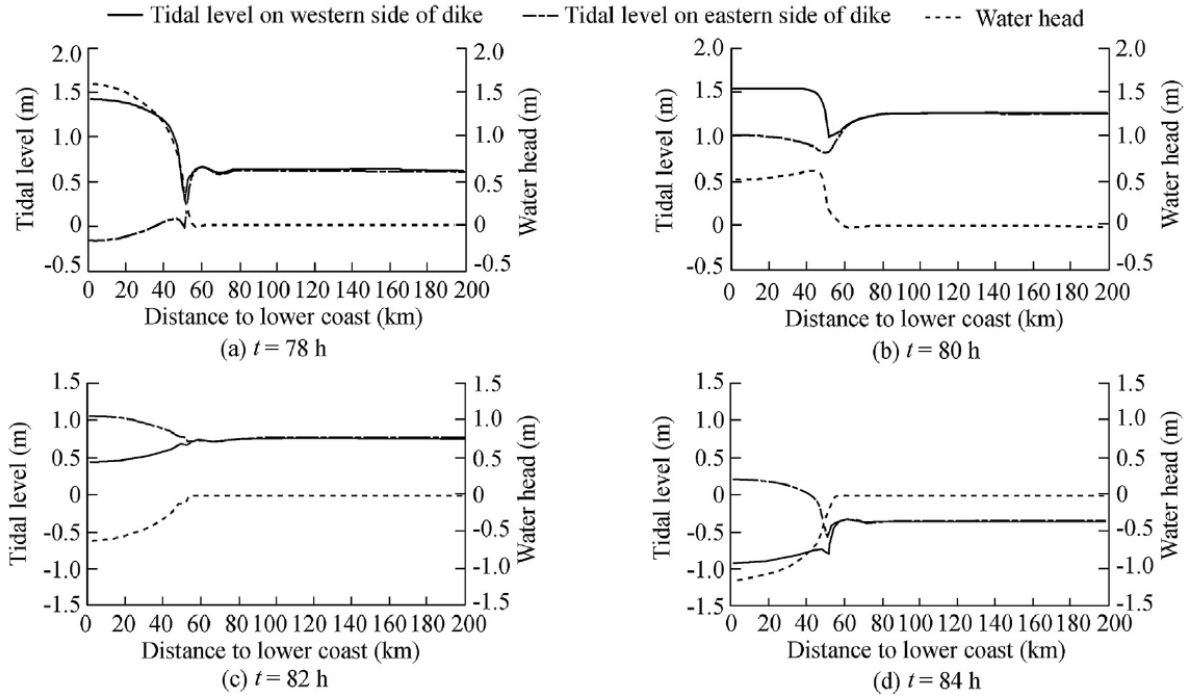

Figure C.1: Sequence of numerical results: water levels and hydraulic head distribution along a DTP dam, retrieved from Dai et al., 2018. As time increases, water levels at the western and eastern sides shift, and the hydraulic head difference shifts from max. 1.6m to -1.2m. The quarter ellipse shape of the hydraulic head can be recognized as well.

C

C.2. Twin dams

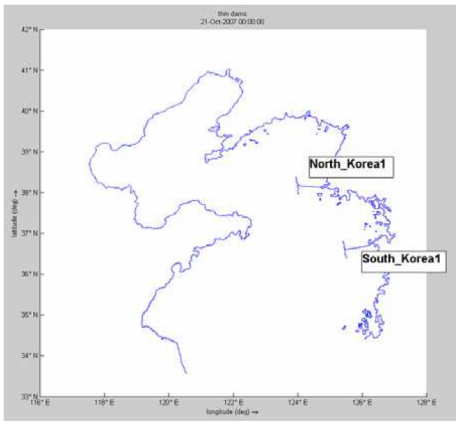

(a) Location of twin dams SK1 and NK1.

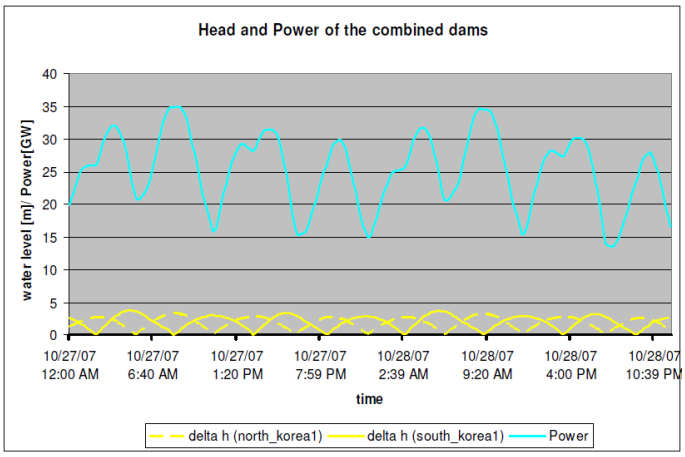

(b) SK1 and NK1 operating as twins. Individual heads, and combined power.

Figure C.2: Twin dams locations, the hydraulic head and the corresponding power output of the paper of Hulsbergen et al., 2008

D

Derivations

D.1. Calculations dispersion relation

The following calculations are derived using several papers (Talstra and Pak, 2020, Anteagroup, 2018, Tidal Bridge bv, 2020), please consult those for further information about the equations.

The oscillating plate from figure B.1 moves with the relative speed of the water in relation to the dam as shown in equation D.1. The derivative of this equation can be found in equation D.2. Because the maximum of a cosine function is 1, the maximum of the derivative can be found in equation D.3, which shows the maximum acceleration per tidal cycle.

$$V(t) = V_{max} \sin(\omega t) \tag{D.1}$$

$$\frac{dV(t)}{dt} = \omega V_{max} \cos(\omega t) \tag{D.2}$$

$$\left(\frac{dV(t)}{dt}\right)_{max} = \omega V_{max} \tag{D.3}$$

where:

V = Speed at which the sheet is moved as a function of time [m/s]
V_{max} = Maximum speed [m/s]
ω = Angular velocity at which the sheet is periodically moved [rad/s]
t = Time [s]

The force on the sheet to move it through the water is derived at equation D.4.

$$F = (m + m_a)\frac{dV}{dt} + \frac{1}{2}\rho V(t)^2 S C_d \tag{D.4}$$

where:

F = Force with which the sheet is moved through the water [N]
m = Mass of the sheet itself [kg]
m_a = Mass of the moving water [kg]
ρ = Specific mass of the water [kg/m3]
S = Wet surface of the sheet [m^2]
C_d = Drag coefficient [-]

The mass of the plate can be disregarded (because in the real case, the plate (dam) is static). In chapter B it was found that the system is inertia dominated, so the drag resistance can be disregarded. With these assumptions, equation D.5 is derived.

$$F_{max} = \rho \pi R^2 Z \omega V_{max} \tag{D.5}$$

$$\Delta \overline{P}_{max} = \frac{F_{max}}{S} = \frac{\rho \pi R^2 Z \omega V_{max}}{Z * 2R} = \rho \pi^2 R \frac{V_{max}}{T} \tag{D.6}$$

where:

$T = \frac{2\pi}{\omega}$ = (Tidal) wave period [s]
D = Diameter of submerged object (length of dam) [m]
Z = Depth of dam [m]
R = Radius of trapped water mass [m]

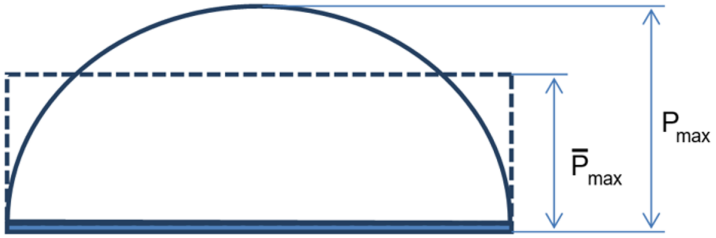

Figure D.1: Maximum and average maximum hydrostatic pressure

$$\Delta H^*_{max} = \frac{\Delta P_{max}}{\rho g} = (\frac{4}{\pi}) \frac{\Delta \overline{P}_{max}}{\rho g} = 2\pi \frac{V_{max} L}{gT} = \frac{2\omega L V_{max}}{g} \tag{D.7}$$

Studies have shown that numerical simulations result in higher hydraulic heads. For example, at IJmuiden the numerical hydraulic head is 1.7 times the analytically calculated hydraulic head (Hulsbergen et al., 2008). To mitigate this difference, the calculated hydraulic head from equation D.7 can be multiplied by a model factor to estimate the numerical results. The study of Hulsbergen et al. suggested a model factor of 1.7 at IJmuiden. This model factor is different on each location.

D.2. Formulation equation 5.9

An equation is needed that described the hydraulic head change relatively to the flow rate through the dam. First, from equation 5.6 the proportional relationship between the flow rate Q and hydraulic head difference Δh is as follows:

$$Q_{in} = Q_{out} = \gamma_s * A_t \frac{\sqrt{2g(1-a)\Delta h}}{1+C} \tag{5.6}$$

$$Q \propto \sqrt{\Delta h}$$

When the dam is closed ($Q = 0$, the hydraulic head level difference is maximum (Δh_{max}). When the dam is fully permeable, the hydraulic head level difference is zero ($\Delta h = 0$) and the flow rate (Q_{dam}) is maximum. Combining this in an equation and applying the proportion derived above gives the following.

$$\frac{\Delta h^\circ_{max}}{\Delta h_{max}} + (\frac{Q^\circ_{max}}{Q_{dam}})^2 = 1$$

Now, in a situation with a partly permeable dam, the Δh°_{max} describes the hydraulic head level difference and Q°_{max} the flow rate. If the flow rate (Q°_{max}) decreases, the hydraulic head (Δh°_{max}) increases since Δh_{max} and Q_{max} stay the same. Rewriting the formula above results in equation 5.9.

$$\Delta h^{\circ}_{max} = \Delta h_{max}[1 - (\frac{Q^{\circ}_{max}}{Q_{dam}})^2] \tag{5.9}$$

D.3. Derivation equation 5.11

The derivation of equation 5.11 is shown below. This derivation uses earlier stated equations: 2.1, 5.6, 5.8, 5.9 and 5.10.

$$\Delta h_{max} = \gamma_{model}\frac{2\omega L V_{max}}{g} \tag{??}$$

$$Q_{in} = Q_{out} = A_{out}V_{out} = C_d * \gamma_s * A_t\sqrt{2g(1-a)\Delta h} \tag{5.6}$$

$$Q_{dam,open} = A_{dam} * V_{max} \tag{5.8}$$

$$\Delta h^{\circ}_{max} = \Delta h_{max}[1 - (\frac{Q^{\circ}_{max}}{Q_{dam,open}})^2] \tag{5.9}$$

$$b = \frac{A_0}{A_{dam}} \tag{5.10}$$

Equation 5.9 can be rewritten to the following:

$$\frac{\Delta H^{o}_{\max}}{\Delta H_{\max}} = \left[1 - \left(\frac{Q^{o}_{\max}}{Q_{\text{dam, open}}}\right)^2\right] \Rightarrow \left(\frac{Q^{o}_{\max}}{Q_{\max}}\right)^2 = \left[1 - \left(\frac{Q^{o}_{\max}}{Q_{\text{dam, open}}}\right)^2\right]$$

$$\left(\frac{Q_{dam,open}}{Q^{o}_{\max}}\right)^2 = 1 + \left(\frac{Q_{dam,open}}{Q_{\max}}\right)^2$$

Combining equations 5.6 and 5.8 with the equation stated above, gives the following equation:

$$\left(\frac{Q_{dam,open}}{Q^{o}_{\max}}\right)^2 = 1 + \frac{(A_{\text{dam}}V_{\max})^2}{C_d^2\gamma_s^2A_0^2 * 2g(1-a)\Delta h}$$

Subsiding equation 5.8 into the equation stated above and rewriting the equation, results in the equation below.

$$Q^{\circ}_{max} = Q_{dam,open}[1 + \frac{(\frac{V_{max}}{b})^2}{C_d^2 * \gamma_s^2 * 2g(1-a)\Delta h_{max}})]^{-\frac{1}{2}}$$

where:

Q°_{max} = Maximum flow rate when partly permeable [m^3/s]
$Q_{dam,open}$ = Maximum flow rate when fully open [m^3/s]
P°_{max} = Maximum hydraulic power output when partly permeable[kW]
Δh°_{max} = Maximum hydraulic head difference when partly permeable [m]

Combining with equations 5.8 and 2.1, this results in equation 5.11 as shown below.

$$Q^{\circ}_{max} = A_{dam} V_{max} * [1 + \frac{(\frac{\Delta h_{max} g}{2\omega L b \gamma_{model}})^2}{C_d^2 * \gamma_s^2 * 2g(1-a)\Delta h_{max}})]^{-\frac{1}{2}} \tag{5.11}$$

Which translates to the following maximum power output:

$$P^{\circ}_{max} = \eta \rho g (a \Delta h^{\circ}_{max}) Q^{\circ}_{max} \tag{5.12}$$

D

D.4. Derivation maximum of a

Factor a expresses the fraction of the hydraulic head that is being used to generate power by the turbine. This factor is introduced to be able to solve the energy balance and calculate the energy extracted by the turbine. To determine the value of a that gives the maximum power output, the power output equation 5.7 should be differentiated to a and set equal to zero, which is done below. It can be noted that at equation 5.7, a is included two times. The first a increases the power output, since this originates from $a * \Delta h = \Delta H_t$ (equation 5.5). The second a originates from the outflow velocity (equation 5.3). This alpha lowers the power output, since an increase in a lowers the outflow velocity and thus the inflow velocity (since $Q_{in} = Q_{out}$ and $A_{in} = A_{out}$).

$$P_{t,max} = \eta \rho g a \gamma_s A_t \frac{\sqrt{2g(1-a)\Delta h^3_{max}}}{1+C} \tag{5.7}$$

Since we are going to differentiate to a, assume the other variables to be constants.

$$P_{t,max} = Constant * a\sqrt{(1-a)} = Constant * \sqrt{(a^2 - a^3)}$$

$$\frac{\partial P_{t,max}}{\partial a} = Constant * \frac{(2-3a)a}{2\sqrt{-(a-1)a^2}}$$

Maximum of a is known when derivative = 0, so:

$$Constant * \frac{(2-3a)a}{2\sqrt{-(a-1)a^2}} = 0$$

$$a = \frac{2}{3}$$

This is also shown at figure D.2, where equation 5.7 is plotted with limits 0 < a < 1 and P > 0.

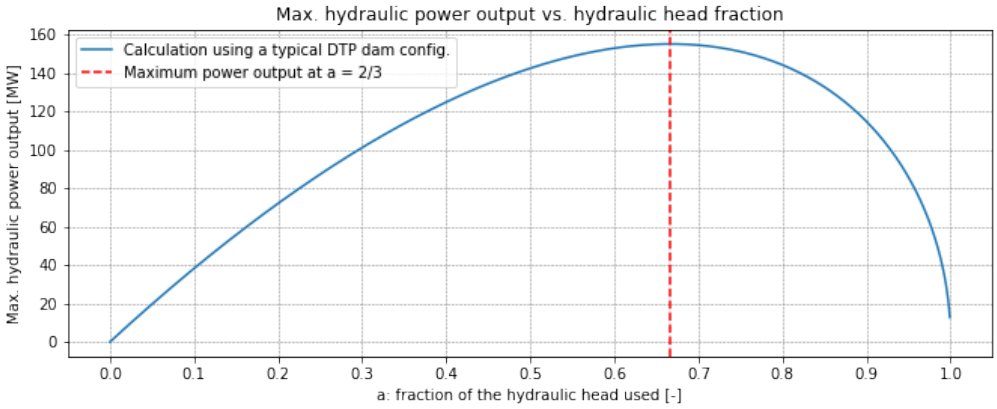

Figure D.2: Calculation using equation 5.7 to find the optimum of parameter a

D.5. Overview hydraulic equations

An overview of the equations used in simplified hydraulic model (orange block of hydraulics) of figure 5.2is shown below, including the names, values, and descriptions of the variables and constants used.

$$\Delta h_{max} = \gamma_{model} \frac{2\omega L V_{max}}{g} \tag{??}$$

$$\gamma_s = \frac{A_t}{A_{in}} \tag{5.4}$$

$$b = \frac{A_0}{A_{dam}} \tag{5.10}$$

$$Q^{\circ}_{max} = A_{dam} V_{max} * [1 + (\frac{\Delta h_{max} g}{2\omega L b \gamma_{model}})^2 \frac{1 + C}{\gamma_s^2 * 2g(1-a)\Delta h_{max}})]^{-\frac{1}{2}} \tag{5.11}$$

$$\Delta h^{\circ}_{max} = \Delta h_{max}[1 - (\frac{Q^{\circ}_{max}}{Q_{dam}})^2] \tag{5.9}$$

$$P^{\circ}_{max} = \eta \rho g (a \Delta h^{\circ}_{max}) Q^{\circ}_{max} \tag{5.12}$$

Variables

Δh_{max}	Maximum hydraulic head difference between both sides of the dam $[m]$
V_{max}	Maximum tidal flow velocity $[m/s]$
L	Dam length $[m]$
ω	Angular velocity $[1/s]$
Q°_{max}	Maximum flow rate when partly permeable $[m^3/s]$
A_{dam}	Total vertical area of the dam $[m^2]$
P°_{max}	Maximum hydraulic power output when partly permeable $[kW]$
Δh°_{max}	Maximum hydraulic head difference when partly permeable $[m]$
γ_s	fraction between rotor and inflow area [-]
b	Permeability [-]

Constants

C	0.76	Loss coefficient [-]
a	$\frac{2}{3}$	fraction of the hydraulic head used for energy generation [-]
η	0.85	Installation efficiency [-]
ρ	1023	Specific water mass $[kg/m^3]$
g	9.81	gravitational acceleration $[m/s^2]$

E

Additional Theory

E.1. Streamlines and currents

The upper part of figure E.1 shows the streamlines around and against a DTP dam. It can be seen that at the base and middle of the DTP dam, the approaching coast-parallel tidal wave is blocked by the dam. These streams decelerate towards zero and their momentum is transformed to an increase in water level. On the other side, the water is withdrawn from the dam (acceleration) because of tidal forces, thus creating a current away from the dam. At the tip of the DTP dam, streamlines are contracted, which results in an increase in flow velocity. A research by Y.H. Park showed that building a DTP dam increases the tidal currents near the head of the dam (Park, 2018). In their case the offshore maximum current speed was nearly twice as fast as in the original situation without a DTP dam.

The lower part of figure E.1 shows the streamlines around a regular breakwater. As can be seen, most streamlines go around the tip of the breakwater. A contraction around the tip can be seen, which results in a severe increase in flow speed. Additionally, a vortex arises at the back of the breakwater.

As explained, a current is flowing around the tip of the DPT dam. However, it is important to note that although there is water flowing around the tip of the dam, in the situation of the DTP dam it is not the entire coast-parallel tidal wave that travels around the dam. Instead, the tidal wave maintains its straight course along the coast (only changing slightly at the tip of the DTP dam). The interaction (blockage) between the dam and the acceleration and decelerating streams of the tidal wave cause an increase or decrease in water level. Thus, the maximum hydraulic head is not related to the vertical tidal range, but depends on the horizontal tidal stream only.

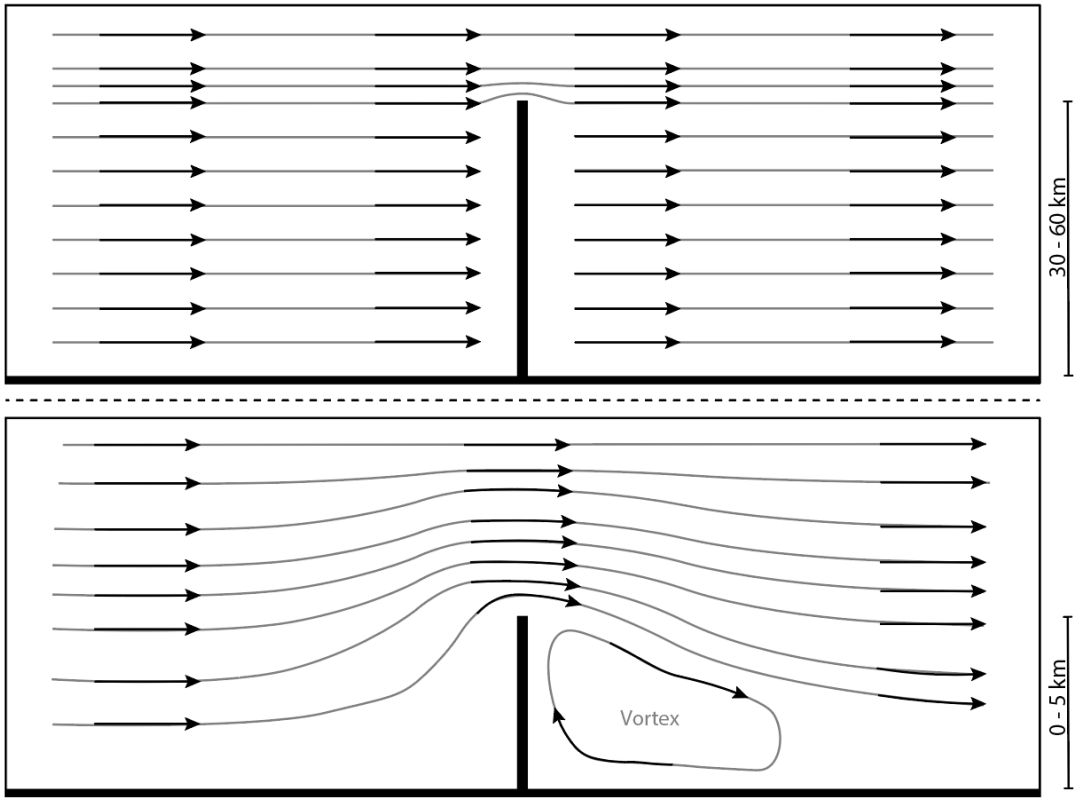

Figure E.1: Flood wave travelling along the coast. Upper figure: Streamlines around and against a DTP dam. Lower figure: streamlines around a regular breakwater. Please note that this situation reverses during ebb time.

E.2. Combine tidal velocities

$$u = A_{M2,u}\cos\left(\omega_{M2,u}t - \theta_{M2,u}\right) + A_{S2,u}\cos\left(\omega_{S2,u}t - \theta_{S2,u}\right) + A_{K1,u}\cos\left(\omega_{K1,u}t - \theta_{K1,u}\right) + A_{O1,u}\cos\left(\omega_{O1,u}t - \theta_{O1,u}\right) \quad \text{(E.1a)}$$

$$v = A_{M2,v}\cos\left(\omega_{M2,v}t - \theta_{M2,v}\right) + A_{S2,v}\cos\left(\omega_{S2,v}t - \theta_{S2,v}\right) + A_{K1,v}\cos\left(\omega_{K1,v}t - \theta_{K1,v}\right) + A_{O1,v}\cos\left(\omega_{O1,v}t - \theta_{O1,v}\right) \quad \text{(E.1b)}$$

E.3. Trapped Kelvin wave

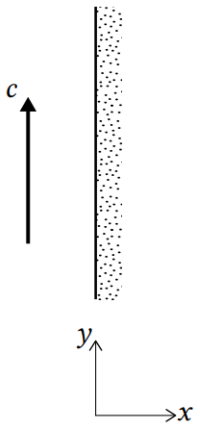

Figure E.2: Closed eastern boundary with direction of tidal (Kelvin) wave propagation in the Northern Hemisphere

E.4. Turbine diameter scale effect

Figure E.3 was produced using results of turbine simulations by the software OpenFOAM. It can be observed that for small flow velocities of 1 m/s, multiple smaller turbines (10 turbines of 2.5m diameter) produce more power than one large turbine with diameter 10m. For higher flow velocities, one turbine of 10m produces more power than 10 turbines of 2.5m diameter. These scale effects are not fully understood yet.

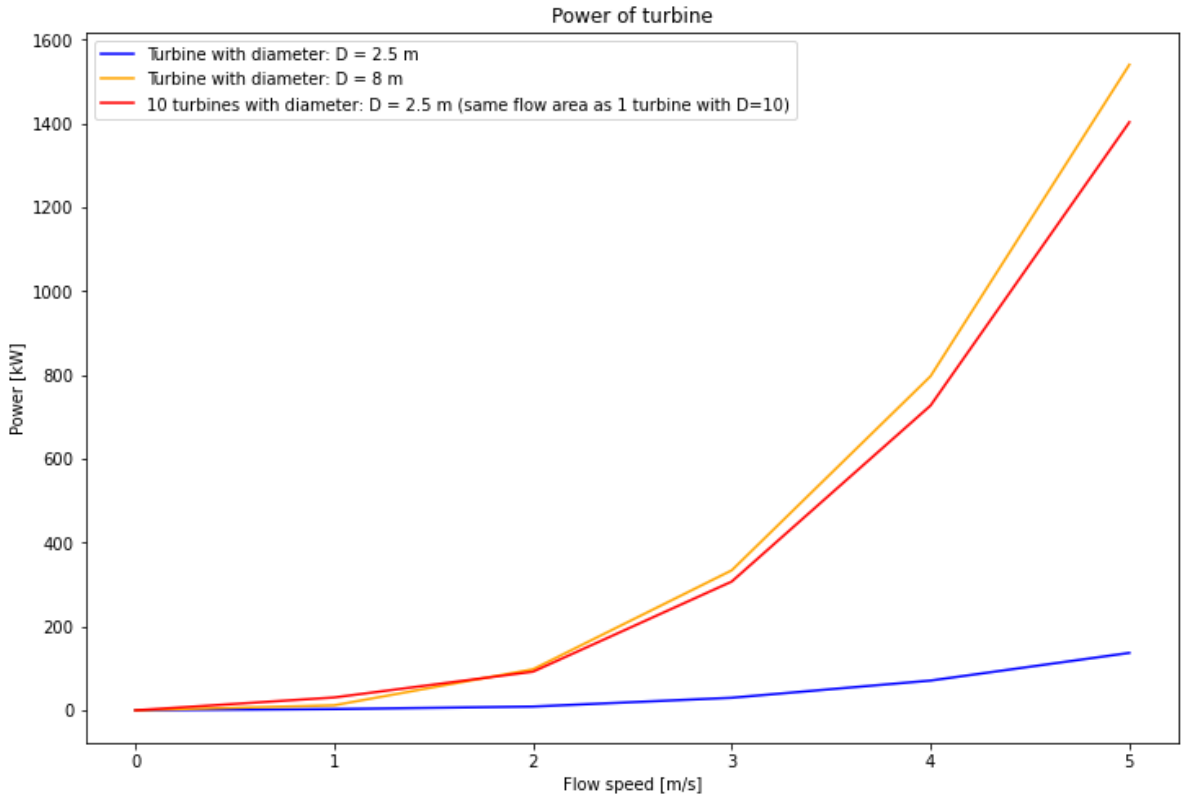

Figure E.3: flow velocity vs power production for multiple turbine diameters

F

Criteria datasets

F.1. Flow velocity dataset: computation time span

Mean and maximum values were calculated for time spans of up to one year for the top 5 most potential locations, seen in figure F.1. As can be seen from table F.1, using a calculation time span of 1 month gives an error between 2% and 2.5% for the mean tidal current velocity values, which is acceptable.

Country	Lat	Lon	Rank potential	Mean velocity error for time span 1 month	Remarks
North Korea	38.1285	124.6875	1st	2.5 %	
Chile	-41.8038	-73.6976	2nd	2 %	Tidal stream method
Myanmar	16	97.563	3th	2.5 %	
Canada	45.3114	-64.4358	4th	1.9 %	
Australia	-11.4993	131.5611	5th	2 %	

Table F.1: Summary of the computational time analysis (figure F.1): top 5 most potential locations and their error for a time span of 1 month.

From this analysis, the following observations are made:

1. For increasing time span, the values approach their correct value.
2. The mean value approaches accurate results after a time span of $\pm$ 1 month (error = 2% to 2.5%).
3. It differs greatly when the correct maximum value is found.

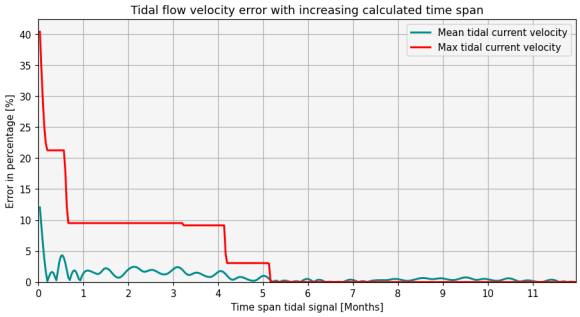

(a) Mean and maximum values of tidal flow velocity signals, calculated for different tidal signal time spans. Location: North Korea, coordinates: (38.1285, 124.6875)

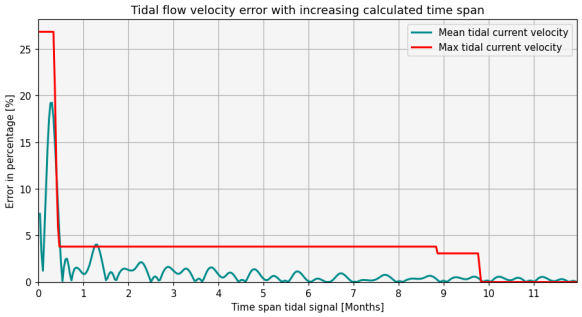

(b) Mean and maximum values of tidal flow velocity signals, calculated for different tidal signal time spans. Location: Chile, coordinates: (-41.8038, -73.6976)

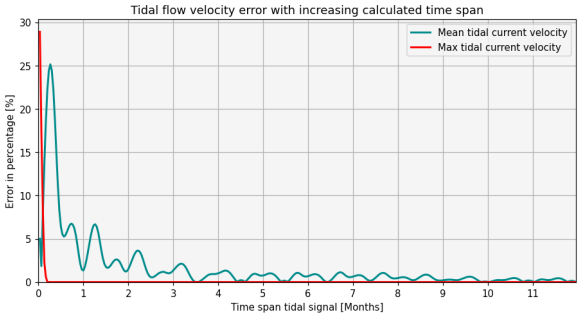

(c) Mean and maximum values of tidal flow velocity signals, calculated for different tidal signal time spans. Location: Myanmar, coordinates: (16, 97.563)

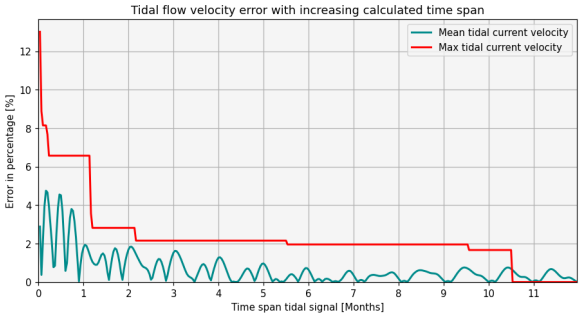

(d) Mean and maximum values of tidal flow velocity signals, calculated for different tidal signal time spans. Location: Canada, coordinates: (45.3114, -64.4358)

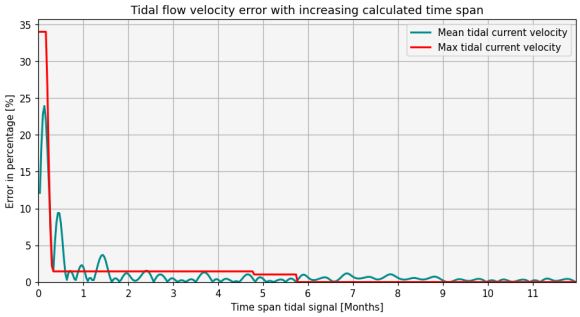

(e) Mean and maximum values of tidal flow velocity signals, calculated for different tidal signal time spans. Location: Australia, coordinates: (-11.4993, 131.5611)

Figure F.1: Computational time analysis: top 5 most potential locations and their error for different time spans

F.2. Technical criteria: datasets

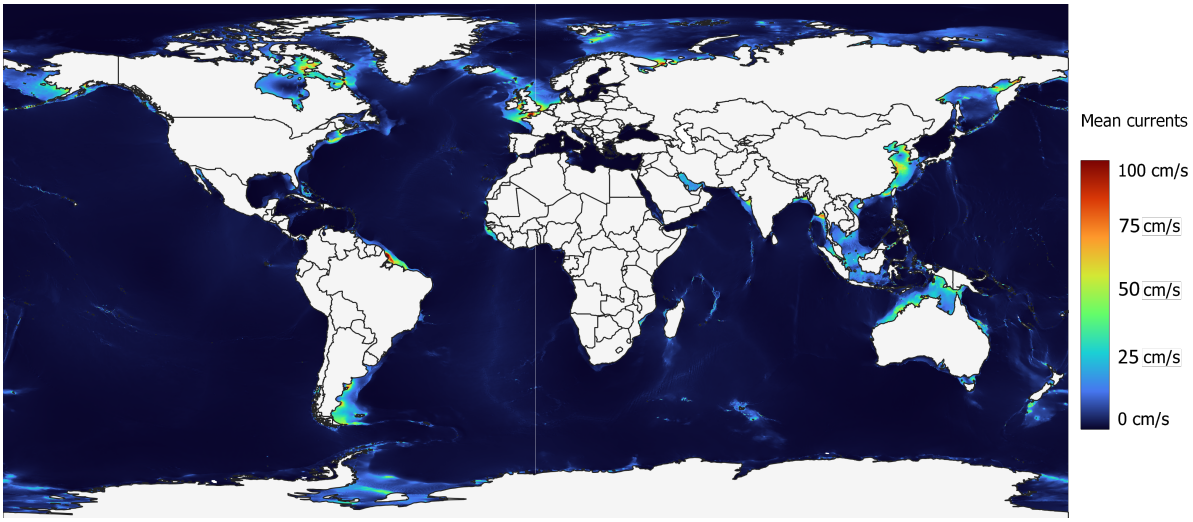

Figure F.2: Technical dataset: global mean tidal currents, produced using the FES2014 tidal model (Noveltis et al., 2016).

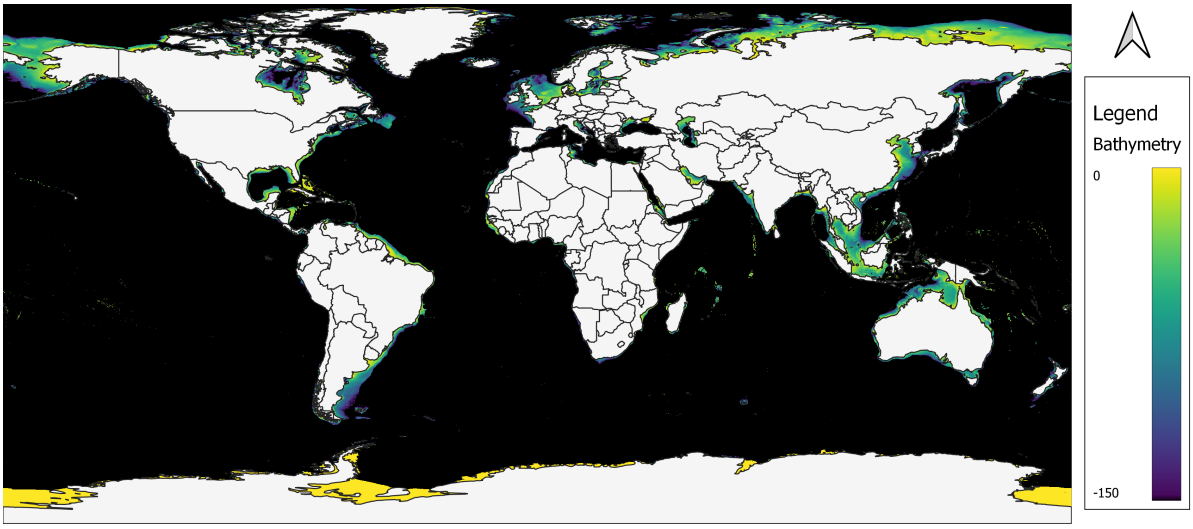

Figure F.3: Technical dataset: global bathymetry (Group, 2022).

F.3. Secondary criteria: datasets

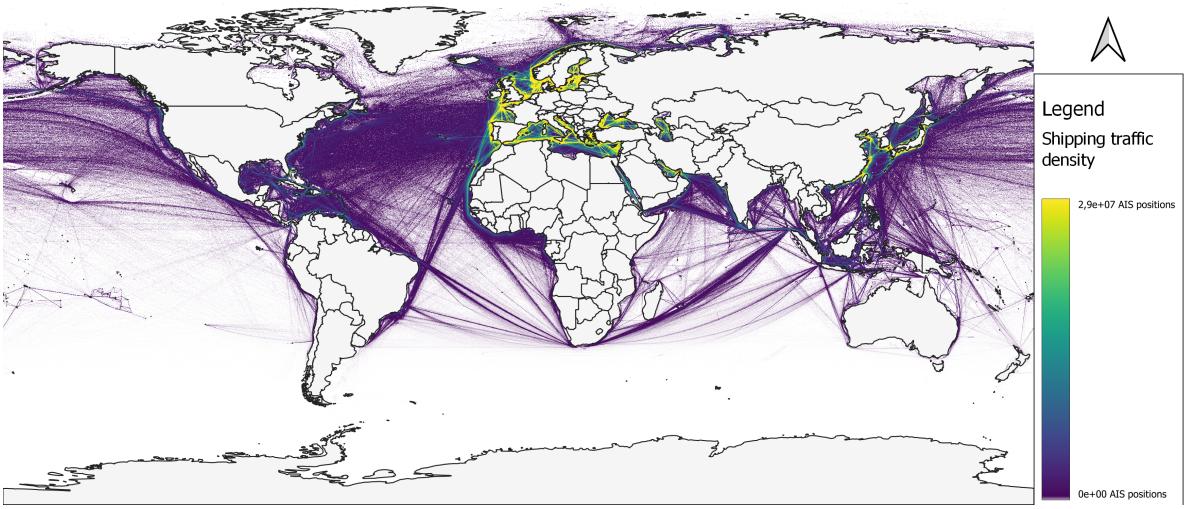

Figure F.4: Secondary dataset: global shipping density [AIS positions / month] (Cerdeiro et al., 2020).

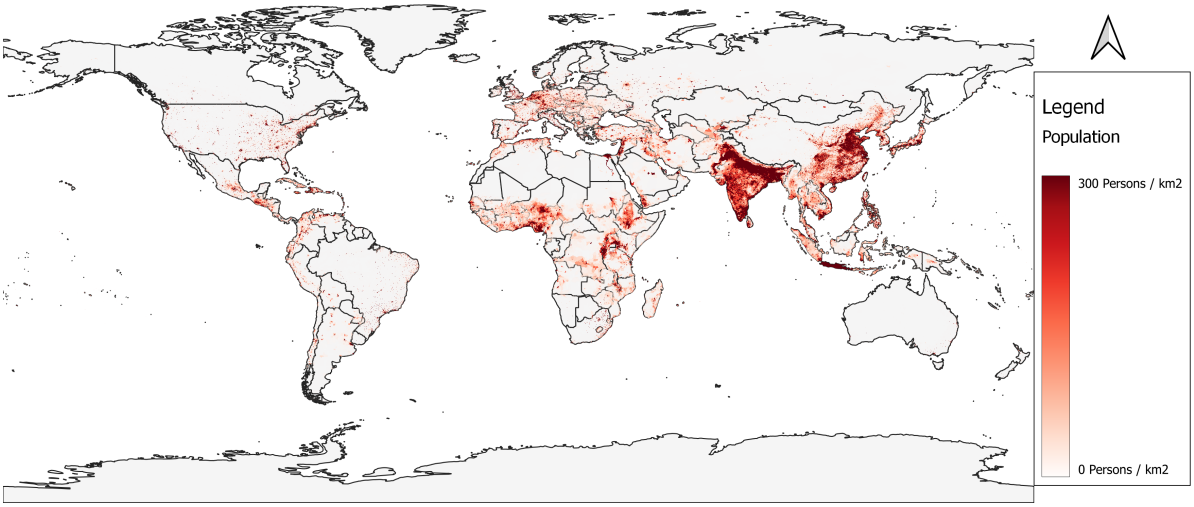

Figure F.5: Secondary dataset: global population density [Persons / km^2] (CIESIN, 2020).

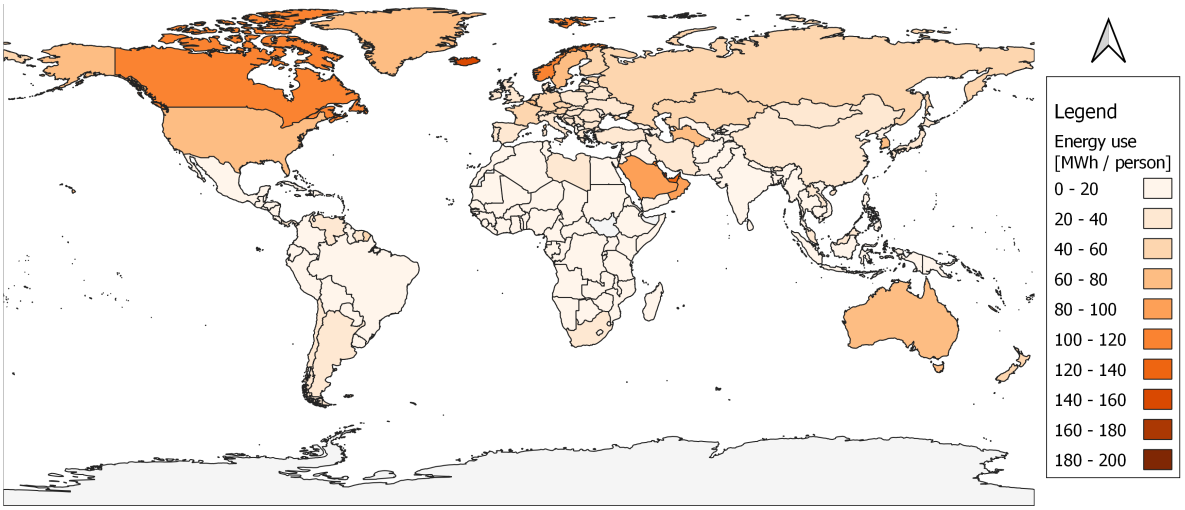

Figure F.6: Secondary dataset: global energy usage per person [MWh] (Bolt & van Zanden, 2020).

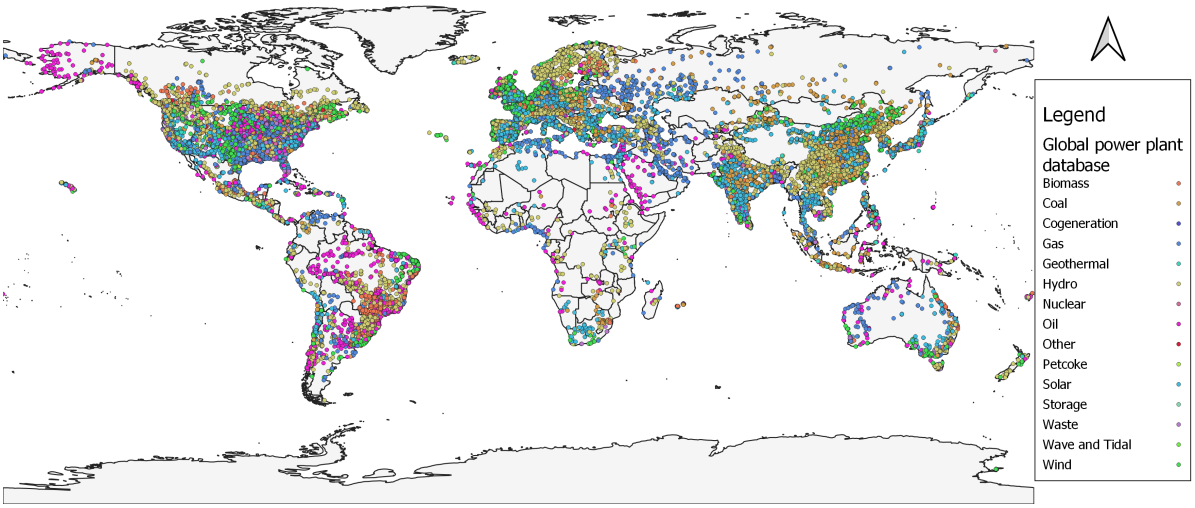

Figure F.7: Secondary dataset: global power plants per category (World Resources Institute, 2021).

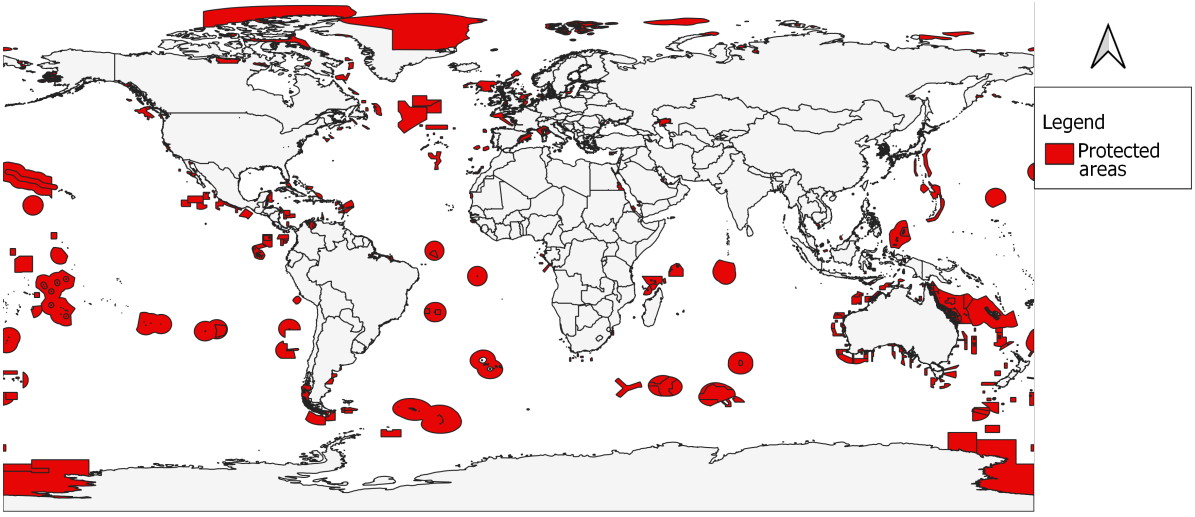

Figure F.8: Secondary dataset: global protected areas (UNEP-WCMC & IUCN, 2023).

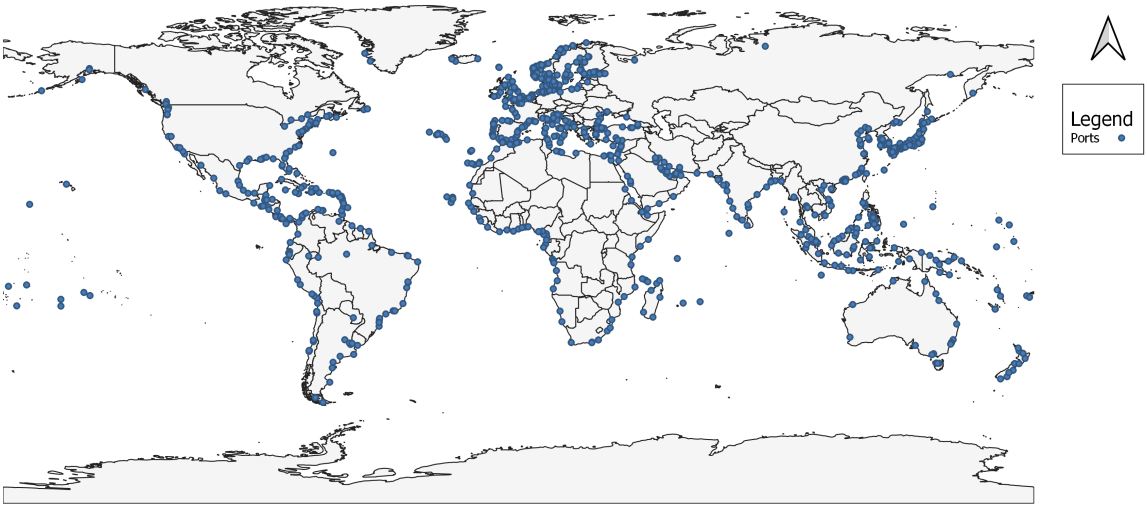

Figure F.9: Secondary dataset: global international ports (The World Bank, 2020).

G

Energy

G.1. Energy mix

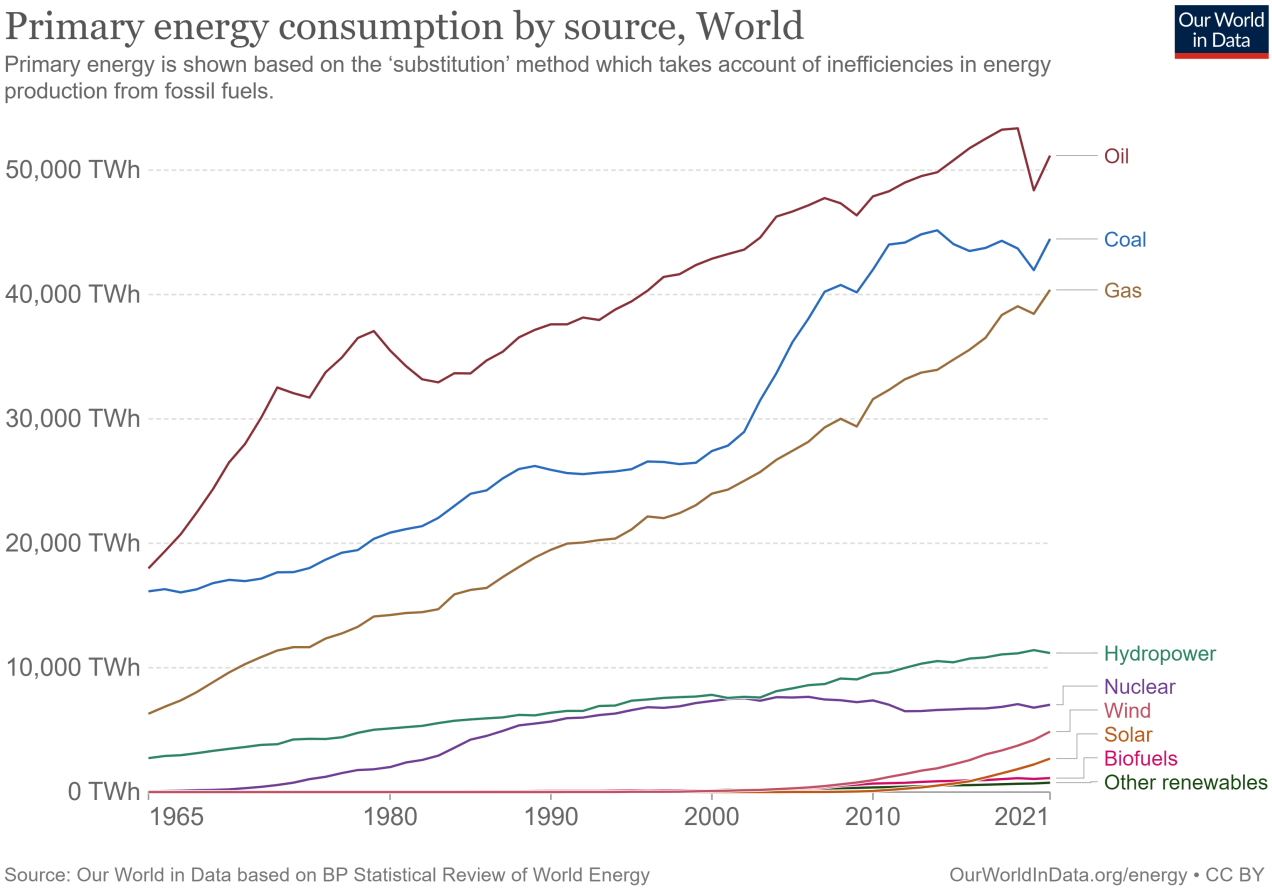

Figure G.1: Global primary energy consumption by source (Ritchie et al., 2022).

G.2. Energy price

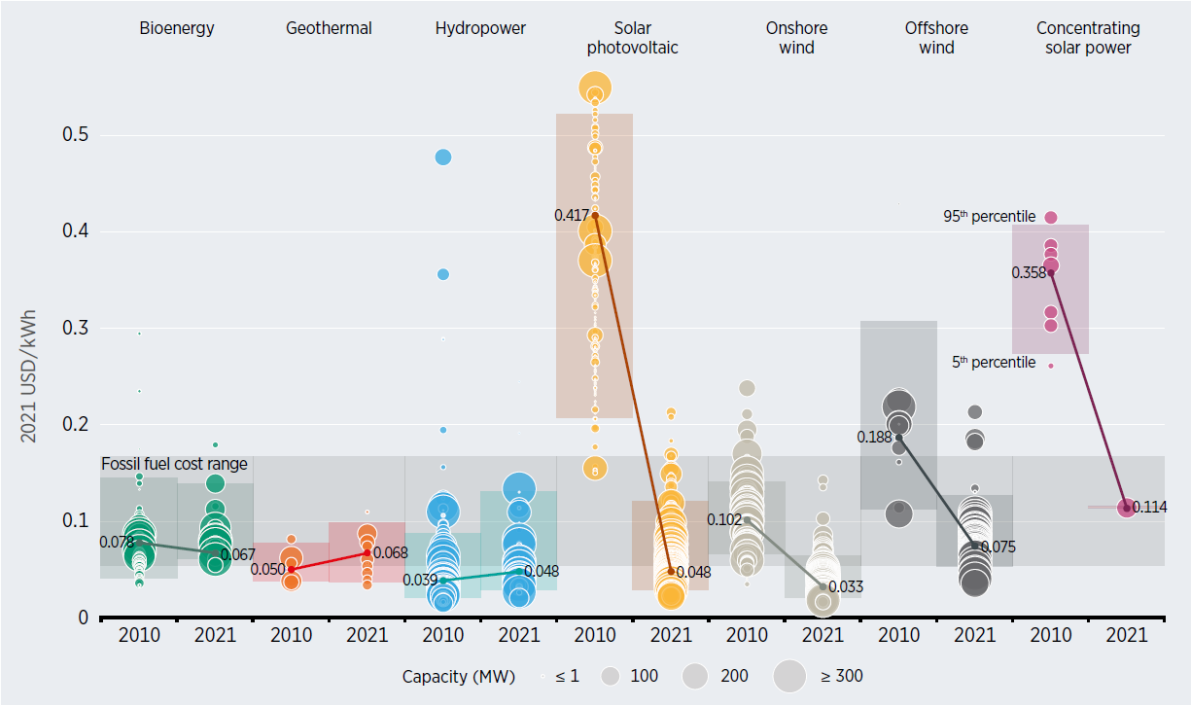

Figure G.2: Global weighted average Levelised Cost of Electricity (LCOE) from newly commissioned, utility-scale renewable power generation technologies, 2010-2021 (IRENA, 2022)

G.3. Area development

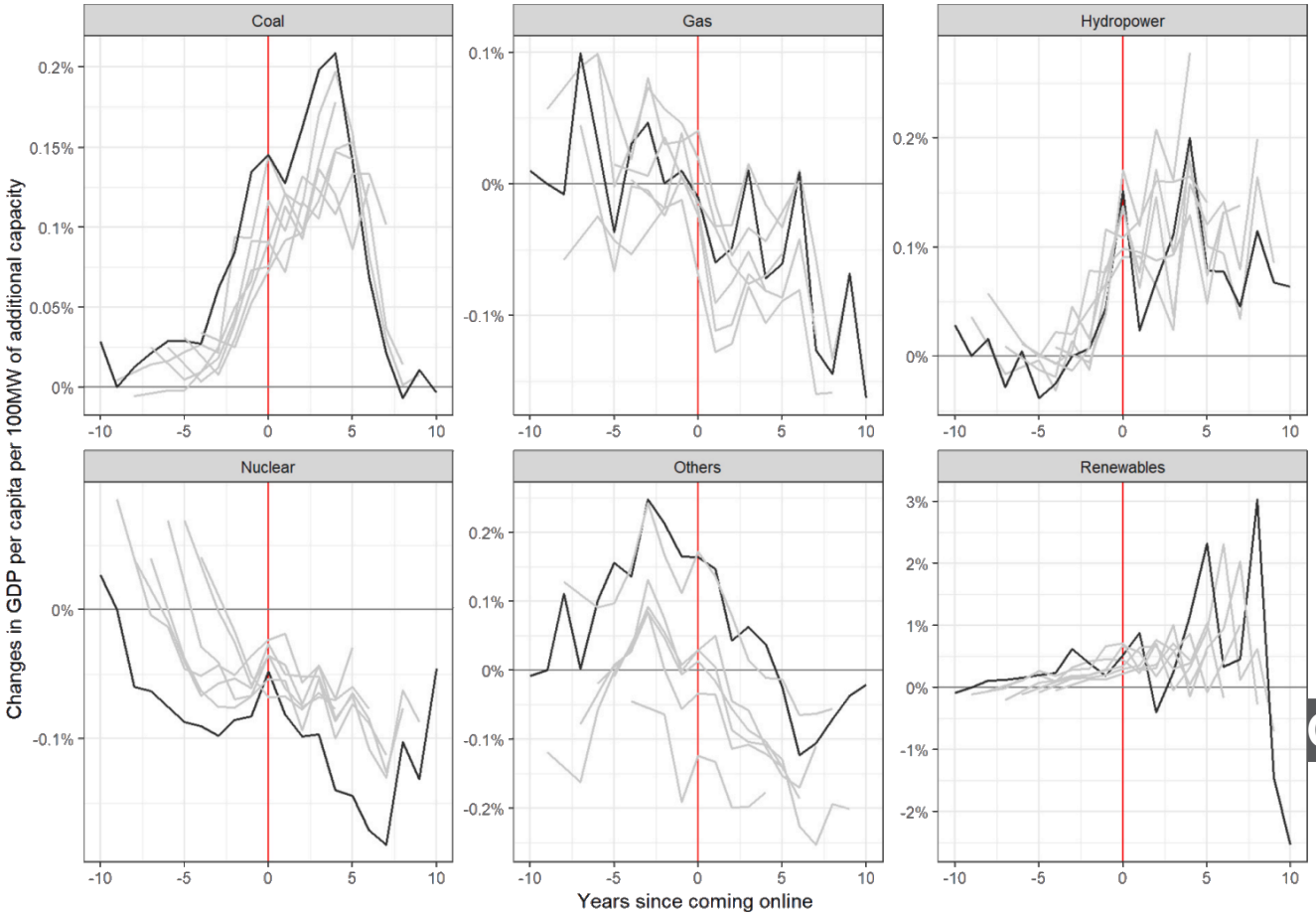

Figure G.3: Event study plot of the relationship between different power capacities and log(GDP per capita) (Montrone et al., 2022)

Additional results

H.1. Threshold analysis additional results

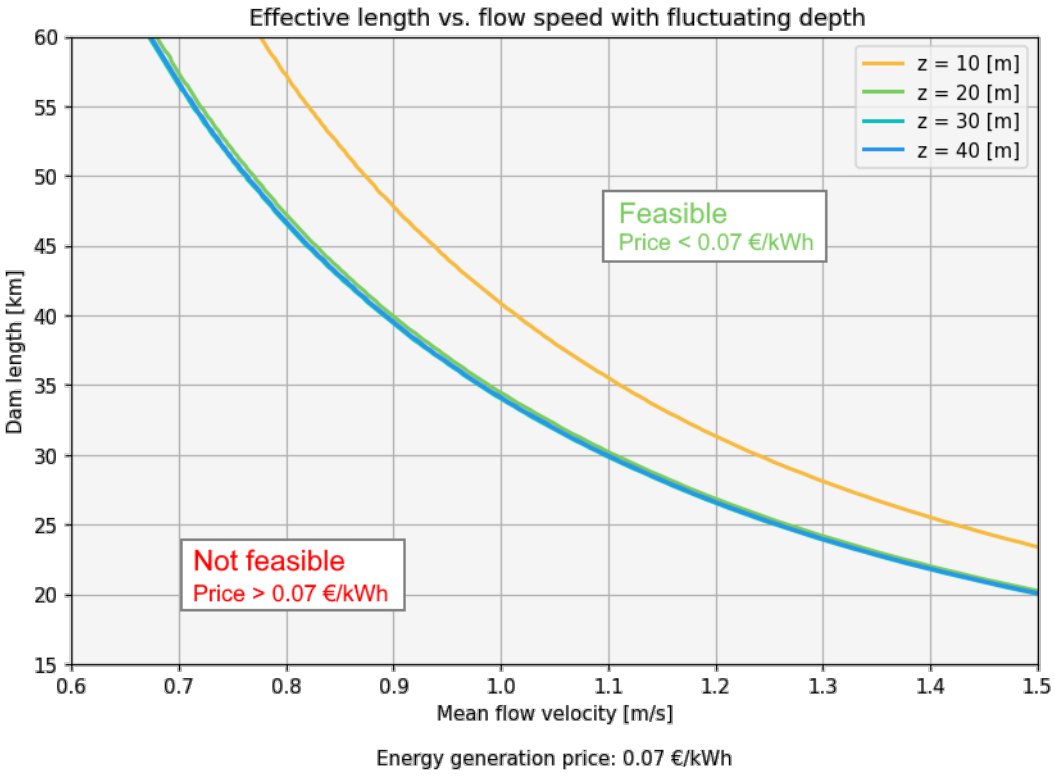

Figure H.1: Effective length and mean flow velocity required to generate energy for 0.07 €/kWh

H.2. Spatial analysis results

Location	Rank	PI score	Potentially feasible	Linkage opportunity: Island		Method	Reason if not feasible
				Model	Manual		
A1	1	0.89	✓	✓	✓		
A2	16	0.53	✓	✓	✓		
A3	23	0.46	✓				
A4	27	0.42	✓				
A5	29	0.42	✓			Detached	
A6	33	0.38	✓	-	✓		
A7	35	0.36	✓				
A8	64	0.14	✓			Detached	
B1	4	0.81	✓	✓	-		
B10	48	0.30	✓	-	✓		
B11	54	0.27	✓				Too far from shore
B12	58	0.20	-				Shipping
B13	60	0.19	-				Bottom slope
B14	61	0.19	-				
B15	65	0.13	✓			Basin	
B2	5	0.79	✓	✓	✓	Stream	
B3	12	0.64	✓	✓	✓	Stream	
B4	14	0.55	✓			Stream	
B5	17	0.53	✓	✓	✓	Stream	
B6_1	18	0.52	✓		✓		
B6_2	22	0.47	✓		✓		
B6_3	32	0.38	✓		✓		
B6_4	45	0.30	✓		✓		
B6_5	50	0.28	✓	✓	✓		
B6_6	55	0.20	✓			Stream	
B7	34	0.37	✓		✓		
B8	38	0.34	✓		✓		Bottom slope
B9	47	0.30	-				
C1	6	0.78	✓	✓	✓		
C2	11	0.67	✓	✓	✓		
C3	21	0.49	✓	✓	✓		Bottom slope
C4	40	0.34	-				
C5	43	0.31	✓		✓		
C6	44	0.31	✓				Bottom slope

Location	Rank	PI score	Potentially feasible	Linkage opportunity: Island		Method	Reason if not feasible
				Model	Manual		
C7	49	0.28	-				
D1	30	0.39	✓				
D2	39	0.34	✓				
D3	57	0.20	✓	✓	-		High tidal amplitude
E1	51	0.28	-				
E2	53	0.27	✓				
F1	3	0.82	✓			Basin	
F2	24	0.45	✓			Detached	
F3	26	0.42	✓	✓	✓		
F4	31	0.38	✓	✓	✓		
F5	46	0.30	✓	✓	✓	Stream	
F6	56	0.20	✓				
F7	59	0.20	✓				
G1	15	0.54	✓		✓		Bottom slope
G2	19	0.51	-				Bottom slope
G3	42	0.32	-				
H1	9	0.71	✓	✓	✓		
H2_1	10	0.67	✓			Basin or Stream	
H2_2	28	0.42	✓			Basin or Stream	
H3_1	13	0.63	✓	✓	-	Stream	
H3_2	20	0.49	✓	✓	-	Stream	
H3_3	62	0.18	✓	✓	-	Stream	
H3_4	66	0.13	✓	✓	-	Stream	
H4	36	0.35	✓				
H5	37	0.34	✓				
I1	2	0.87	✓			Stream	
I2	25	0.45	✓		✓		Bottom slope
I3	52	0.27	-				Bottom slope
J1	7	0.78	-				
J2	8	0.74	✓			Basin	
J3	41	0.32	✓				
J4	63	0.15	✓				

Table H.1: Overview of manual assessment: potential locations

Caisson design

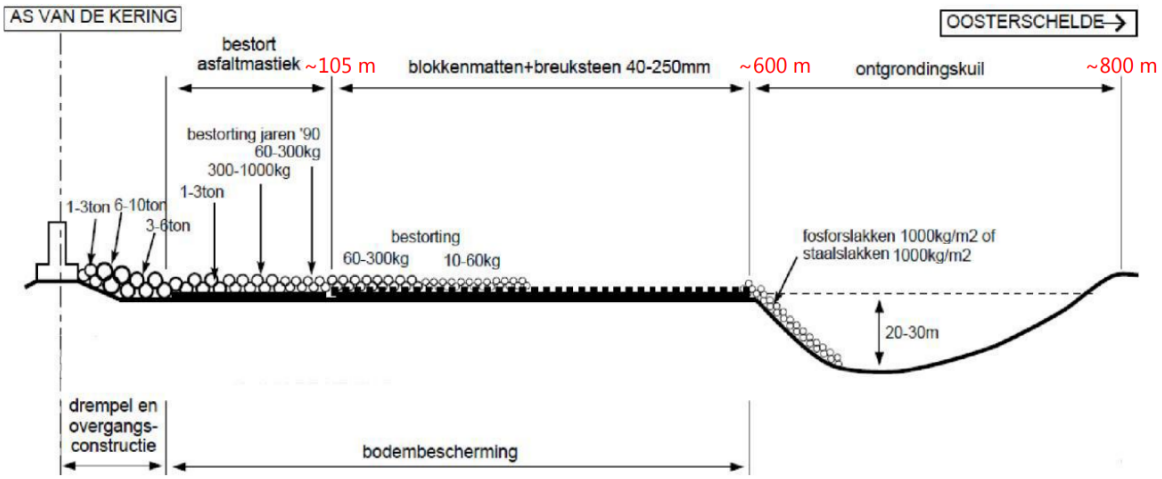

Figure I.1: Scour protection of the Eastern Scheldt barrier (Witteveen+Bos, 2017)